UNIVERSITY OF Southampton

University of Southampton Research Repository
ePrints Soton

http://eprints.soton.ac.uk

UNIVERSITY OF SOUTHAMPTON

Moving Approximate Entropy and its Application to the Electromyographic Control of an Artificial Hand

by

Siti Anom Ahmad

A thesis submitted in partial fulfillment for the
degree of Doctor of Philosophy

in the
Faculty of Engineering, Science and Mathematics
School of Electronics and Computer Science

June 2009

UNIVERSITY OF SOUTHAMPTON

ABSTRACT

FACULTY OF ENGINEERING, SCIENCE AND MATHEMATICS
SCHOOL OF ELECTRONICS AND COMPUTER SCIENCE

Doctor of Philosophy

by Siti Anom Ahmad

A multiple-degree-of-freedom artificial hand has been developed at the University of Southampton with the aim of including control philosophies to form a highly functional prosthesis hand. Using electromyographic signals is an established technique for the control of a hand. In it simplest form, the signals allow for opening a hand and subsequent closing to grasp an object.

This thesis describes the work carried out in the development of an electromyographic control system, with the aim to have a simple and robust method. A model of the control system was developed to differentiate grip postures using two surface electromyographic signals. A new method, moving approximate entropy was employed to investigate whether any significant patterns can be observed in the structure of the electromyographic signals. An investigation, using moving approximate entropy, on twenty healthy participants' wrist muscles (flexor carpi ulnaris and extensor carpi radialis) during wrist flexion, wrist extension and co-contraction at different speeds has shown repeatable and distinct patterns at three states of contraction: start, middle and end. An analysis of the results also showed differences at different speeds of contraction. There is a low variation of the approximate entropy values between participants. This result, if used in the control of an artificial hand, would eliminate any training requirement. Other methods, mean absolute value, number of zero crossings, sample entropy, standard deviation, skewness and kurtosis have been determined from the signals. Of these features, mean absolute value and kurtosis were selected for information extraction. These three methods: moving approximate entropy, mean absolute value and kurtosis are used in the feature extraction process of the control system. A fuzzy logic system is used to classify the extracted information in discriminating the final grip posture. The results demonstrate the ability of the system to classify the information related to different grip postures.

DECLARATION OF AUTHORSHIP

I, Siti Anom Ahmad, declare that the thesis entitled "Moving Approximate Entropy and its Application to the Electromyographic Control of an Artificial Hand" and the work presented in it are my own. I confirm that:

- This work was done wholly or mainly while in candidature for a research degree at this university;

- where any part of this thesis has previously been submitted for a degree or any other qualification at this University or any other institution, this has been clearly stated;

- where I have consulted the published work of others, this is always clearly attributed;

- where I have quoted from the work of others, the source is always given. With the exception of such quotations, this thesis is entirely my own work;

- I have acknowledged all main sources of help;

- where the thesis is based on work done by myself jointly with others, I have made clear exactly what was done by others and what I have contributed myself;

- Parts of this work have been published as:

    1. Siti A. Ahmad and Paul H. Chappell,"Surface EMG Pattern Analysis of the Wrist Muscles at Different Speeds of Contraction", Journal of Medical Engineering and Technology, Vol. 33, Issue 5, pp. 376-385, July 2009.

    2. Siti A. Ahmad and Paul H. Chappell,"Moving Approximate Entropy Applied to Surface Electromyographic Signal", Biomedical Signal Processing and Control, Vol. 3, pp. 88-93, 2008.

Signed: ....

Date:..

Contents

List of Figures

List of Tables

Glossary

Abduction	Movement away from the midline of the body
Adduction	Movement toward the midline of the body
Afferent	A nerve which transmits impulses from the tissues to the brain and spinal cord
Anterior	Toward the front of the body
Anthropomorphic hand	Mechanical hand made to resemble a human hand
Concentric	A shortening contraction
Contraction	An increase in muscle tension
Deep muscle	Away from the body surface or skin
Distal	Farther from the centre or median line, or from the trunk
Eccentric	A lengthening contraction
Efferent	A nerve which transmits impulses from the brain and spinal cord to the muscle and organ
Electromyography	An electrical activity associated with muscular contraction
Extension	Straightening movement in the posterior direction
Flexion	Bending movement in the anterior direction
Isometric	Increase in tension without change in muscle length
Isotonic	Increase in tension with muscle length
Lateral	Away from the median plane or midline
Medial	Towards the media plane or midline
Posterior	To the rear or behind
Pronation	Rotation of the forearm with the palm turned inward
Prosthesis	An artificial replacement for a part of the body
Rotation	Rotation of a limb segment, medial or lateral direction
Superficial muscle	Close to the surface of the body or skin
Superior	Above
Supination	Rotation of the forearm with the palm turned outward

Nomenclature

ANN	Artificial neural Network
ApEn	Approximate Entropy
AR	autoregressive
bpm	beeps per minute
CNS	Central Nervous System
DOF	Degree of freedom
EMG	Electromyography
ECR	Extensor carpi radialis
ECS	Electromyographic control system
FC	Fuzzy Clustering
FCU	Flexor carpi ulnaris
FL	Fuzzy Logic
FSM	Finite State Machine
GMM	Gaussian mixture model
LDA	Linear discriminant analysis
MF	Membership function
MLP	Multilayer perceptron
MMG	Mechanomyography
MU	Motor unit
MUAP	Motor Unit Action Potential
PCA	Principal Component Analysis
RP	Recurrence Plot
SampEn	Sample entropy
SD	Standard deviation
SEMG	Surface electromyography
SOFM	Self-organizing Featured Map
STFT	Short-time Fourier transform
WPT	Wavelet packet transform
WT	Wavelet transform

Acknowledgements

First and foremost, I would like to offer my sincerest gratitude to my supervisor, Dr Paul Chappell, who has supported me throughout my PhD with his encouragement, guidance and knowledge. Without him, my PhD would not have been completed. One simply could not wish for a better or friendlier supervisor.

I would like to thank Barry Bailey for letting me use his lab without limit and in the same time being my UK history teacher. To Richard Howell, a person I will turn into for components and Martin Warner, for teaching me about EMG stuff, something that I know nothing about before doing my PhD.

In my daily work, I've been blessed with helpful and cheerful colleagues and friends, particularly Somphop, Stephen, Evo, Gaithaa, Asmahan, Darryl and Andy. You're all are amazing friends. My special thanks to Noreha, Cheryl and Ann-Marie for our coffee breaks - thank you for the motivation.

My thanks also go to the Electronic Systems and Designs group that has provided the support and equipment I have needed to produce and complete my PhD. I would like to acknowledge the Universiti Putra Malaysia and government of Malaysia for their financial support.

To my family in Malaysia, thank you for all the love, constant encouragement and prayers throughout my study.

Last but not least, to my beloved husband, Syawal and my wonderful children, Syafique & Syra, thanks for being so understanding and supportive especially when I was piled up with the PhD work.

Chapter 1

Introduction

The human hand is a complex biological system with twenty seven bones. A multitude of muscles and tendons provide multiple degrees of freedom of movements and an array of over 17,000 tactile sensors for sensory feedback mechanisms [Carrozza et al., 2002a]. Prosthetic hands have been designed to provide either functional and/or visual replacement for individuals with amputation or a natural birth defect. Commercial hand prostheses provide the user with limited dexterity and functionality due to the restricted number of grip patterns that may be achieved. The last few decades have shown continuous work on prosthetic hand developments with the ultimate aim of developing a prosthetic hand that is able to mimic the functionality and control of the human hand. For example, the US Department of Defense's Advanced Research Project Agency has put a large investment into prosthetic arm research with the aim to have a mechanical limb with significant function and sensory perception of a natural limb controlled via the amputee's nervous system [Evans-Pughe, 2006].

To improve the functionality of the artificial hand, two main factors have to be considered in the development process. Those two factors are the structural design of the artificial hand and the control mechanism of the hand. Rapid growth in the structural design of the artificial hand can be seen and there is renewed interest in the development of hands with multiple degrees of freedom that lead to multiple grip hand postures [Mitchell, 2008; TouchBionics, 2007]. The Southampton Hand has multiple degrees of freedom that are able to adopt six different hand grip postures; spherical, lateral, power, tripod, tip and extension[Light et al., 2002a]. Unlike most other artificial hand designs that have only three active digits, the Southampton Hand has four digits and a thumb that is able to do multiple grip postures. This lighter weight (about 400g) hand uses six gearboxes that can flex/

extend the four digits, and the thumb can flex/extend and also rotate. It also has some sensors (slip, force and temperature) that could improve the functionality of the prosthetic hand [Cotton et al., 2007; Cranny et al., 2005b]. Generally, the Southampton Hand is about the structure of an artificial hand but also included is any control philosophy that could form a high functionality prosthetic hand in the future.

The control mechanism has become the main concern in the prosthetic hand development process. Various methods have been proposed in controlling the operation of an artificial hand and surface electromyography has become an established technique as the control mechanism for prosthesis control application. The concept of using surface electromyography signal for prosthesis control started in the 1940s [Plettenburg, 2006]. By using the residual muscles on the amputee's arm, they have been used as the control channel to determine the final movement of the hand. The most simple application is to either open or close a hand.

Attempts to recognize patterns in the surface electromyography signal for control purposes have been investigated and it has been demonstrated that this control method is robust for the prosthesis control. Pattern recognition aims to classify the surface electromyography data based on statistical information extracted from the signal and determine the final output of the device operation. Even though the amputees may not have fully functioning muscles, it has been shown that they are able to generate repeatable surface electromyography patterns during movements [Asghari Oskoei & Hu, 2007]. The control channel can be varied from single to multiple surface electromyography channels. There is a trade off between the number of control channels and the complexity of the system. A single channel would give a less complex structure whereas multiple channels will cause more complexity in the construction but could give higher accuracy in the system performance. An example of electromyographic control system is an investigation on four channels of surface electromyography signals with the task to discriminate four multiple classes of hand and wrist movement [Englehart & Hudgins, 2003]. Their system was very accurate in its performance (98% classification rate) as each control channel was used in determining one different movement.

Electromyography (EMG) is used to evaluate and record the electrical activity of skeletal muscles during their contraction. It can be divided into two types: surface EMG (SEMG) and needle EMG, requiring transcutaneous insertion or needles. The former is the most widely used as it is a non-invasive technique, cost effective and more convenient to use. SEMG signals are the summation of

motor unit action potentials when the neuromuscular activities are detected using surface electrodes placed on the skin surface. It has been used in numerous fields including biomechanics, motor control, muscle fatigue monitoring, functional electrical simulation and many other applications [Bilodeau et al., 2003; Bonato et al., 2001; Eom et al., 2000; Manette & Maier, 2004]. Also, repeatable SEMG patterns can be observed during different muscle contractions enabling use in prosthetic control.

Various signal processing techniques have been used to analyze the SEMG signals, depending on which application is carried out. Root mean square and median power frequency are two popular methods in the analysis of fatigue muscle [de Andrade et al., 2006; Jansen et al., 1997]. By determining the signal to noise ratio and using the Teager-Kaiser energy operator, the onset time when the muscle contracts can be detected from a SEMG signal [Li et al., 2007; Li & Aruin, 2005]. In an electromyographic control system for prostheses applications, the mean absolute value (MAV) has been the most widely used method to extract information from a SEMG signal [Hudgins et al., 1993; Y. Al-Assaf, 2005; Chan et al., Sept. 2000; Englehart & Hudgins, 2003].

1.1   Objective

The objective of this research is to develop an EMG control system (ECS) that is based on pattern recognition to control a six degrees of freedom prosthetic hand, specifically the Southampton Hand by using information from two SEMG signals (flexor and extensor muscle) as the control channel. A new method, moving approximate entropy is used as the main method in feature extraction of the SEMG signal, which is part of the ECS.

To achieve this objective, a detail investigation of moving ApEn has been carried out. Since its computation involves two parameters, the behaviour of different variable conditions have been investigated thoroughly before the final parameters are chosen. The ApEn algorithm is also tested on different data sets, from regular and random numbers to raw and rectified SEMG. This thesis emphasize the investigation on the SEMG signals using this method, as well as the ECS development process where a fuzzy logic system is used to classify the extracted features in selecting the final output.

The aim of the research is, by integrating the ECS with the Southampton Hand, the hand should be able to do multiple grip postures (multiple degree of freedom) to form a prosthetic hand with better functionality.

1.2   List of Publications

The research on the development of the ECS has been been presented and published through the following research papers:

1. Siti A. Ahmad and Paul H. Chappell,"Surface EMG Pattern Analysis of the Wrist Muscles at Different Speeds of Contraction", Journal of Medical Engineering and Technology, Vol. 33, Issue 5, pp. 376-385, July 2009.

2. Siti A. Ahmad and Paul H. Chappell,"Development of electromyographic control system based on pattern recognition for prosthetic hand application", in the Proceedings of the Sixth IASTED International Conference on Signal Processing, Pattern Recognition and Applications (SPPRA'09), Innsbruck, Austria, pp. 120-125, February 2009.

3. Siti A. Ahmad and Paul H. Chappell,"Surface EMG Classification using Moving Approximate Entropy and Fuzzy Logic for Prosthesis Control", in the Proceedings of the Myoelectric Controls/Powered Prosthetics Symposium (MEC'08), New Brunswick, Canada, pp. 136-138, August 2008.

4. Siti A. Ahmad and Paul H. Chappell,"Moving Approximate Entropy Applied to Surface Electromyographic Signal", Biomedical Signal Processing and Control, Vol. 3, pp. 88-93, 2008.

5. Siti A. Ahmad and Paul H. Chappell, "Surface EMG Classification Using Moving Approximate Entropy", in the Proceedings of the International Conference on Intelligent and Advanced Systems (ICIAS'07), Kuala Lumpur, Malaysia, November 2007.

1.3   Document Structure

The structure of this report reflects the sequence of the development of ECS based on pattern recognition. The organization of the thesis is as follows:

Chapter 2 reviews the research in the development of prosthetic hands. The commercial prosthetic hands available are described as well as the current development of the hand. The Southampton Hand operation and latest development are also described. A brief overview of functional anatomy of the upper limb and the physiology of SEMG signals are presented in this chapter.

Chapter 3 describes the state of the art of the electromyographic control system based on pattern recognition. Various methods used in different stages of pattern recognition based control are reviewed.

Chapter 4 describes the theoretical background of the proposed method, moving approximate entropy. This includes some of the applications that using ApEn. The continuous form of entropy measure and other algorithms are also described and discussed.

Chapter 5 details the investigation of the surface EMG signals of the wrist muscles during different movements at a different speeds including results, analysis and findings.

Chapter 6 describes the development of the electromyographic control system based on pattern recognition in detail. The classification process of the extracted features obtained in the previous chapter is discussed in detail . The stages involved are also described along with the analysis.

Chapter 7 discusses the main issues arise from the results and findings obtained during the development process.

Chapter 8 draws the conclusions from the development and testing of the electromyographic control system based on pattern recognition. An outline for potential future work is described.

Chapter 2

Review of Prosthetic Hands

This chapter reviews the current status of the prosthetic hand development covering their function, mechanical structure and control mechanisms. A brief history and commercially available prosthetic hands are also included in this chapter. An introductory explanation of the human hand and physiology of surface EMG signal are also included.

2.1 The human hand

The upper limb is associated with the lateral aspect of the lower portion of the neck. Its main function is for positioning the hand in space as well as assisting to regulate the body's movement to compensate for changes in the body's centre of gravity. Based on the position the upper limb's component bones and major joints, it can be divided to shoulder, arm, forearm and hand.

The hand function is as mechanical tool (to grip and manipulate objects) and sensory tool (to discriminate between objects based on touch). Grip postures can be divided into six types that are commonly used when completing a task, namely spherical, lateral, tripod, tip, power and extension (Figure 2.1)

The hand independent movements are effected by different muscle groups. Some muscles are located entirely in the hand itself (intrinsic muscles) and some are located at the forearm (extrinsic muscles). The intrinsic muscles mainly execute precision movement with the fingers and thumb. The extrinsic muscles are connected to the fingers by tendons and responsible in the wrist movement and power gripping in hand. The central nervous system (CNS) sends a signal to the spinal
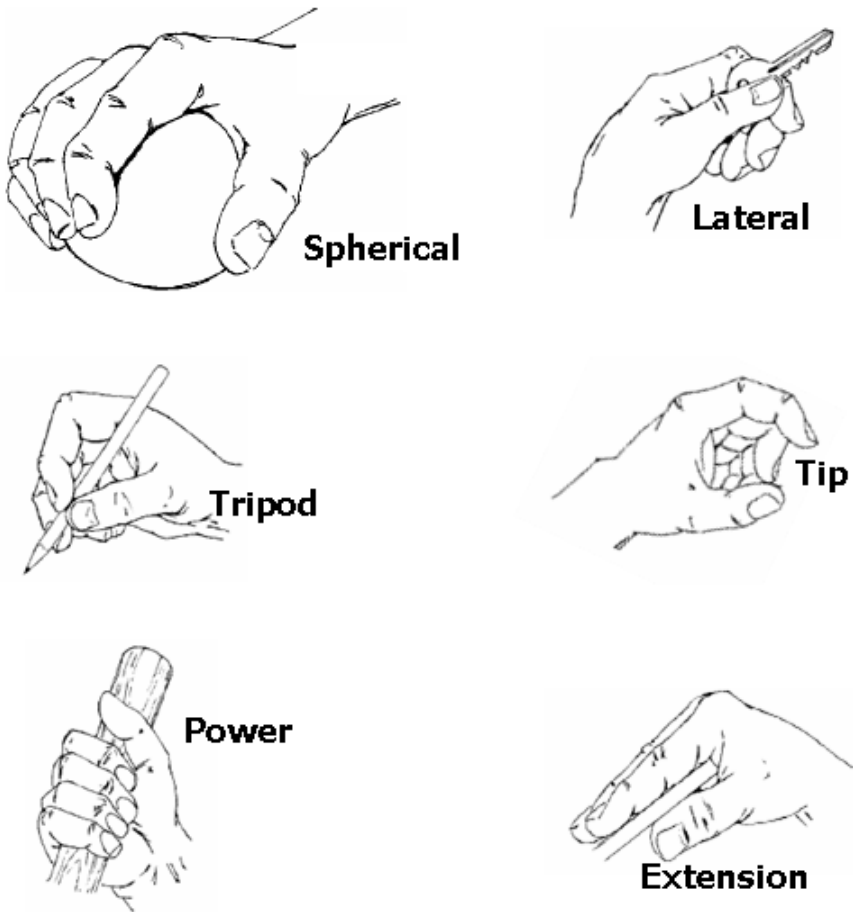
FIGURE 2.1: Six patterns of hand grip postures [Light et al., 2002a]

cord which then activates the appropriate muscles in performing the hand movement. Figure 2.2 shows the view of the forearm with an extending hand (top) and a flexing hand (bottom).

2.2 Prosthetic hands

Prosthetic hands are designed to provide a replacement for upper limb amputees and they range from the passive type to functional types. A passive prosthesis is a cosmetic type where it just provides visual replacement of the amputation, while the functional prostheses are used to mimic the function of a natural hand. The simplest operation they can do is just either open or close the hand. The functional type can be divided into two categories; body powered and externally powered.
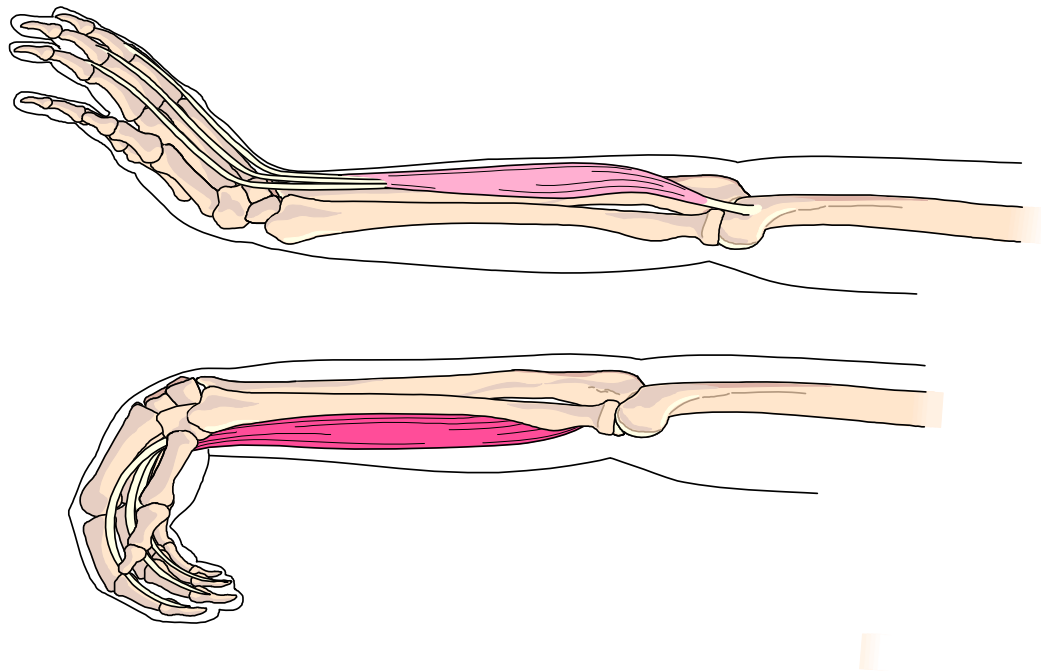
FIGURE 2.2: Lateral view of the forearm with an extending hand (top) and a flexing hand (bottom)

Body powered prosthesis is when the prosthesis is powered and controlled by body movements. This is done by putting a harness system on the shoulder or upper arm, which is attached to a cable that is connected to the hand (see Figure 2.3). It is highly durable type of prosthesis with low maintenance cost. They provide some sensory feedback to the shoulder through the cable and harness. Also, a person can become dexterity in holding an moving everyday objects. However they have limited functionality and maybe uncomfortable to the wearer.

Externally powered prostheses normally use small electronics devices that can be put on the hand or wrist to control the hand movement. Control techniques are used in this type of prosthesis, for example EMG control, servo control and nerve control. Rechargeable batteries are used to power the device. Even though the externally powered prostheses is much heavier compared to other type of prostheses, they require less maintenance once fitted to the amputees where typical maintenance is in every six months. With the rapid growth in the technology, the weight problem could be overcame in the future.

2.2.1 Brief history of prosthetic hands

Prosthetic hands have been found centuries ago with the main aim was tried to provide the amputees with a replacement part. It had been found as early as
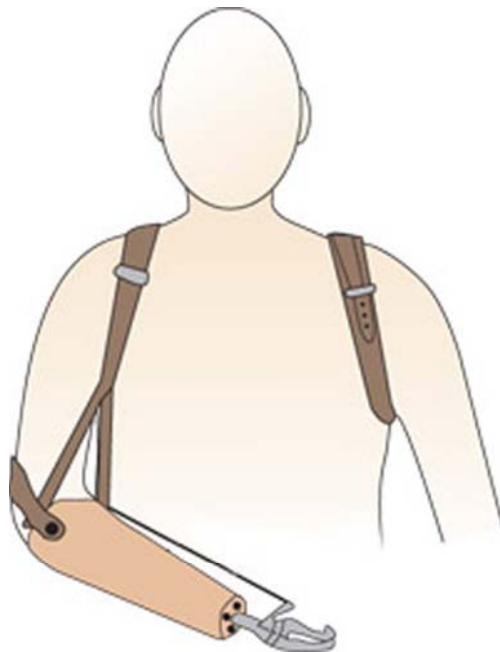
FIGURE 2.3: Below elbow body powered prosthesis [Disaboom, 2008]

330BC on an Egyptian mummy which was a cosmetic hand prosthesis [Plettenburg, 2006]. In the 15th century, passive hand prostheses were developed and used for several decades. Passive prosthetic hands involve a moveable thumb only or by using knob activation to lock the thumb and fingers configuration to select the chosen position [Plettenburg, 2006]. One example of a passive prosthetic hand was the Jagsthauser Hand (Figure 2.4) worn by a German knight, Gotz von Berlichingen. The $1500g$ steel hand uses knob activation where both thumb and the paired fingers of the hand are capable of being independently locked in several positions by means of an elaborate system of ratchets and spring-operated pawls.

The beginning of 19th century showed the start of actively operated prostheses. The prosthesis is called body powered where a harness is tied to the shoulder and connected to device via a cable. When the user moves the shoulder, the cable is tightened and will cause the device to open and close. Count of Beaufort from France had designed a body powered prosthesis back in 1860 where the hand was made of wood and the moveable thumb was controlled by a cable connected to a shoulder girdle [Plettenburg, 2006]. The hand can also be operated by the abduction and the extension of the arm.

World War I had caused a large number of amputees. The development and use of the body powered prostheses were boosted during this time and several other body powered designs can be found with different functionality. The most popular design was the split hook and this type of prosthesis is still widely used today. The
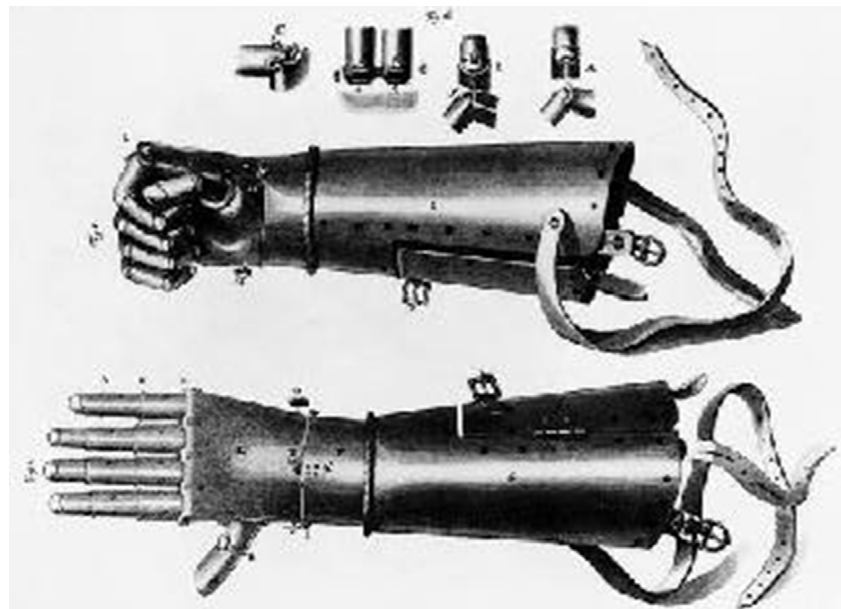
FIGURE 2.4: The Jagsthauser Hand [von Berlichingen, 2007]

hook has two fingers where one finger is static and the other one is moveable. It is operated by a control cable connected to the extension finger and the finger is opened against a spring (rubber band). Plastic materials were introduced into prosthetics after the Second World War and further development on the body-powered prostheses continued with gradual growth.

External powered prostheses were introduced at the end of 19th century and can be divided to types: pneumatically and electrically powered. Pneumatically powered used carbon dioxide to power up the prostheses while electrically powered used rechargeable batteries. However , the pneumatically powered device was not practical as it was noisy and more difficult to operate. Later, electromyographic prostheses had been introduced where an electrical signals generated when the muscle contracts to control the prosthetic device. When a skeletal muscles contracts, small voltages can be detected on the skin surface which are amplified and conditioned to operate an electrically powered prosthesis. It has been reported that the electromyographic prosthesis was first proposed and built by Reiter in 1948 and by the end of the sixties and early seventies, the electromyographic prostheses became popular in this field [Plettenburg, 2006].
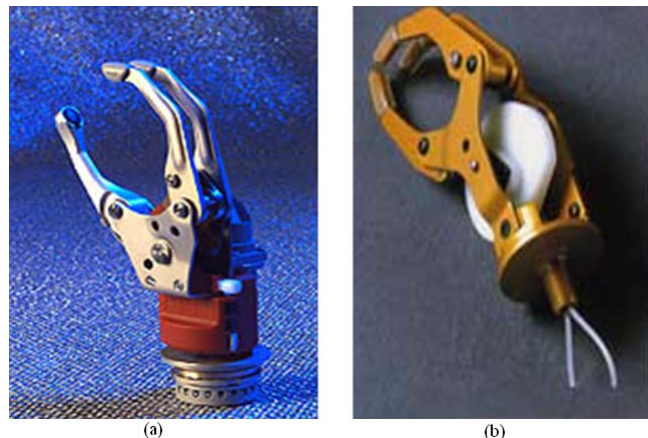
FIGURE 2.5: The Otto Bock Prosthetic hands: (a) The SensorHand and(b) The SystemHand [OttoBock, 2007]

2.3 Commercially available prosthetic hands

A wide variety of commercial upper limb prostheses are available nowadays. They range from body powered to externally (electrically) powered prostheses to passive hands. Most of the commercial prosthetic hands are three fingered (2 fingers and a thumb) devices with a single degree of freedom (DOF) and restrictive function. All of these prosthetics come with a cosmetic glove which provide a natural appearance to the wearer.

In Germany, the Otto Bock SensorHand (Figure 2.5(a)) is one example of an externally powered prostheses. It is myoelectrically controlled and is able to open/ close with a speed of 300 mms^{-1}. The device incorporates an auto grasp feature, which can prevent the object held from slipping by monitoring and changing the gripping force accordingly.

The SystemHand (Figure 2.5(b)) also manufactured by Otto Bock, is a cable-controlled arm prosthesis that is powered through the body residual limb and/or the shoulder girdle. The hand is closed when the cable is pulled intentionally and the grip force will be increased if the cable is pulled further [OttoBock, 2007].

The ProHand, one of the prosthetic hands developed by Motion Control uses EMG signals from the remnant limb to control the prothesis [MotionControl, 2007]. The operation is almost similar to the Otto Bock hand with an extra feature, flexion/extension of the wrist (Figure 2.6) The wearer is able to flex and extend the wrist and could allow the hand to act like a natural hand in performing tasks.
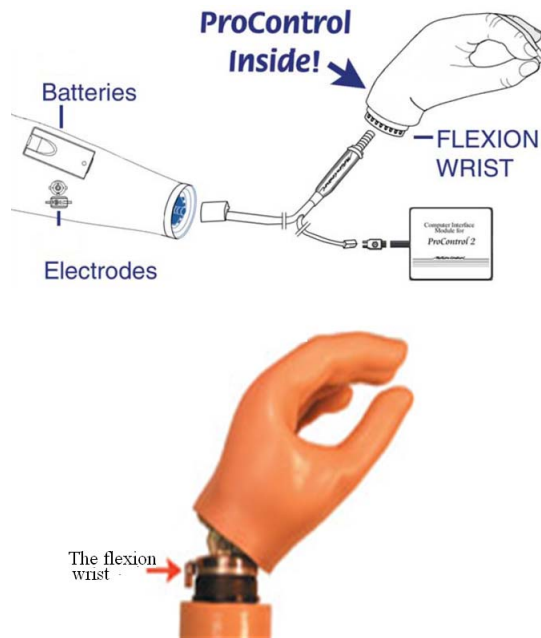
FIGURE 2.6: The ProHand by Motion Control. Top: The system setup, Bottom: the hand with the wrist flexion feature [MotionControl, 2007]
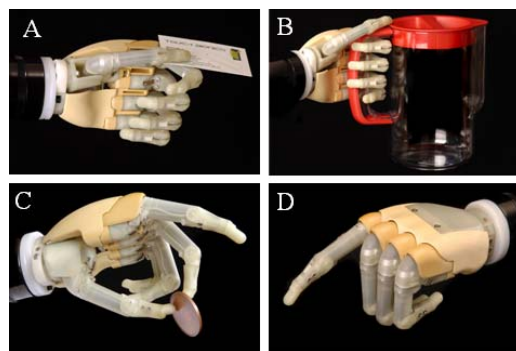
FIGURE 2.7: The Touch Bionics i-Limb hand. A: key grip, B: power grip, C: precision grip and D: index point [TouchBionics, 2007].

Touch Bionics (Edinburgh, Scotland) developed the lighter weight i-Limb hand that uses two EMG signals to control the system [TouchBionics, 2007]. While other commercial prosthetic hands can only perform one DOF, the i-LIMB hand consists of five active digits that can perform three most common gripping configurations used by humans: power, precision and key grip by rotating unpowered the thumb (Figure 2.7). These grip postures are done by rotating the thumb to different positions (using a human hand to do this). The hand is also able to perform index point posture where it is very useful for operating a computer keyboard, automatic teller machine (ATM) and other daily requirements [TouchBionics, 2007].

2.4 Current research into the development of prosthetic hands

A significant amount of research has been devoted to the improvement of the prosthetic hand's functionality. This section reviews some of the currently active research on upper limb prosthetics.

2.4.1 The Southampton Hand

The research into upper limb prostheses at the University of Southampton began in the 1960s. The hand was originally built with 4 DOF, weight about 1.4kg and discrete logic components were used to control it. The work had seen innovative development of the prostheses in different aspects as follows: mechanical design, control system design and also sensor incorporation for automation process [Todd, 1970; Codd, 1976; Moore, 1980; Storey, 1978; Swain, 1982]. The main objectives of this research is to increase the grasping pattern and also to improve the sensory feedback control of the hand.

Kyberd [Kyberd, 1990; Kyberd & Chappell, 1994; Kyberd et al., 1995] had continued the enhancement of the Southampton hand where sensors that could detect object slippage, contact force and angle were incorporated on the palmar surface of the hand. The Southampton Adaptive Manipulation Scheme (SAMS) is a hierarchical control format that had been developed to control the Southampton hand. This control scheme is initiated from the central nervous system principles of a human system. Figure 2.8 shows the state diagram of the SAMS. The SAMS uses EMG or the sensor inputs to grip the object with minimal force by maximizing the contact area between the object and the hand. Two channel EMG inputs are used to control the hand, which are flexor and extensor muscles of the forearm. The power consumption can also be optimized with this scheme where the object will be gripped if the user issues the instruction or if slip is occurring. When no instruction is given, the hand will be in idle condition and no power will be consumed.

The Southampton Hand was then being redesigned by Light [Light & Chappell, 2000; Light, 2000; Light et al., 2002b] which is called the Southampton Remedi Hand. It is a five fingered device, formed by a thumb and four fingers to have a more hand-like appearance. Manufactured using carbon fibre epoxy composite for
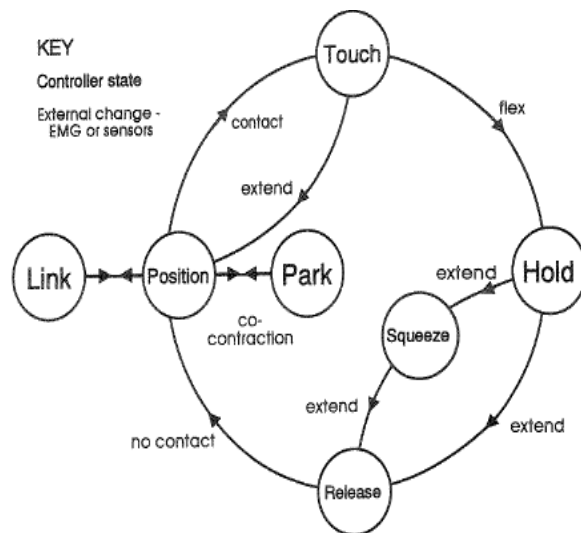
FIGURE 2.8: State diagram of the SAMS [Kyberd & Chappell, 1994]

the linkage and polymer thermoplastic, a lighter weight (400g) hand with good bearing properties is produced. The hand has six DOF which builds on the four DOF Southampton hand. The thumb is able to do two different movement; flexion/ extension and adduction/ abduction that can adapt to six prehensile pattern: power (Figure 2.9(a)), tip, extension, lateral (Figure 2.9(b)), tripod and spherical. The hand is used with a hierarchical controller, SAMS to ensure the adaptable prehension. To investigate the functionality of the prosthesis and the controller, an assessment procedure was developed. The Southampton Hand Assessment Procedure (SHAP) is used to evaluate the hand's functionality in clinical setting [Light et al., 2002a; Light, 2000].
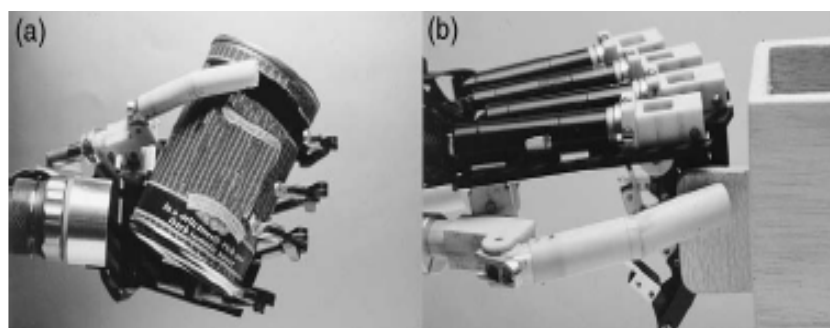
FIGURE 2.9: The Southampton Remedi hand in (a) power and (b)lateral prehension [Light & Chappell, 2000]

The Southampton Remedi Hand was destroyed in a major fire at the University which resulted in the design and construction of a new hand with improved properties. The new lighter hand can mimic the motion of the human hand and also

has sensors (Figure 2.10). The sensors have been designed using thick-film printing technology [Cranny et al., 2005b,a; Cotton et al., 2007] that could be placed at each fingertip of the hand. These piezo-resistive sensors can be used to monitor force, where it can detect how much forces is exerted to the tip. The sensor information is converted to electrical signals that are fed to a processor which will then allows the hand to hold the object with sufficient force. Another sensor is a slip sensor placed on the finger tips where when the object begins to slip. It will automatically control the hand to tighten the object. Temperature sensors are also included to avoid thermal damage to the prosthesis.
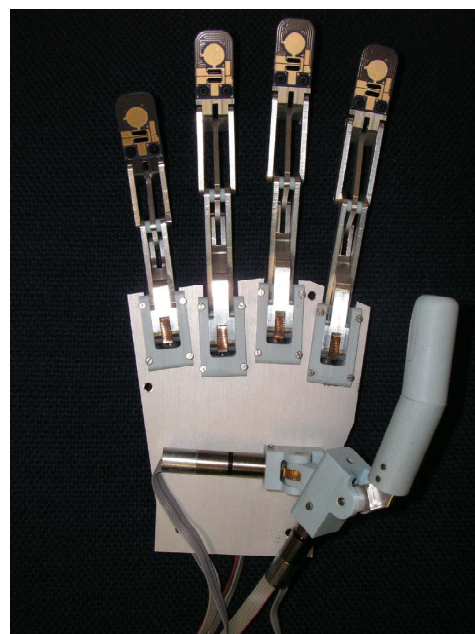
FIGURE 2.10: The new Southampton Hand with sensors at each fingertip of the hand

2.4.2   The Biomechatronic hand

Researchers from Advanced Robotics Technology and Systems Laboratory (ARTS) Lab in Italy have been actively involved in designing and developing prosthetic hands for several years. Carrozza et al. [2001, 2002b] developed a mechanical 'human-like' hand embedded with electronics and sensors to form a biomechatronic hand. The hand has three active fingers (thumb, index and middle) device and two passive fingers that are able to perform cylindrical (power) and tripod (precision) grasps. In order to make a light weight hand, micromotors are used to actuate the fingers where they are integrated in the hand structure. Force sensors are placed at the fingertips to monitor the grip control and also position sensors to monitor the displacements of the active joints.

FIGURE 2.11: The CyberHand prosthesis [ARTSLab, 2008]

The development of the biomechatronic hand has led to further enhancement of the prostheses. The CyberHand [Carrozza et al., 2003, 2004; Cipriani et al., 2006; Carrozza et al., 2006] prosthesis was developed by re-designing the biomechatronic hand where a five fingered device is produced (Figure 2.11). It has sixteen DOF and able to perform cylindrical, lateral, spherical, bidigital and tridigital grasping postures. Included in the design are twenty-one position sensors, eight force sensors and fifteen touch sensors to monitor and control the position, force and velocity between the object and the hand. The wearer also can feel the prosthesis as specific afferent nerves are stimulated to give natural sensory feedback. By using efferent nerves as the control channels, the system will interpret the user's intention of grasp selection or grasping force. However, it is possible that this control method will cause discomfort to the users as it requires surgery, in comparison with the SEMG that is more flexible to perform. Also, the control algorithm of the device consisting of high and low level control would require more complex circuitry for the real time implementation.
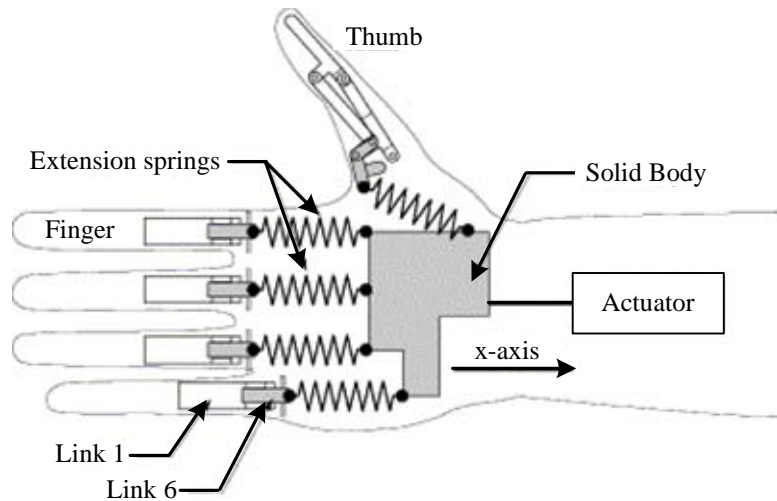
FIGURE 2.12: The TBMs' adaptive grasp system [Dechev et al., 2001]

2.4.3 The Toronto/Bloorview Macmillan Hand

A hand prosthesis has been specifically designed for children in the 7 - 11 years group age at the University of Toronto and the Bloorview MacMillan Centre. The Toronto/Bloorview Macmillan (TBM) hand [Dechev et al., 2001] is a five fingered (four fingers and a thumb) that used mechanical approach in performing the grasp. The adaptive grasp system used no sensors or electronics devices, instead springs are used. The hand is actuated using a single motor and the five digits are each connected to an extension spring. All the springs are connected to solid body which is connected to the actuator. To grasp an object, the digits will flex inwards independently and conform the shape of the object.

2.5 Control strategies for the externally powered prosthesis

The control algorithm has become one of the important criteria in the prosthetic hand design. The conventional control method used a mechanical tool to power and control the prosthesis. Nowadays, the natural control channels have become most popular in controlling the prosthesis.
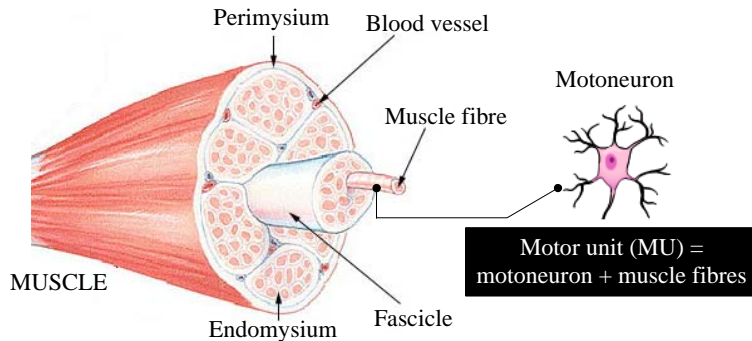
FIGURE 2.13: Structure of a skeletal muscle

2.5.1 Surface electromyographic control

The most widely used control channel is via surface electromyographic (SEMG) signal. An SEMG-based control system for prosthesis application will be described in detail in Chapter 3.

Electromyography (EMG) is used to evaluate and record the electrical activity of skeletal muscles during their contraction. As mentioned earlier in Chapter 1, it can be divided into two types. Needle EMG involves inserting a needle through the skin into a muscle and provides information about a single muscle fibre. Surface EMG involves placing electrodes on the skin overlying the muscle to detect the electrical activity and provide information about the overall muscle function. Surface EMG is the most common method of measurement because it can be conducted with minimal risk to the subject.

Muscle consists of many individual fibres which vary in length, shape and width. Bundles of fibres (fasciculi) are bound together by connective tissue covering. The whole muscles are formed by groups of fasciculi that are bound together. The combination of a single alpha motor neuron and all the muscle fibres it activates is called motor unit (MU) (Figure 2.13). The muscle fibres are located near its motor unit. However the MUs overlap other parts of a muscle. The number of fibres per MU and the MUs size varies depending on the muscle's function. For example; eyes are organized into smaller MU and have about 10 fibres per motor unit while the quadriceps muscles are organized into larger MUs with about 2000 fibres per motor unit.

The contraction of the muscle is controlled by central nervous system (CNS) and the concept is shown in Figure 2.14. The muscle fibres are activated by neurons whose cell bodies are located in the spinal cord. The nerve fibres of the neurons leave the spinal cord and distributed to the motor nerve which will cause the
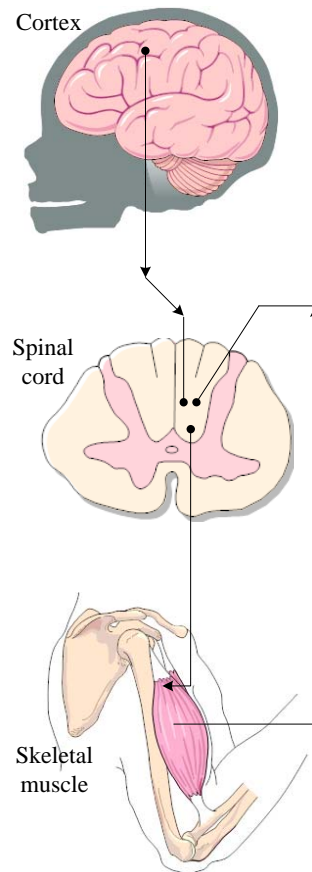
FIGURE 2.14: A schematic representation of basic motor control mechanisms and of the motor unit and its components

activation of muscle fibres. As the signal propagates along its surface and the the fibre twitches, a muscle fibre is depolarized. This depolarization generates an electrical activity at the area of the muscle fibres and is called muscle fibre action potential. The muscle fibre action potentials from all the muscle fibres of each motor unit are combined and produce a motor unit action potential (MUAP). The summation of the electrical activities created by each motor unit is called electromyography (EMG) signal (Figure 2.15).

The degree of tension during muscle contraction depends on two factors: recruitment and firing rate of the MUs. The recruitment of the MUs are depend on the size factor. Smaller MUs are recruited first during muscle contraction. Smaller MUs have fewer muscle fibres and low threshold to activate. Larger MUs are progressively recruited as the demand for tension increased. The smaller MUs are also slow units, compared to larger MUs that are composed of fast twitch fibres. The second factor is the firing rate. Different MUs have different rate where slower units have lower firing rate. The force of tension is increases with the increase of the firing rate.
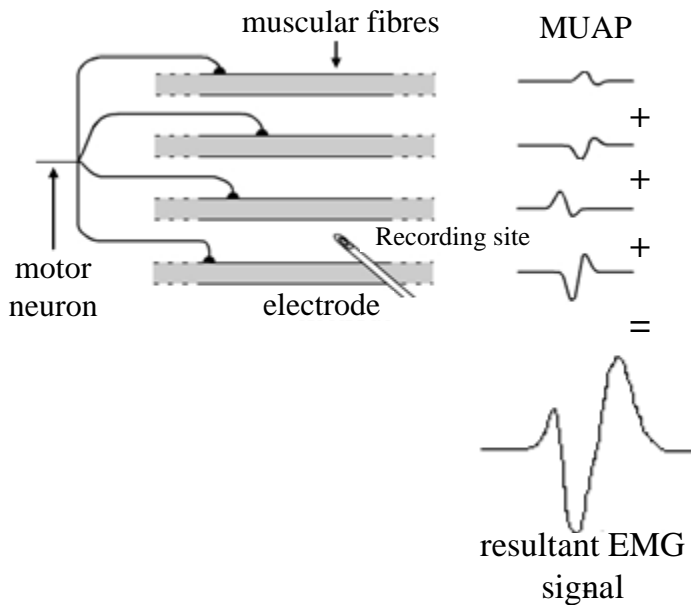
FIGURE 2.15: The resultant EMG signal are the summation of the MUAP, generated from four muscular fibres [Delsys, 2009]

SEMG signals can be detected using electrodes. The amplitude of the surface EMG signal varies from a μV to a low mV range (0.2mV) and can have a frequency content up to 2 kHz, and these properties are dependant on the intensity of a muscle activity. Normally, the signals will be amplified where a differential amplifier is typically used. The signals are often filtered, where the low and high frequencies, or other possible artifacts are eliminated to get a smoother signal. Then the EMG signals are processed and there are various methods have been used in analyzing them. One common method is to rectify and average the signal.

SEMG has been used widely in many applications. Generally, it has been used clinically in neurological and neuromuscular problems. It is also been used by clinicians in biofeedback and ergonomic assessments. EMG is also used in many research laboratories including biomechanics, motor control, movement disorder, gait analysis, exercise physiology and also to control powered upper limb prostheses.

2.5.2 Mechanomyography control

Mechanomyography (MMG) is an acoustic myography where it detects the sound of a muscle contracting. The MMG-based method is almost similar to the EMG-based method except that the MMG has lower frequency range where, typically it is bandpass filtered at 5 - 100Hz where EMG is filtered at 10 - 500Hz [Perry

et al., 2001]. Silva et al. [2004, 2003b,a] has investigated the use of muscle sounds or MMG to activate and control the prosthesis where a silicon-embedded MMG sensors are developed for the detection of the MMG signals. They were using root-mean square values based detection and root-mean square values based classification for the signal detection and classification. They also found that the control method used could provide adequate information for the detection and classification of muscle activity like SEMG based system. The drawback of this method is with a very low frequency range, it is prone to acquire noise signal during the acquisition process.

2.5.3 Nerve control

Another method of control is by using the nerve. Electrodes are implanted in the targeted efferent nerve that will send a signal to the brain. The afferent nerve will be stimulated and communicate with the artificial hand [Carrozza et al., 2003, 2002b, 2006]. However this method is difficult to implement as it involves the expert skills of a surgeon before it can be performed. Also, this method is more costly compared to the previous two methods mentioned above.

2.6 Summary

Current developments of prosthetic hands have been described in this chapter. From the comparison between the commercial and research devices, it can be seen that an integration of extra numerous features, whilst preserving the life like appearance, has been achieved in prototype form.

Chapter 3

Review of Electromyographic Control Systems

This chapter gives an overview of electromyographic control systems, with an emphasis on pattern recognition control. The various methods used in the different stages of the pattern recognition based control system are reviewed. The non-pattern recognition based control is also discussed.

3.1 Electromyographic Control

The concept of using EMG for prosthesis control started in the 1940s. Electromyographic control is when the signal is used as the input for the control of powered prostheses. The signal is used to select and modulate a function of a multifunction prosthesis [Roberto Merletti, 2004].

As described in Chapter 1, there are two types of EMG; needle and surface EMG. Hargrove et al. [2007] had carried out an investigation to compare the performance of these two types of EMG for prostheses control application. In the investigation, both signals were acquired simultaneously and processed using the same methods. They found that both EMG types gave high classification accuracies which is between 95% to 99%. Even though there is no difference between SEMG and needle EMG in terms of accuracy, SEMG is the most preferred method as it is non-invasive and more convenient to use.

Figure 3.1 shows the block diagram presenting the relationship between normal and electromyographic control system. For the amputees, the natural motor control
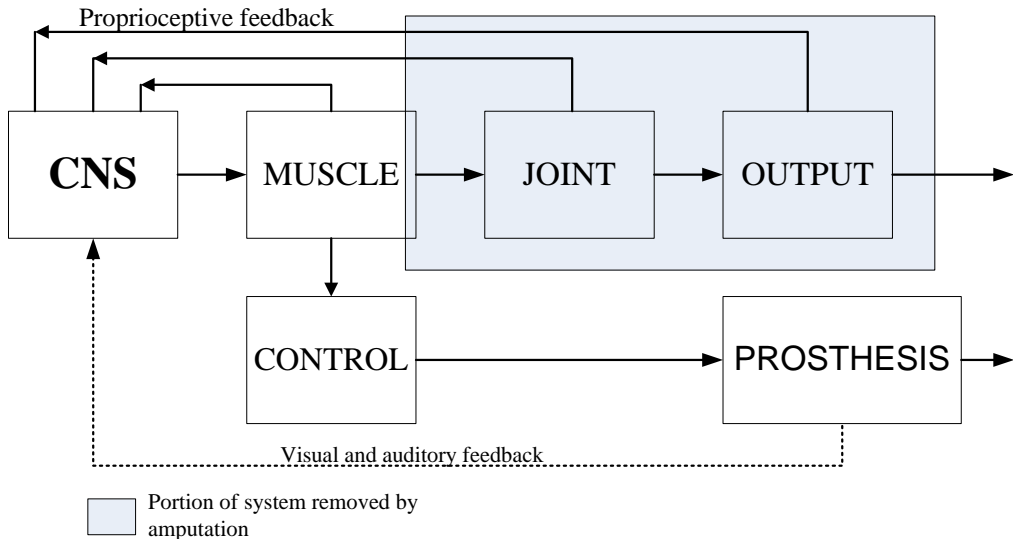
FIGURE 3.1: Block diagram presenting relationship between normal and myo-electric control system (shaded area is removed by amputation)[Parker et al., 2006]

system which consist of the joint and the output (the shaded area in the diagram) are replaced with the control mechanism and the prosthesis respectively. The SEMG signal generated from the remnant muscle is used as the control channel of the system.

Generally, electromyographic control can be divided into two; non-pattern recognition based and pattern recognition based. Non-pattern recognition based control is basically constructed using hierarchical control, threshold control, proportional control or finite state machines. Most of the commercial prosthetic hands use this method which is either amplitude or level coding of the EMG signal generated during an active control muscle of the user to control the prostheses. For example, the Otto Bock two-state system incorporated this technique to assign each prosthetic limb function to a separate control muscle [Scott & Parker, 1988; Parker et al., 2006; Roberto Merletti, 2004]. The operation of the system is shown in Figure 3.2a where each muscle is assigned with its threshold value (S1 for muscle 1 and S2 for muscle 2). When the muscle exceeds the cutoff threshold, it is activated and the associated function is selected. Only one function will be activated at one time and this is implemented using appropriate logic circuitry. Figure 3.2b shows another amplitude coding technique that is based on the different level of muscle contraction. A fixed threshold value is assigned to different level and each level is assigned to different function. The drawback of this method is the function per muscle is limited to two. In proportional control method, the strength of the muscle contraction controls the speed of the performed function and the Boston elbow
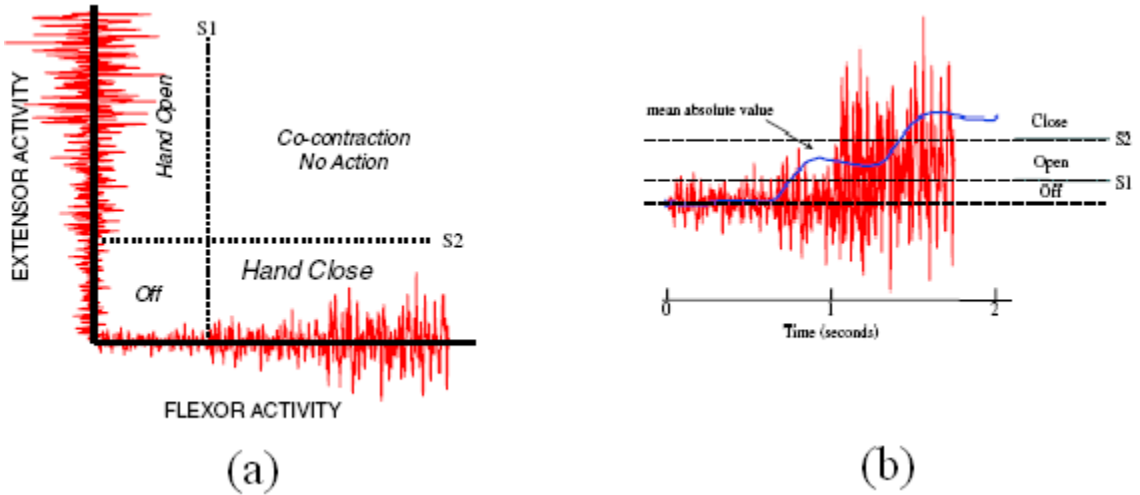
FIGURE 3.2: (a)Two channel amplitude coded ,(b)One channel amplitude coded myoelectric control[Parker et al., 2006]

used this type of control. The hierarchical control format has been described in Chapter 2. Carrozza et.al [Carozza et al., 2005] have used Finite State Machine (FSM) to control the opening and closing of the hand prosthesis. The grasping force during the closure is also controlled using FSM.

The state of the art of pattern recognition based control is described in the next section.

3.2   ECS based on pattern recognition

Even though the SEMG signals are stochastic, repeatable EMG patterns can be observed from different muscle contractions and this also can be seen in amputees, even though they may not have fully functioning muscles. SEMG also has been proven as an effective input for powered upper limb prostheses [Englehart & Hudgins, 2003; Hargrove et al., 2007].

Pattern recognition aims to classify data based on statistical information extracted from the patterns and determines the control signal that will select the final output of the device operation. Figure 3.3 shows the basic components in an ECS based on pattern recognition. Three main modules of ECS are: pre-processing,feature extraction and classification.

Control channels 1 and 2 labeled in Figure 3.3, are the SEMG signals. The SEMG data are acquired from the surface of the skin by placing electrodes over the person's muscle (Figure 3.4). Different muscles responsible on different movement.
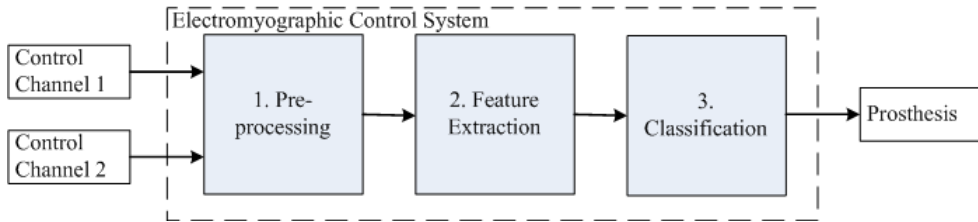
FIGURE 3.3: The block diagram of an electromyography control system (ECS) based on pattern recognition

Therefore, the electrode must be placed on the muscles that are to be investigated. For example, the extensor and flexor muscles are responsible for wrist flexion/extension movement. It is important to place the electrode on the accurate location as correct placement of the electrodes will give strong SEMG signals and gives a good distinction between movements. Inaccurate placement of the electrodes will affect the performance of the classifier [Hargrove et al., 2006, 2007]. Normally, the electrodes are accompanied by miniature pre-amplifiers. In common practise, the EMG signal will be amplified, usually using an instrumentation amplifier with a gain of 1000 - 5000 [Ajiboye & Weir, 2005; Karlik et al., 2003; Chu et al., 2006; Hudgins et al., 1993; Y. Al-Assaf, 2005]. The SEMG signals are then being filtered using bandpass filter (low cut-off frequencies,$f_{cl} = 450$ - 500Hz and high cut-off frequencies,$f_{ch} = 10$ - 20Hz) to eliminate noise before transferred to the ECS [Ajiboye & Weir, 2005; Karlik et al., 2003; Chu et al., 2006; Chen et al., 2006; Y. Al-Assaf, 2005]. The SEMG signal is then sampled digitally, where in common practice the sampling frequency is above 1000Hz [Ajiboye & Weir, 2005; Karlik et al., 2003; Chu et al., 2006; Hudgins et al., 1993; Chen et al., 2006; Y. Al-Assaf, 2005].

The ECS block diagram shown in Figure 3.3 is the basic implementation of the control system. Each module plays important role for the success of the system but they can be adjusted (merge or omit) depend on the implementation of the system. Another important factor to consider is the computation time for this control system. Scott et. al [Scott, 1984] has reported that 200 to 300 ms is a clinically recognized maximum delay for the response of the prosthesis. Therefore, the calculation of the control system that is within 300ms is generally adopted to avoid a longer delay [Chan et al., Sept. 2000; Chu et al., 2006; Chan & Englehart, 2005]
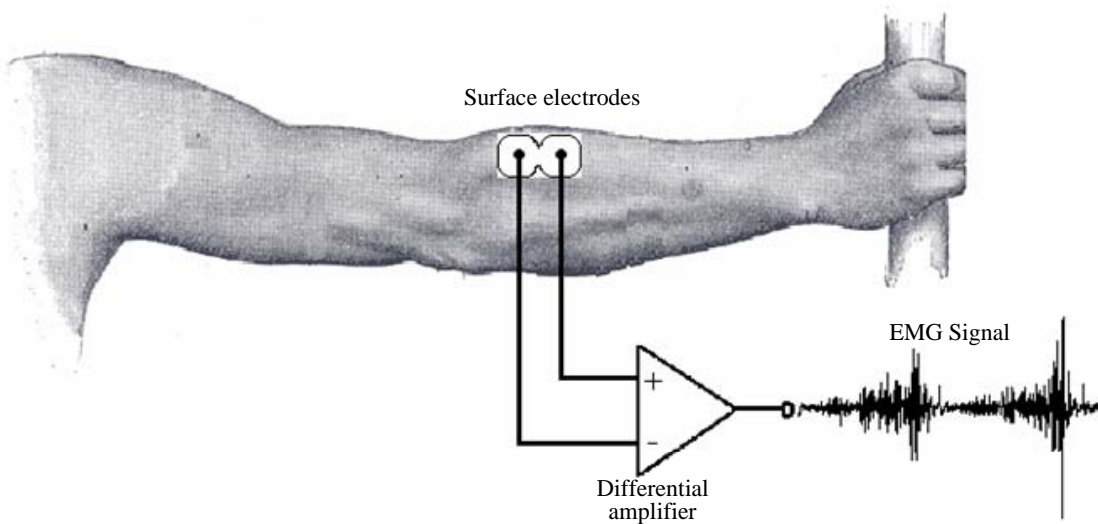
FIGURE 3.4: The acquisition of SEMG signal using surface electrodes [Delsys, 2009]

3.2.1 Pre-Processing

There have been various techniques in handling the EMG data before feature extraction. Usually, data segmentation will be used and could improve the accuracy and response time of the controller. For each divided segment, a feature set (section 3.2.2) will be computed which will be then fed to the classifier (section 3.2.3) and these processes are continuous. The data length and the windowing technique are two main points that need to be considered.

Englehart & Hudgins [2003] had investigated the effect of different length on the classification error. Figure 3.5 demonstrates that the classification error is related to the segment length, where the length is varied between 32ms and 256ms. The transient and steady state shown in the plot are the states in SEMG signal. A transient state is when a muscle goes from a relax to voluntary contraction level and steady state is where the contraction in a muscle is maintained. There will be also a trade off between the accuracy and response time. Farina & Merletti [2000] showed a segment length that is less than 128ms will leads to high bias and variance of features that will degrade the classifier's performance.

There are two main methods used for the data windowing; adjacent and overlapping. The adjacent windowing technique (Figure 3.6), is where adjacent disjoint segments with predefined length are used feature extraction and classification after a certain processing delay, τ. The τ depicted in Figures 3.6 and 3.7 is the time required to calculate the feature and classify the data. The drawback of this
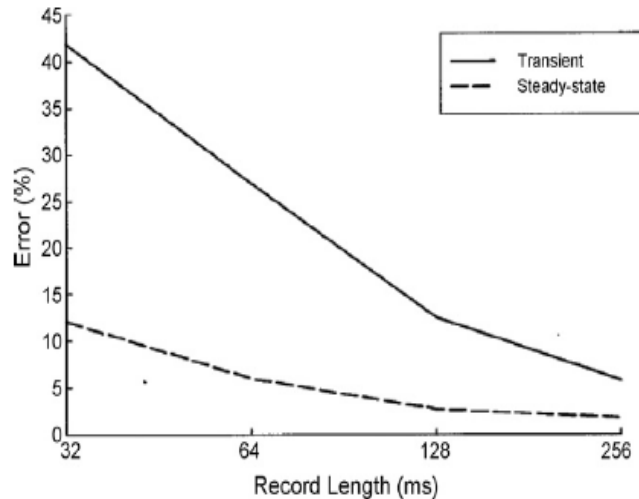
FIGURE 3.5: Classification error compared to segment length[Englehart et al., 2001]

technique, is that the τ is just a small portion of the segment that will cause the processor to stay at idle condition during the remaining time of the segment length. This matter is overcome with overlapped windowing technique (Figure 3.7). With this technique, the new segment slides over the current segment and the increment time is less than the segment length. For example, Hudgins et al. [1993] processed the signal in every 40 ms in a 240ms adjacent window. Yonghong et al. [2005] implemented the same technique with 32ms window increment. Englehart & Hudgins [2003] had reported that shorter segment increment produces a more dense but semi-redundant stream of class decision that could improve response time and accuracy. The overlapping windowing technique is the most common method due to the ability to preserve the important information in the EMG signals where there is limited time for signal processing then the non-overlapping technique is used.

3.2.2 Feature Extraction

The feature extraction process is where the raw SEMG signal is represented into a feature vector which is then used to separate the desired output, e.g. different hand grip postures. The success of the ECS based on pattern recognition depends on the selection and extraction of features [Asghari Oskoei & Hu, 2007]. The feature extraction techniques can be grouped into two main categories:
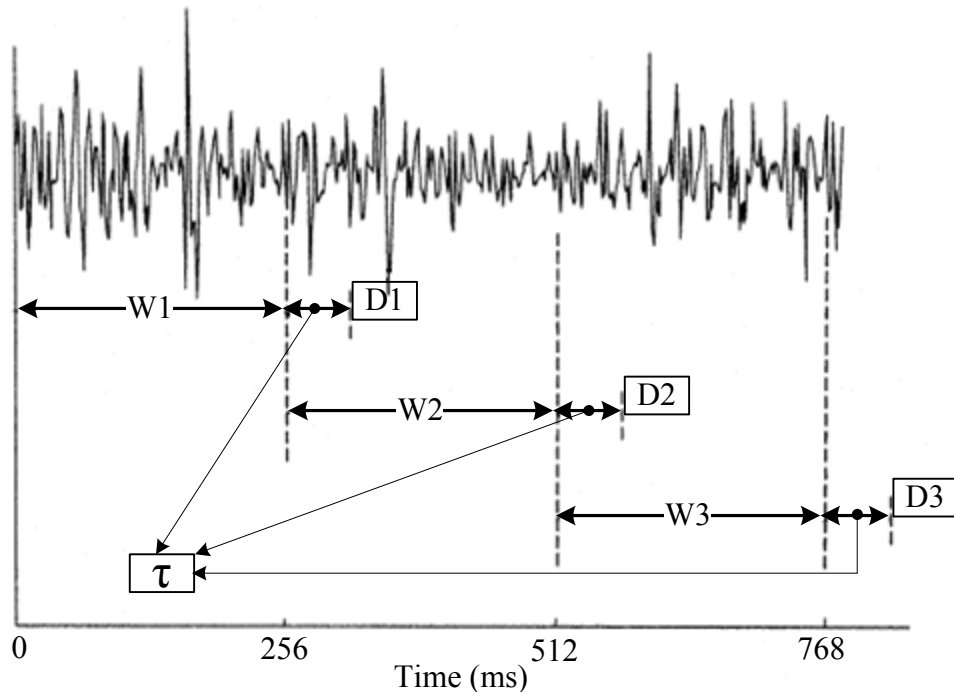
FIGURE 3.6: Adjacent windowing technique. W: Window, D:Delay,τ:time delay
[Englehart & Hudgins, 2003]

3.2.2.1 Time domain feature

The time domain (TD) feature is based on the signal amplitude and is the most common method used in ECS for upper limb prosthesis application as the computational complexity is low. The features can be obtained in a short time using a simple algorithm executed in a microprocessor. The amplitude gives an indication of either activation level, duration or force of the SEMG signal which is influenced by the following factors: the location of the electrodes, the tissues' thickness, the system used to acquire the signal and the distribution of motor units in muscle fibre [Asghari Oskoei & Hu, 2007].

Various methods have been reported for feature extraction of the SEMG. Hudgins et. al. [Hudgins et al., 1993] used mean absolute value (MAV), mean absolute value slope, slope sign changes (SSC), waveform lengths and zero crossings (ZC). Chan et. al [Chan et al., Sept. 2000] also used the same features as them except SSC. Other reported features are variance, root mean square (RMS), mean and standard deviation (SD) [Ajiboye & Weir, 2005; Yonghong et al., 2005]

Autoregressive (AR) models also have been used for the EMG classification [Graupe et al., 1982; Zardoshti-Kermani et al., 1995; Karlik et al., 2003]. With AR, the value at the current point of a time series of an EMG signal can be predicted
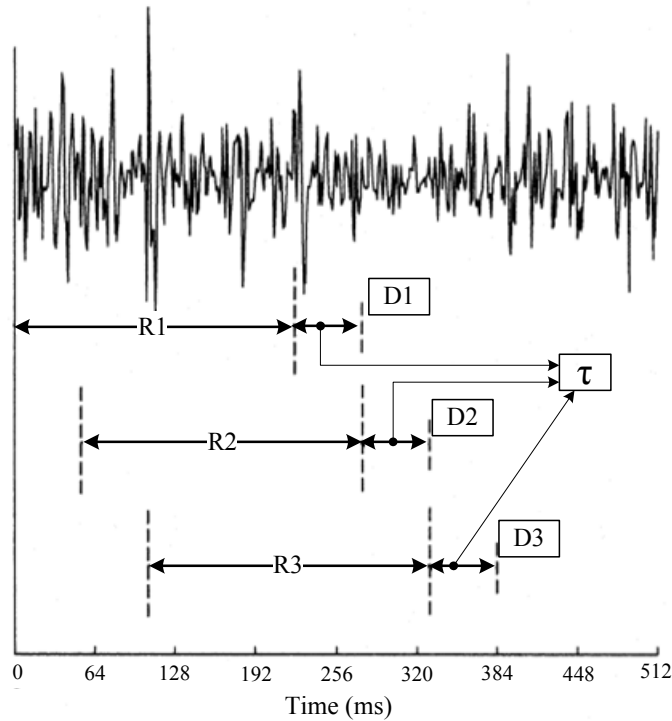
FIGURE 3.7: Overlapped windowing technique. R: Window, D:Delay,τ:time delay[Englehart & Hudgins, 2003]

by several previous points. This method can produce high separability between different limb functions, however it requires a more complicated computation process.

3.2.2.2 Time-frequency domain feature

The time-frequency domain (TFD) method is to overcome the limitation of the TD method, which is acceptable for a stationary signal. However, the EMG signal is a non-stationary signal which show a high frequency characteristics and with TFD, the performance of the control system could be increased.

Some of the methods used in TFD are short time Fourier transform (STFT), wavelet transform (WT) and wavelet packet transform (WPT). In general, the difference between these methods are the partitioning of the time-scale axis (Figure 3.8). In short-time Fourier transform (STFT), the EMG signal is mapped into frequency components that present within an interval of time (window). A suitable window size must be determined prior to this as small window will give good time resolution but poor frequency resolution and vice versa. The partitioning ratio of the STFT is fixed: once specified, each cell has an identical aspect ratio. To overcome the resolution problem in STFT, WT was developed [Polikar, 2007].

The WT has a variable partitioning ratio where the aspect ratio of the cells varies such that frequency resolution is proportional to centre frequency. WPT is the generalization of the WT method allows the best adapted analysis of the signal. WPT provides as adaptive partitioning - complete set of partitions are provided as alternatives, and the best for a given application is selected [Englehart et al., 2001].
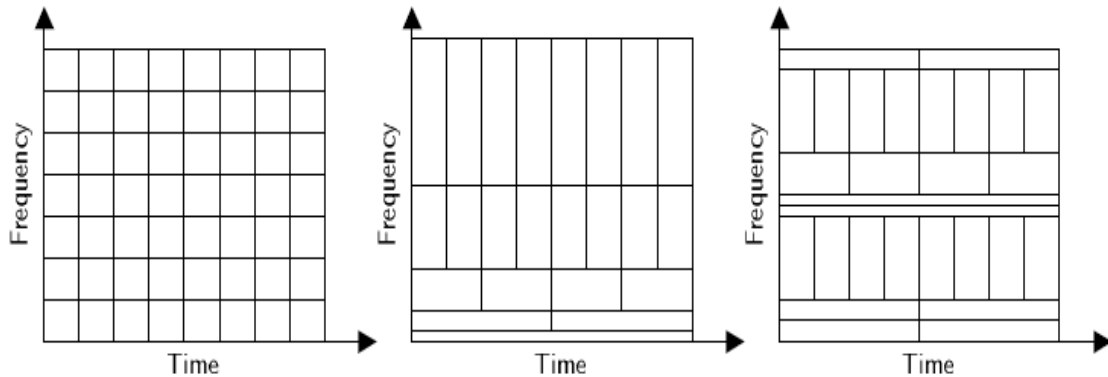
FIGURE 3.8: Time frequency domain method. From left to right: STFT,WT,WPT [Englehart et al., 1999a].

Englehart et al. [2001, 2000] has conducted a comparison between TD features used by Hudgins Hudgins et al. [1993] and TFD methods. Based on the results of the classification error, WPT was the most effective method. However, he also suggested that there is no clearly superior method between them [Englehart et al., 2001]. Chai et al. [1999] had used WT to discriminate between four motions: hand grasp,hand extension, forearm supination and forearm pronation. Their system has an average accuracy 90% by extracting twelve parameters from two channel EMG signals and with the nature of the WT method, the system might have a high computational time.

TFD method may cause high resolution representations and AR model yields high dimensional feature vectors. However, these factors cause long processing time and delays. To avoid these problems, dimensionality reduction was introduced which reduce the dimensionality of the data while maintaining its discrimination capability. This technique also helps to reduce memory requirement, as well as the classifiers' speed [Chu et al., 2006]. In general, there are two methods of dimensionality reduction; feature selection and feature projection. There are many strategies for feature selection, such as sequential forward selection, sequential backward selection, simulated annealing and genetic algorithm [Asghari Oskoei & Hu, 2007; Wang et al., 2006; Asghari Oskoei & Hu, 2006]. Feature projection is mostly used when using the TFD method. WT produces many coefficients to

represent time scale features and they need to be mapped into a lower dimension. Principal component analysis (PCA) and linear discriminant analysis (LDA) are the most commonly used method for feature projection [Chu et al., 2006; Englehart et al., 2001, 1999b].

3.2.3   Classifier

The information obtained during feature extraction will be then fed into a classifier. A classifier should be able to map different patterns and match them appropriately. An efficient classifier should be able to classify patterns in a short duration to meet the real-time constraint of prosthetics device. However, due to the nature of EMG signal it is possible to see a large variation in the value of the feature used. This variation may be due to the electrode placement or sweat.

In early EMG control systems, statistical classifiers had been used widely until about the mid-1980s [Roberto Merletti, 2004]. A statistical classifier also known as linear discriminant analysis (LDA) searches for feature vectors which best discriminate amongst motion classes as opposed to those which best describe the data [Martinez & Kak, 2001]. The LDA classifier is simpler to implement and has shown high classification accuracies [Asghari Oskoei & Hu, 2007; Farrell, 2005]

Then, the application of artificial neural network (ANN) began to appear. ANN has been used in most of the EMG classification systems reported in the literature [Hudgins et al., 1993, 1994; Englehart et al., 1995c,b, 1998, 1999b, 2000, 2001; Englehart & Hudgins, 2003; Ajiboye & Weir, 2005; Zhao et al., 2006a; Jingdong et al., 2006]. An ANN consists of many simple processing units (neurons) that can be globally programmed for computation. They are trainable and the main advantage of the ANN is its ability to represent both linear and nonlinear relationships. Figure 3.9 shows one example of ECS that using ANN. A variety of ANN architecture and learning algorithm have been conducted; such as simple feedforward multilayer perceptrons [Hudgins et al., 1994, 1993; Del Boca & Park, 1994], dynamic networks [Englehart et al., 1995a] and self organizing feature maps [Christodoulou & Pattichis, 1995].

Another technique that has been used for the classification of the SEMG data is fuzzy logic (FL) system. The most useful property of fuzzy logic is that it provides a simple way to arrive at a definite conclusion just based upon imprecise input information which mimics how a person would make a decision. Due to
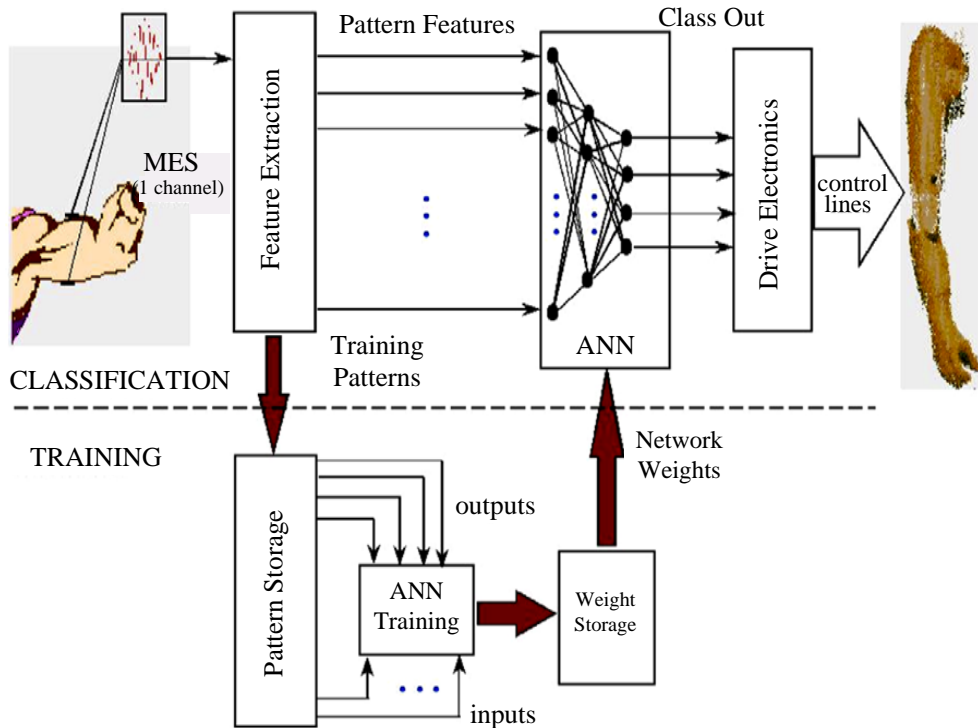
FIGURE 3.9: Electromyographic control system using ANN as the classifier
[Parker et al., 2006]

the biomedical signal characteristics, which is not always repeatable, FL is an advantageous control technique in biomedical signal processing and classification.

Basically, FL system consists of three stages: input, processing and output stages. Figure 3.10 shows the general block diagram of FL system. At the input stage, also known as fuzzification module, the signal features used will be converted into grade or signals (for example OFF. LOW, MED and HIGH in Figure 3.11) that is called membership function (MF) and truth values. At the processing stage which is also called the inference rule base stage, all the information will be processed based on the rules generated in IF-THEN form. The appropriate rule will be invoked at this stage, generates result for each rule which are then combines the results of the rules. The output stage which also has its own membership function will then convert the combined results obtained at the previous stage into one final output value. This procedure is called defuzzification.

Weir & Ajiboye [2003]; Ajiboye & Weir [2005] used a heuristic fuzzy logic approach to multiple EMG pattern recognition for multiple prosthesis control. Chan et al. [Sept. 2000] also used FL to classify single channel EMG signal for multifunctional prosthesis control. Some FL systems used in conjunction with a neural network to classify the EMG data. Karlik et al. [2003]; Del Boca & Park [1994] have reported the used of this method, where the EMG features are clustered using fuzzy c-means
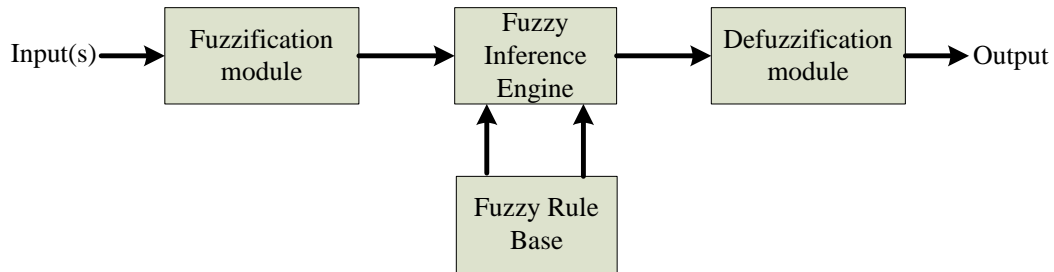
FIGURE 3.10: General block diagram of a fuzzy logic system

algorithm which is then presented to ANN system. All the FL systems reported high classification accuracies which is about 95%.
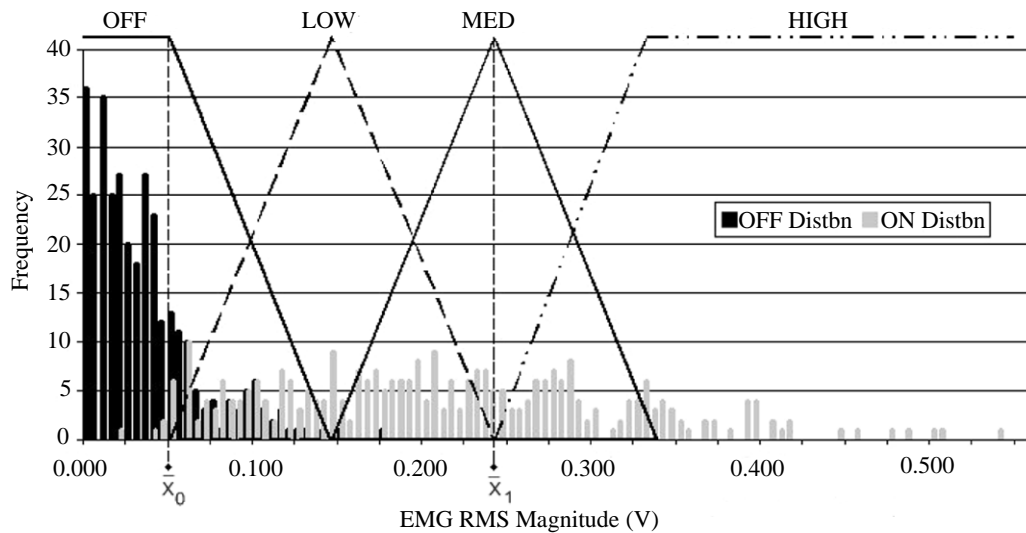
FIGURE 3.11: EMG histogram used in the construction of the input membership function for the FL system [Ajiboye & Weir, 2005]

3.2.4   The Control System

Table 3.1 summarizes some of the methods used for feature extraction and classification processes for the ECS based on pattern recognition for upper-limb prosthesis control. It can be seen that the methods used for the feature extraction varies between TD and TFD method, and it has been reported that there is no superior method between these two processing techniques. As for the classifier, ANN is the most used method to discriminate the final output of the system.

The most right column of the table shows the accuracy of the electromyographic control systems and the success of the system depends upon the classification accuracy. It measures the number of correct classification achieved for a number of trials. From the table, it shows that all accuracies are between 90% to 98%.

TABLE 3.1: Summary of ECS based on pattern recognition for upper limb prosthesis

Reference	Feature	Classifier	Accuracy
Englehart et al. [2001, 1999b]	STFT,WT,WPT	PCA/LDA	98%
Chu et al. [2006]	WPT	SOFM, PCA	97%
Karlik et al. [2003]	AR	FC-ANN	96.1%
Chan et al. [Sept. 2000]	MAV,ZC,waveform length	FL	95%
Zhao et al. [2006a]; Jingdong et al. [2006]	SampEn,WT, integrated EMG	ANN	95%
Yonghong et al. [2005]	AR, RMS	GMM	95%
Y. Al-Assaf [2005]	MAV,WT,PCA	ANN	94.9%
Weir & Ajiboye [2003]; Ajiboye & Weir [2005]	mean,SD	FL	94%
Englehart et al. [1999a]	STFT,WT,WPT	MLP-ANN/LDA	93.7%
Hudgins et al. [1993]	MAV, ZC, SSC, waveform length	ANN	90%

However, the percentage obtained by each study is subjective. It is depends upon the number of control channels used and the number of final movements that want to be achieved. For example, Englehart et al. [2001, 1999b] investigated four channel SEMG signal in classifying four types of upper limb motion by using the TFD method. With a single EMG channel used to control one limb motion it is expected to have a high classification accuracy. In comparison with Hudgins et al. [1993] that used two SEMG channel in discriminating four types of upper limb motion, a lower classification rate was obtained. However, even though Ajiboye & Weir [2005] also used four SEMG channels in their study but they have a lower classification accuracy compared to the work of Englehart et al. [2001, 1999b]. This is possibly due to the feature used to extract the information from the SEMG signal that might be not accurate enough in giving the best information.

Based on the information shown in Table 3.1, the misclassification of the system can be determined. For example, for an ECS with 98% accuracy, it tells that in one hundred trials, there are two times that the system misclassifies the data (classification error, 2%) and gives an inaccurate output. Figure 3.12 shows projection on numbers of the misclassification occur on certain number of trials.
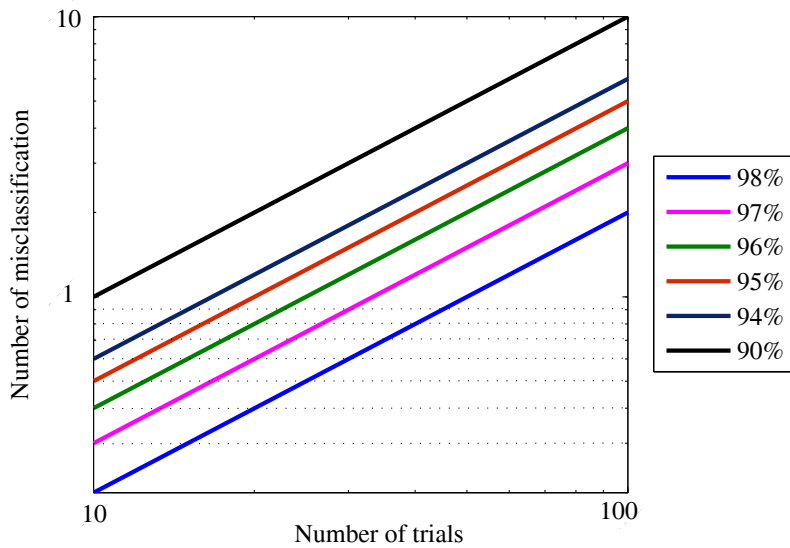
FIGURE 3.12: The misclassification error projection for numbers of trial based on the data in Table 3.1.

3.3 Summary

A SEMG control based system in controlling upper limb prosthesis has been reviewed. Two types of control system were discussed which are non-pattern recognition and pattern recognition based. The review emphasized on the pattern recognition based control system where various methods used in the application are discussed. Continuous research in this field is still needed in order to provide a control system with a high classification rate. From the summary in Table 3.1, it can be concluded that there are various factor that effect the performance of the electromyogaphic control system. This includes the number of control channel used and also methods used in the feature extraction process. A reasonable number of control channel with good feature extraction method will give a high classification accuracy of the control system.

Chapter 4

Moving Approximate Entropy

The chapter describes the theoretical basis of the approximate entropy and also the motivation behind the chosen method. A brief explanation on entropy is given. An explanation on another entropy, sample entropy is described which is then being compared with approximate entropy.

4.1   Entropy

Entropy is a word to describe the amount of a 'disorder' of a system. It was introduced by Claude E. Shannon [Shannon, 1948] and is defined as a measure of the average information content associated with a random outcome. An understanding of information entropy relates to the amount of uncertainty about an event associated with a given probability distribution. Basically, the entropy measure is continuous where if all the outcomes are equally likely, then entropy should be maximal and if the outcome is certainty, then the entropy is zero.

There are different kinds of measures of entropy and they depend upon the application. Some of the entropies are Shannon entropy, Kolmogorov entropy, Kolmogorov-Sinai entropy, maximum entropy and differential entropy [Schug et al., 2005; van Drongelen et al., 2003; Samanta et al., 2004; Simpson, 1994; Gautama et al., 2003]. All these entropies have been used for biomedical signal analysis. It has been reported that ApEn is useful for pattern recognition application [Pincus et al., 1996b]. This makes ApEn as the most suitable technique for this research where in ECS; it uses the pattern information extracted from the SEMG signals in determining the final hand motion.

4.2 Approximate Entropy

Approximate entropy (ApEn) was first introduced by Pincus [Pincus, 1991] in 1991. It is a technique that can be used to quantify the irregularity of a signal when applied to a short and noisy time series of data.

It has been reported that ApEn is particularly useful in nonlinear dynamic signals (e.g. biosignals) and is applicable to noisy and short data length (between 100 and 5000 data points) [Pincus & Goldberger, 1994]. For example, Pincus used ApEn to evaluate the heartbeat of infants to determine whether they were healthy or sick [Pincus, 1991]. The evaluation showed that the sick infants had lower ApEn compared to healthy infants. ApEn has been used mainly to analyze heart rate variability [Pincus et al., 1993; Pincus & Viscarello, 1992; Pincus et al., 1991; Kalon et al., 1997], endocrine hormone [Pincus et al., 1996b,a] and electroencephalogram (EEG) signals [Ferenets et al., 2006]. Pincus et al. [1996b] has applied ApEn to a finite (150) data length in investigating the pattern of two hormones to study the aging process between young and old people.

There has been little research using ApEn on SEMG signals and the technique has not been investigated for use with the control of a prosthesis. ApEn has confirmed that the SEMG signal is a nonlinear deterministic signal and not just a random signal [Meng et al., 2005, 2001]. Chen et al. [2006] have improvised the standard ApEn algorithm and developed an improved ApEn algorithm to study the supination and pronation of the forearm in thirty subjects. In their improvised ApEn algorithm, the SEMG data was divided into clusters and the formed vector sequence for the ApEn calculation were normalized. By normalizing the SEMG data, they add additional process to the signal processing and this might increase the processing time of the whole system.

4.2.1 The ApEn algorithm

Two input parameters are required, prior to the calculation of ApEn and they are:(1) m, a positive integer as the embedding dimension of the vector to be formed and (2) r, a filter factor. First, the m-vectors $X(1), X(2), ..., X(N-m+1)$ are formed, which can be defined by:

$$X(i) = [x(i), x(i+1), ..., x(i+m-1)]; i = 1, N-m+1 \qquad (4.1)$$

Then, the distance between $X(i)$ and $X(j)$ are defined as:

$$d[X(i), X(j)] = \max_{k=0,m-1} [|x(i+k) - x(j+k)|] \tag{4.2}$$

For each $i = 1, (N - m + 1)$, the $C_i^m(i)$ are calculated where:

$$C_r^m(i) = \frac{\text{number of } d[X(i), X(j)] \leq r}{N - m + 1} \tag{4.3}$$

Then the quantity of $\phi^m(r)$ is calculated as:

$$\phi^m(r) = \frac{1}{N - m + 1} \sum_{i=1}^{N-m+1} lnC_r^m(i) \tag{4.4}$$

The above process is repeated for $m+1$ and the ApEn is finally obtained as follow:

$$ApEn(m, r, N) = \phi^m(r) - \phi^{m+1}(r) \tag{4.5}$$

The result from ApEn calculations is a positive real number, where a smaller value shows high regularity while a large value shows low regularity in the data [Pincus & Singer, 1996; Pincus, 1991]. For example, a series of the same numbers will return $ApEn = 0$ and a continuous sine waveform will return a lower ApEn compared to series of random numbers.

The flowchart shown in Figure 4.1 shows the step by step procedure of the ApEn calculation. To give a clear understanding of the calculation, an example is given and shown in Appendix A.

It has been tested on different data sets such as random and regular numbers. Table 4.1 shows the results of the ApEn calculation for different data sets. For each calculation, the data length is set to 200 data points, the same data length used in this work.

TABLE 4.1: The results of ApEn calculation for various sets of numbers

Numbers	ApEn
Constant numbers (1)	0
Regular numbers 1 $(1, 2, 3, ..., 200)$	0.0049
Regular numbers 2 (triangular waveform)	$6.48 X 10^{-5}$
Random numbers 1 (between 0 and 1)	0.9581
Random numbers 2 (between 10 and 500)	0.9342

```
                      ( Start )
                         │
                         ▼
  ┌────────────────────────────────────────────┐
  │ Input data: X(1), X(2),….., X(N)            │
  │                                              │
  │ Initialization:                              │
  │ - Given threshold, r                         │
  │                                              │
  │ - Initial dimension, m₀                      │
  │                                              │
  │ - Nᵐ(i) = Nᵐ⁺¹ (i) = 0 for all i            │
  └────────────────────────────────────────────┘
                         │
                         ▼
  ┌────────────────────────────────────────────┐
  │ From the N*N binary distance matrix s:      │
  │  i.   Find d(i,j) = |X(i)-X(j)|, i = 1,N, j>I│
  │  ii.  s(i,j) = 0 if d(i,j) > r;s(i,j) = 1 if d(i,j) < r │
  │  iii. s(i,j) = s(j,i); s(i,i ) = 1, i = 1, N │
  └────────────────────────────────────────────┘
                         │
                         ▼
                   [ m = m₀ ]
                         │
                         ▼
                    [ i = 1 ]
                         │
                         ▼
                    [ j = 1 ]
                         │
                         ▼
  ┌────────────────────────────────────────────┐
  │ Cᵣᵐ(i, j) = s(i, j) ∩ s(i+1, j+1) ∩ …. ∩ s(i+m−1, j+m−1) │
  │ if Cᵣᵐ(i, j) = 1, then Nᵐ(i) = Nᵐ(i) + 1    │
  │ Cᵣᵐ⁺¹(i, j) = Cᵣᵐ(i, j) ∩ s(i+m, j+m)      │
  │ if Cᵣᵐ⁺¹(i, j) = 1, then Nᵐ⁺¹(i) + 1        │
  └────────────────────────────────────────────┘
                         │
                         ▼
                  [ j = j + 1 ]
                         │
                         ▼
              < j > N-m+1 >  ── No ──┘ (loop back to j=1)
                         │ Yes
                         ▼
  ┌────────────────────────────────────────────┐
  │ Cᵣᵐ(i) = Nᵐ(i) / (N−m+1)                    │
  │ Cᵣᵐ⁺¹(i) = Nᵐ⁺¹(i) / (N−m)                  │
  └────────────────────────────────────────────┘
                         │
                         ▼
                  [ i = i + 1 ]
                         │
                         ▼
              < i > N-m+1 >  ── No ──┘ (loop back to i=1)
                         │ Yes
                         ▼
  ┌────────────────────────────────────────────┐
  │ φᵐ(r) = (1/(N−m+1)) Σ ln Cᵣᵐ(i)             │
  │ φᵐ⁺¹(r) = (1/(N−m)) Σ ln Cᵣᵐ⁺¹(i)           │
  └────────────────────────────────────────────┘
                         │
                         ▼
            [ ApEn(m,r) = φᵐ(r) − φᵐ⁺¹(r) ]
                         │
                         ▼
                      ( End )
```

The relevant equations from the flowchart:

$$C_r^m(i, j) = s(i, j) \cap s(i+1, j+1) \cap \dots \cap s(i+m-1, j+m-1)$$
$$\text{if } C_r^m(i, j) = 1, \text{ then } N^m(i) = N^m(i) + 1$$
$$C_r^{m+1}(i, j) = C_r^m(i, j) \cap s(i+m, j+m)$$
$$\text{if } C_r^{m+1}(i, j) = 1, \text{ then } N^{m+1}(i) + 1$$

$$C_r^m(i) = N^m(i) / (N-m+1)$$
$$C_r^{m+1}(i) = N^{m+1}(i) / (N-m)$$

$$\phi^m(r) = \frac{1}{N-m+1} \sum_{i=1}^{N-m+1} \ln C_r^m(i)$$
$$\phi^{m+1}(r) = \frac{1}{N-m} \sum_{i=1}^{N-m} \ln C_r^{m+1}(i)$$

$$\text{ApEn}(m,r) = \phi^m(r) - \phi^{m+1}(r)$$

FIGURE 4.1: The flowchart of the calculation of ApEn
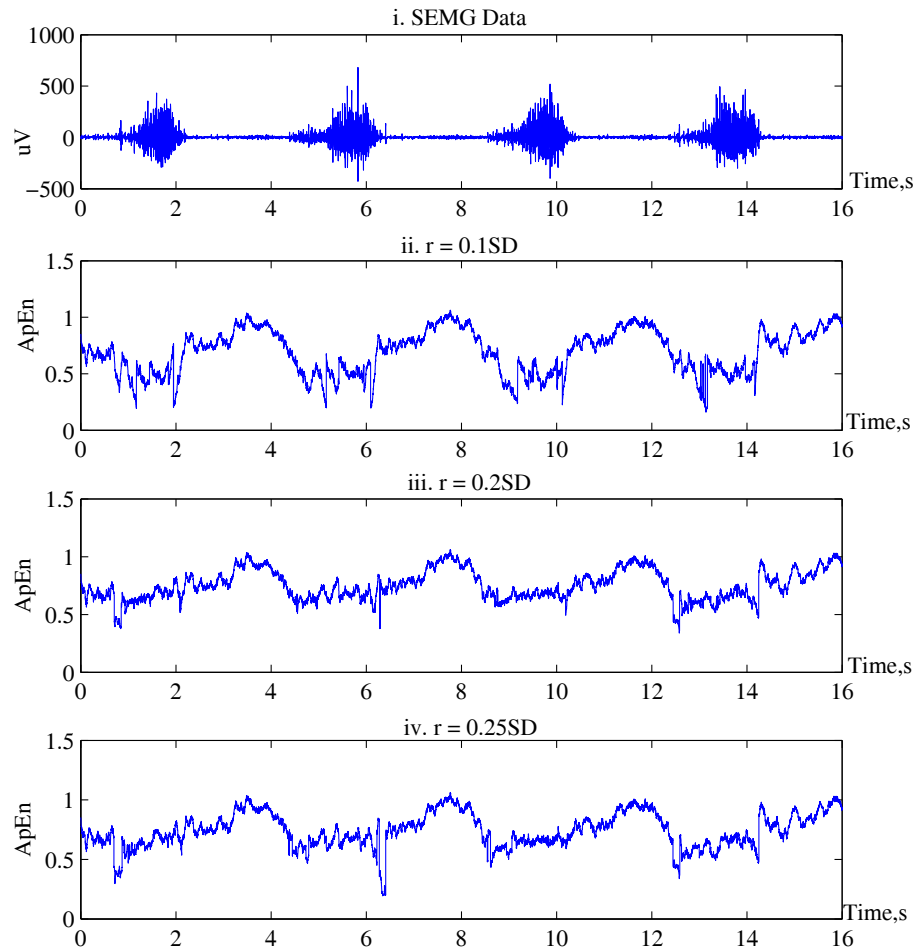
FIGURE 4.2: The ApEn evaluation during wrist extension for $m = 2$ and different r; (ii)$r = 0.1SD$, (iii)$r = 0.2SD$ and (iv)$r = 0.25SD$

In this research, the appropriate values for the embedding dimension, m and the filter factor, r are chosen. The ApEn algorithm was tested on the raw SEMG data for a range of m values (1 to 3) and r values (0.1, 0.2 and 0.25 of the standard deviation of the data) with 200 points data length. The SEMG data was acquired from one healthy subject during wrist flexion and extension. Figure 4.2 shows the result of the ApEn evaluation on the signal obtained during wrist extension with m fixed to 2 and r varies from 0.1 to 0.25 of the SD of the data. Appendix B shows the evaluation results for $m = 1$ and $m = 3$ at different r values.

Careful selection of the r value must be considered as a larger r will cause loss of useful information in the signal and a smaller r will cause unstable probability estimation due to the conditioning part in equation 4.3. As for the m value, lower m will give higher ApEn values which shows more irregularity in the data and higher m will cause lower ApEn values. Also, a value of m = 1 means that a data

is compared with itself and therefore is of no practical use. Table 4.2 shows the statistical analysis of the ApEn evaluation carried out. From the evaluation, it had been observed that $m = 2$ and $r = 0.25SD$ are the suitable parameters for the SEMG data. They were consistent with the parameters suggested by Pincus [Pincus, 1991]. The evaluation was also carried out on the rectified SEMG data and the signal appeared to have little effect in the ApEn values, so the raw signals are used. The algorithm was implemented using MATLAB 7.0.

TABLE 4.2: Statistical analysis of the ApEn evaluation on different m $(1, 2$ and $3)$ and $r(0.1, 0.2$ and 0.25 of the SD)

		average	min	max	SD
	0.10SD	1.491	0.839	1.816	0.204
m = 1	0.20SD	1.254	0.529	1.617	0.217
	0.25SD	1.113	0.270	1.552	0.232
	0.10SD	0.526	0.160	0.981	0.138
m = 2	0.20SD	0.662	0.339	0.981	0.080
	0.25SD	0.638	0.195	0.981	0.102
	0.10SD	0.222	0.005	0.736	0.147
m = 3	0.20SD	0.441	0.144	0.736	0.080
	0.25SD	0.475	0.172	0.736	0.076

Further information about ApEn can be found in the previous research [Pincus, 1991; Pincus et al., 1993; Pincus & Viscarello, 1992; Pincus et al., 1991].

4.3   Moving approximate entropy

SEMG signals consist of a long data series of data and based on the literature discussed in Chapter 3, section 3.2.1 which discusses the pre-processing of the signals in ECS, it is important to determine the right approach at this stage because it will affect how much information can be extracted from the SEMG signal, as well as the computation time. The overlapping windowing technique in pre-processing the data has became the most widely used method as it preserves the information in the signal. It has been reported that ApEn works accurately in a short finite data series. Since the SEMG data is long data series, in normal practice they are divided into shorter segments. Also, to preserve the information in it, the overlapping windowing technique as mentioned above is used when being analyzed.

Moving approximate entropy was developed where ApEn is calculated repeatedly when a moving window is applied to the SEMG data. A literature search showed that this technique has not been used for signal analysis in any application. Figure 4.3 shows the arrangement where each window is set to a fix data samples and they are overlap with a delay one between the first and the next window. The number of the data samples, N of the window depends upon the sampling rate of the acquisition of the SEMG signal.
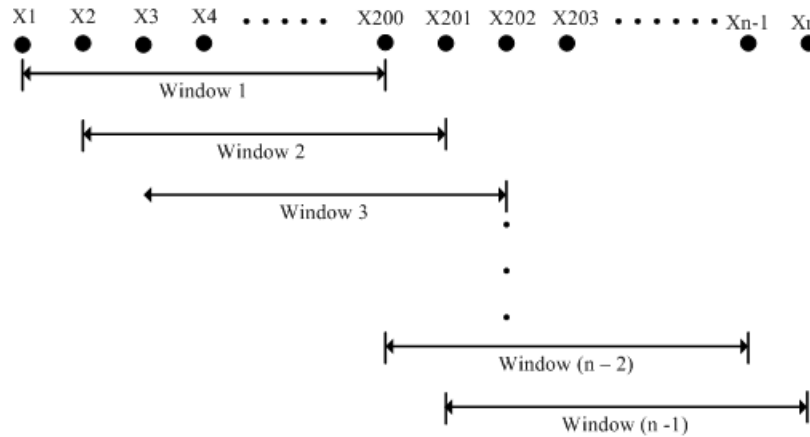
FIGURE 4.3: Adjacent overlapping window with delay 1

4.4 Recurrence Plot

Recurrence plots (RP) were first introduced by Eckmann et al. [1987]. This method is used to detect recurrence patterns and non-stationary sequence in dynamic system. Fundamentally, it is a graphical representation of the distances matrix $D_{I,J}$, with dark pixels located at coordinates (I, J) correspond to a distance value between I and J vectors which are lower than a predetermined cut-off (or radius) [Belaire-Franch et al., 2002]. The plot is symmetric ($D_{I,J} = D_{J,I}$), and the main diagonal is always darkened ($D_{I,J} = 0$, I=J). The mathematical expression for the RP can be written as:

$$R_{(i,j)} = \Theta(\varepsilon_i - \|x_i - x_j\|), x_i \in \Re^m, i,j = 1 \ldots N \tag{4.6}$$

Where N is the number of data values, x_i ; ε_i is a threshold distance; $\| \cdot \|$ is a norm and is the Heaviside function [Marwan, 2003]. Prior to determining a plot, the following parameters must be chosen: (1) the embedding dimension, m, (2) the time delay,τ and (3) the threshold, ε.

Recurrence quantification analysis (RQA), proposed by Webber and Zbilut [Webber & Zbilut, 1994] is used to quantify complex structures. Based on measures in RQA, RP have become very popular and have been applied to various experimental data [Thiel et al., 2004]. The advantage of RP is that their structure instantly shows whether a system is periodic or chaotic. The structural changes in data or similarities in pattern across a time series can be seen from the plots. Figure 4.4 shows some examples of the RP patterns for different time series. All the RP analysis on the EMG waveforms were carried out using the recurrence plots toolbox developed by Marwan [Marwan, 2003] and was run in MATLAB 7.0.

4.5 Comparison with sample entropy

Although ApEn is widely used, it has been reported that it is inherently biased because self matches are counted to avoid the occurrence of natural logarithm of zero in the calculation [Richman & Moorman, 2000; Lake et al., 2002; Chen et al., 2005]. Sample entropy (SampEn) was introduced by Richman and Moorman [Richman & Moorman, 2000] to overcome this limitation. Both methods, ApEn and SampEn have similar algorithm and are easily implemented. There is only one small difference between these two entropies.

Like ApEn, SampEn requires two parameters prior to the calculation which are: the embedding dimension, m and the filter factor, r. From a time series of $X(1), X(2), ..., X(N - m + 1)$, SampEn is defined by forming m-vectors:

$$X(i) = [x(i), x(i+1), ..., x(i+m-1)]; i = 1, N - m + 1 \qquad (4.7)$$

Then, the distance between $X(i)$ and $X(j)$ are defined as:

$$d[X(i), X(j)] = \max_{k=0, m-1} [|x(i+k) - x(j+k)|]; i \neq j \qquad (4.8)$$

and this is where SampEn is different from ApEn (refer Equation 4.2) where in ApEn, $i = j$ is included in the calculation but not in SampEn.

Let $N^m(i)$ be the number of vectors $X_m(j)$ within r of $X_m(i)$, define the function:

$$B_r^m(i) = \frac{N^m(i)}{N - m - 1}, B^m(r) = \frac{1}{(N - m)} \sum_{i=1}^{N-m} B_r^m(i) \qquad (4.9)$$
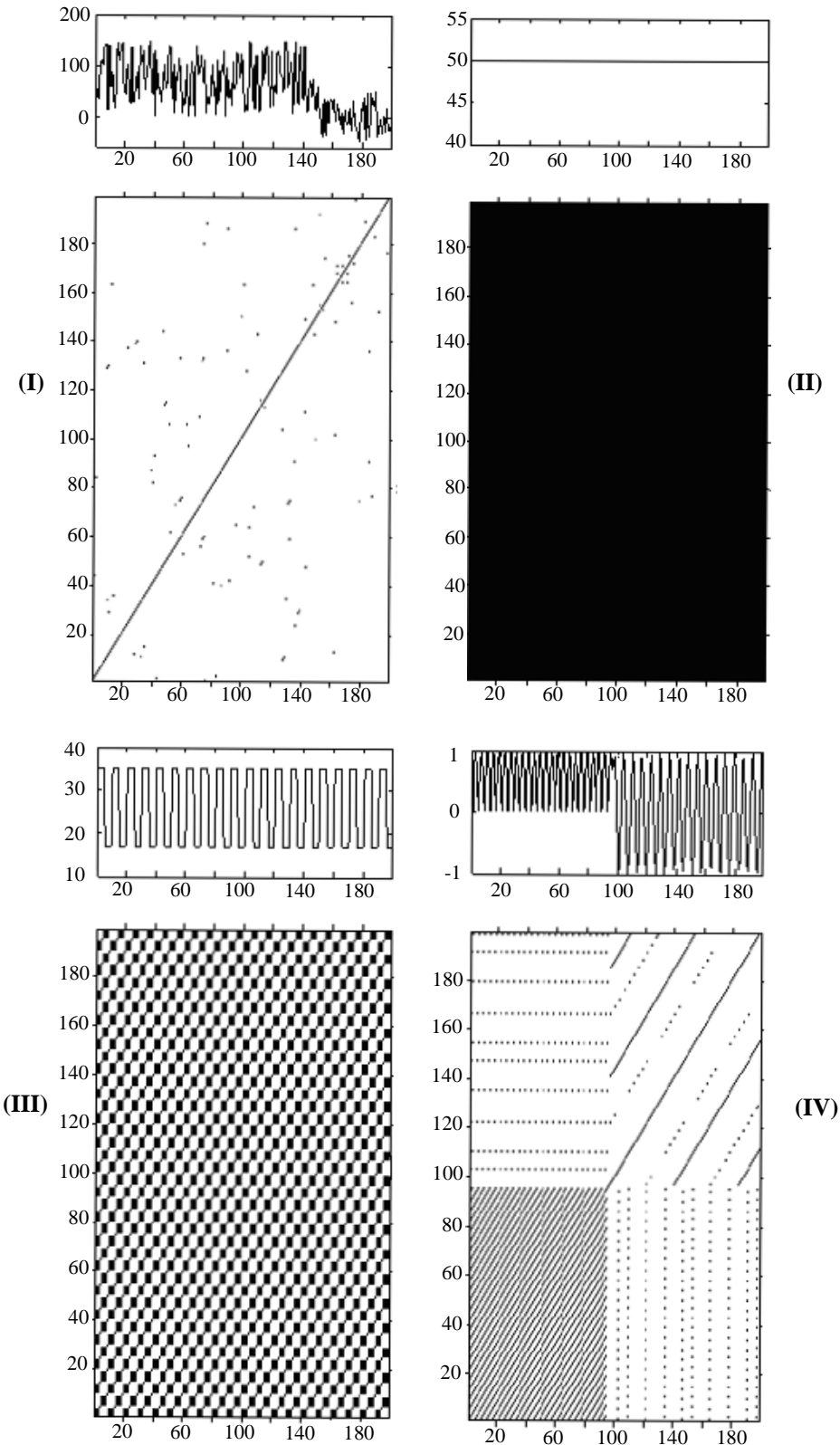
FIGURE 4.4: Four examples (I,II,III and IV) of recurrence plots analysis: top row - time series; bottom row - corresponding recurrence plots. From (I) to (IV): uncorrelated stochastic data (noise/random), constant number, periodic and harmonic oscillation with different amplitudes (sinusoidal waveforms). The data has a length of 200, embedding dimension, m = 2, the threshold, $\varepsilon = 5$ (first three signals) and $\varepsilon = 0.1$ (sine wave)

The above process is repeated for $m + 1$ and the following function is defined:

$$B^{m+1}(r) = \frac{1}{N-m} \sum_{i=1}^{N-m} B_r^{m+1}(i) \tag{4.10}$$

and the SampEn is finally obtained as follow:

$$SampEn(m, r, N) = -\ln(B^{m+1}(r)/B^m(r)) \tag{4.11}$$

There is one example of the use of SampEn in EMG control; it had been used by Zhao et al. [2006a]; Jingdong et al. [2006] to identify flexion and extension of the thumb, the index finger and the middle finger from three SEMG channels measured from the flexor digitorum profundus, flexor pollicis longus and extensor digitorum. Besides SampEn, they also used WT in processing the signals and this adds to the calculation time of the whole system as both methods require longer calculation time.

4.6   Summary

A new method, moving ApEn has been developed for the application to the electromyographic control system for upper limb prosthetic application. The findings from the investigation on SEMG signals using the proposed method will be discussed further in Chapter 5. A comparison between ApEn and SampEn, as well as RP analysis will also be presented in the next chapter.

Chapter 5

Feature Extraction of the Surface EMG Signal

This chapter describes an investigation of the surface EMG (SEMG) signals of the wrist muscles during different movements at a different speeds. The study focuses on the wrist muscles which are the flexor carpi ulnaris (FCU) and extensor carpi radialis (ECR). This pair of antagonistic muscles were selected as they are the muscles responsible for the wrist movement. Typically the flexor and extensor muscles are used in the SEMG control application [Ajiboye & Weir, 2005; Karlik et al., 2003; Zhao et al., 2006b; Asghari Oskoei & Hu, 2006]

The signals were then analyzed using moving ApEn as the main method. Other features had also been used in this investigation and they were sample entropy (SampEn), number of zero crossings (NoZC), standard deviation (SD),mean absolute value (MAV), skewness and kurtosis.

An overview of the protocol and experimental setup procedures are described, including selection of the participants in the investigation, overview of the equipment and description of the extraction process.

5.1 Method

5.1.1 Subjects

Twenty subjects (10 men and 10 women) aged between 20 and 30 years (mean: 25.4, SD: $\pm$ 2.28) agreed to participate in the study. The participants were recruited from the University of Southampton's student population and they were either right or left hand dominant. Table 5.1 shows the demographic data of the subjects.

TABLE 5.1: Demographic data of the subjects

Subject	Sex	Age	Dominant hand
A	Female	29	Right
B	Female	26	Left
C	Female	28	Right
D	Female	27	Left
E	Male	23	Right
F	Male	25	Right
G	Female	28	Right
H	Male	30	Left
I	Female	23	Right
J	Female	27	Left
K	Female	21	Left
L	Male	24	Left
M	Female	27	Right
N	Female	24	Left
O	Male	24	Left
P	Male	24	Left
Q	Male	26	Right
R	Male	25	Right
S	Male	23	Left
T	Male	25	Right

The exclusion criteria for this study were as follows: No history of nerve or physiological injury, no present discomfort that may effect the movement of their upper limb and no allergies to sticky plasters or cleansing wipes. The experimental protocol was approved by ethics committee of School of Electronics and Computer Science at the University of Southampton. A written consent was obtained from each subject prior to testing.

5.1.2   Experimental procedure

This investigation focused on the wrist muscles and the participants were asked to do movements that related to these particular muscles. The SEMG signals were acquired using Noraxon Ag/AgCl dual electrodes (diameter 15 mm, centre spacing 20mm). They were placed on the forearm above FCU and ECR with a reference electrode at the elbow. To obtain a stable and maximum pickup area of the surface EMG signals [Hargrove et al., 2006] from each subject, the procedure for surface electrodes placement were referred from SENIAM [Hermans et al., 1999]. Prior to the electrode placement, the electrodes sites were prepared by cleansing the skin surface with rubbing alcohol to reduce the impedance at the surface. The protocol to determine the correct arrangement for the electrodes are as follows:

1. Flexor carpi ulnaris

   The dual electrodes were positioned on a line from the medial epicondyle of the elbow to the radial styloid (base of the thumb), one third distant from the medial epicondyle (Figure 5.1 (left)).

2. Extensor carpi radialis

   The dual electrodes were positioned on a line from the lateral epicondyle of the elbow to the 2^{nd}metacarpal, 50 - 70 mm distant from the lateral epicondyle (Figure 5.1 (right)).

The test was conducted with the subject sitting in a chair that was positioned parallel with the table and Figure 5.2 shows the experimental setup for the study. The SEMG data were recorded during three tasks, which were wrist flexion/ extension, co-contraction and isometric contraction. The subjects were first seated with their elbow bent at ninety degrees. They were asked to do the three tasks at a speed of 60 beep per minute (bpm) where the speed was controlled using a metronome. The subjects were first instructed to perform wrist flexion and extension with their dominant hands. Once the contraction was established, the SEMG data were recorded. Then, they were asked to co-contract their muscles. Isometric contraction of the flexor and extensor was then achieved by restraining a subject forearm/ hand flat on a table. The SEMG signals were sampled at 1,500 Hz using a Noraxon 2400T in conjunction with Noraxon Myoresearch XP Master Edition (version 1.06) software. Table 5.2 shows the summary of the procedure of the experiment.
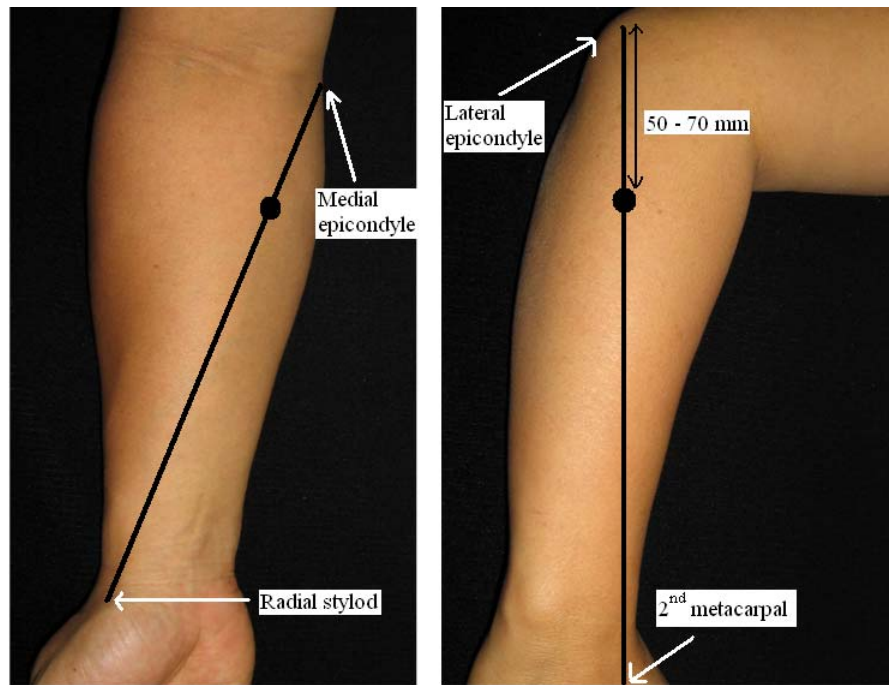
FIGURE 5.1: SEMG electrodes placements for FCU (left) and ECR (right)

TABLE 5.2: The protocol of the investigation on the SEMG of the upper limb

Movement	Clinical test	Movement speed (bpm)			
Wrist flexion/ extension	The subjects voluntary flexes and extends their wrist	60	90	120	max
Co-contraction	The subject will close the hand with maximum voluntary contraction. The subject can feel that both flexor and extensor muscles are tensed at the same time	60	90	120	max
Isometric	Restrain the forearm and hand flat on a table	60	90	120	max

Each trial was repeated for another three times at a different speed, which were 90bpm, 120bpm and maximum speed. During the maximum speed, the participants were asked to perform the task based on their ability. To avoid fatigue, each trial was spaced. The SEMG were recorded about 5 s after the task was initiated and ended immediately after the subject was asked to stop. Each recording was about 10 s to 15 s which contained about 5 to 10 muscle contractions. For one subject, there are twenty four recorded SEMG data sets (2 muscles × 4 speeds × 3 movements).
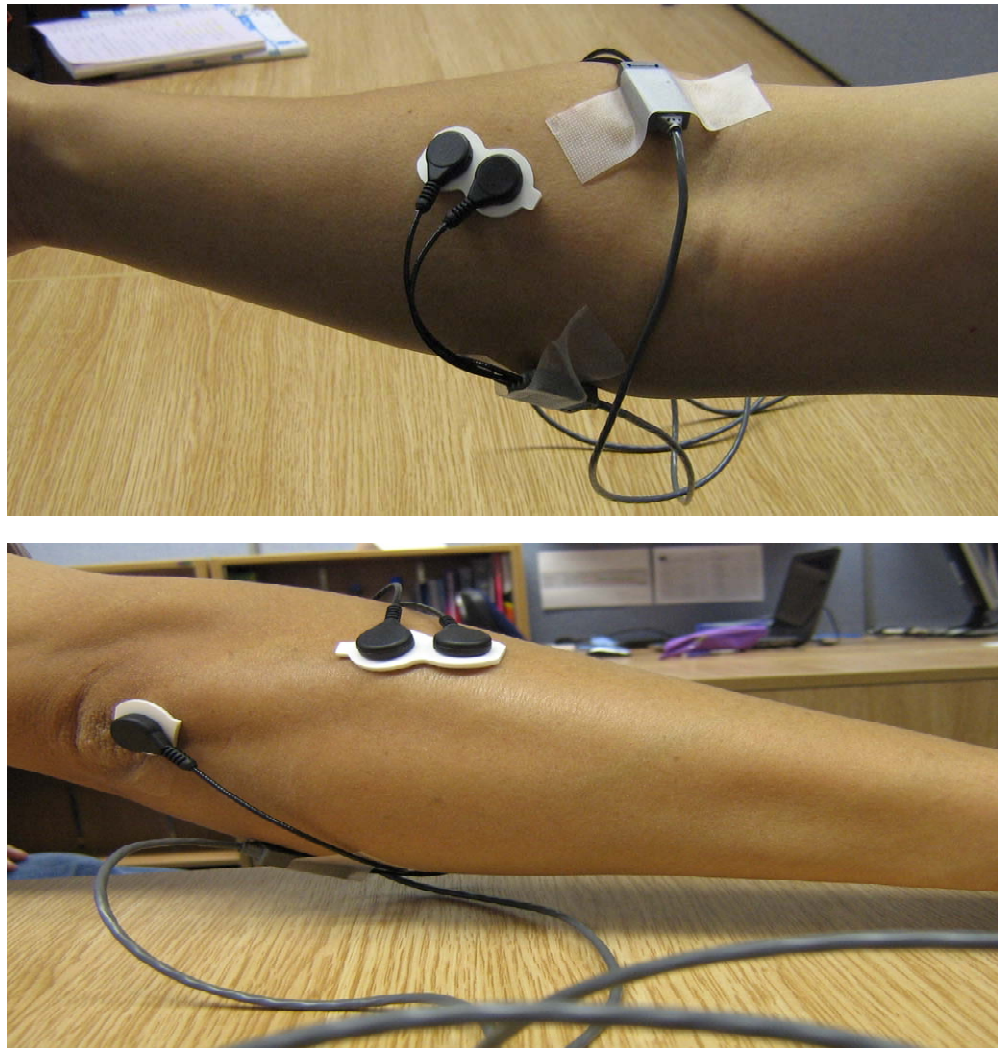
FIGURE 5.2: The experimental setup and the actual placements of the electrodes for FCU (top) and ECR (bottom)

5.1.3 Data Analysis

All the raw SEMG data were post-processed using the moving ApEn algorithm and other methods. The investigation focus on the analysis of the moving ApEn and other methods were used to support the performance of the moving ApEn.

The whole data was first divided into overlapping segments of length 200 data values (N), which is about 130 ms duration with a delay of one point to the next segment. For prosthetic control, calculations should be less than 200ms. Otherwise the delay would be too long for practical use. Based on the literature (Chapter 3.2.1), a sample window of 200 samples (130 ms) is a very good balance between having enough sample to give robust estimated of ApEn and delay time. A moving data window was applied to the data sequence and ApEn within the

data is calculated repeatedly. The moving ApEn is obtained as the windows moves point by point along the time axis. Detail explanation on the windowing technique has been discussed in section 4.3, Chapter 4. This windowing technique is also used for the calculation of other methods.

The RP analysis was then carried out to support the information obtained from the moving ApEn analysis. The RP analysis was applied to the SEMG data during, before and after a muscle contraction. For the analysis, the chosen parameter values are same as the values for the ApEn calculation. For each plot, the data length, N is set to 200, the embedding dimension, m = 2, the time delay, $\tau = 1$ and the threshold, $\varepsilon = 4\sigma$.

Using the same windowing technique discussed above, the SEMG signals were also analyzed using the following methods:

1. Sample entropy (SampEn)

   This method has been explained in section 4.2, Chapter 4

2. Number of zero crossings (NoZC)

   A measure to count how many times the signal crosses zero.

3. Standard deviation (SD)

   A statistical dispersion to measure how spread out the values in a data set, X_i that can be defined as:

$$\sigma = \sqrt{\frac{1}{N} \sum_{i=1}^{N} (X_i - \bar{X})^2} \tag{5.1}$$

   where $\bar{X}$ is the mean and N is the number of data points.

4. Mean absolute value (MAV)

   An estimate of the mean absolute value of the signal X_i in segment i which is N samples in length is given by:

$$\bar{X}_i = \frac{1}{N} \sum_{k=1}^{N} |x_k|; i = 1, ..., I \tag{5.2}$$

   where x_k is the kth sample in segment I and I is the total number of segments over the entire sampled signal [Hudgins et al., 1993].
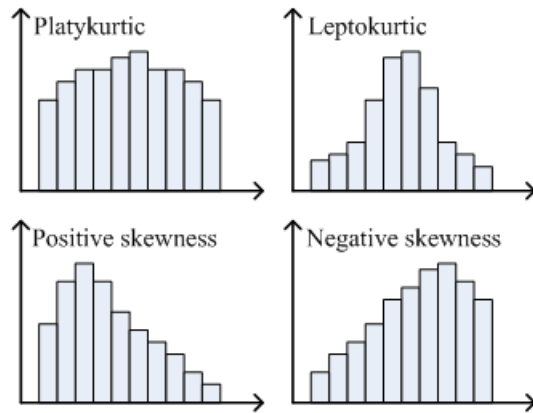
FIGURE 5.3: Top: kurtosis distribution, bottom: skewness distribution

5. Skewness

   A measure of symmetry of a distribution/data set, X_i that can be defined as:

   $$skewness = \frac{\sum_{i=1}^{N}(X_i - \bar{X})^3}{(N-1)\sigma^3} \tag{5.3}$$

   where $\bar{X}$ is the mean, σ is the SD and N is the number of data points.

   The skewness for a normal distribution is zero. negative (-ve) values of skewness indicate data are skewed left (left tail is long relative to the right tail) and positive (+ve) values indicate data are skewed right (Figure 5.3 (bottom)). Skewness >1 or skewness <-1 is indicated as highly skewed while 0.5<skew<1(or -1<skew<-0.5) is moderately skewed.

6. Kurtosis

   A measure of whether the data are peaked or flat relative to a normal distribution and is given by:

   $$kurtosis = \frac{\sum_{i=1}^{N}(X_i - \bar{X})^4}{(N-1)\sigma^4} - 3 \tag{5.4}$$

   where $\bar{X}$ is the mean, σ is the SD and N is the number of data points.

   The kurtosis for normal distribution is 3. Positive kurtosis indicates a 'peaked' (leptokurtic) distribution while a 'flat' (platykurtic) distribution is indicated by a negative kurtosis (Figure 5.3 (top)). A skewed distribution is always leptokurtic.

The above methods were selected for various reasons. SampEn is chosen to compare with the ApEn method as SampEn is the revised version of ApEn and it is

essential to analyze the SEMG data using it. Method 2 to method 6 had been used in the control system for prosthetic hand application and have been discussed in the literature (Chapter 3).

Further analysis were carried out on the extracted data. The analysis focuses on two aspects which are the information on the speeds and states of a contraction. The average values of the moving ApEn from 20 subjects at four different states during these three movements were computed. The four states are: start, middle and end of contraction and also when the muscle is relaxed. The average values for the other methods were also calculated.

5.2 Results and Discussion

Figure 5.4 shows several recorded SEMG for the first 350ms from the flexor and extensor muscles during wrist flexion/ extension, co-contraction and isometric contraction at 60bpm. The plots show which muscle was activated corresponding to the related movement.
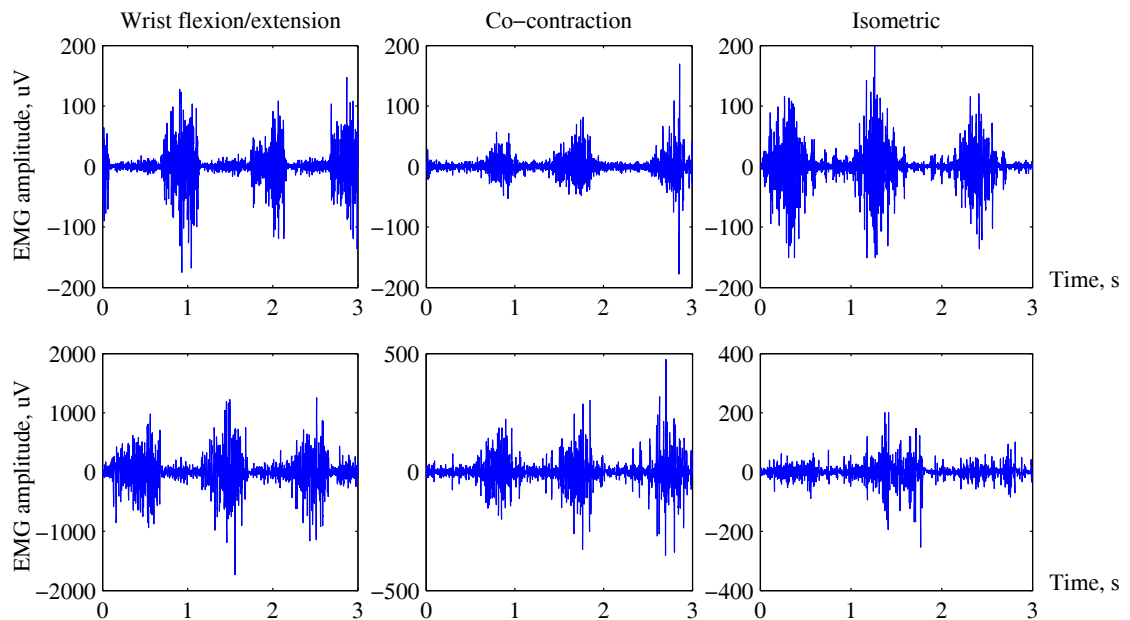
FIGURE 5.4: Examples of recorded SEMG signal during 3 tasks at 60bpmfrom two muscles, FCU (top) and ECR (bottom)

The results will be divided into two sub-sections, which are the results from the ApEn analysis and the results from the other methods. The result from the SampEn analysis will be included in the first section as these two methods are closely related.

5.2.1 Moving Approximate Entropy analysis

Figure 5.5 and Figure 5.6 show the moving ApEn analysis from one subject during wrist flexion and wrist extension respectively at a speed of 60bpm. The result of an ApEn calculation for each window of 200 points is plotted below the EMG signal with respect to the 200th point of the EMG signal (a delay of 130ms). From visual inspection, the results demonstrated differences during the contraction at different speeds. For example, dips can be seen at the start and end of a contraction. All the results show repeatable and constant patterns in other movements at all speeds carried out on other subjects.

From the plots, shown in the waveform of Figure 5.5 (regions B, D and F) and in Figure 5.6 (regions I and K) are drops in the ApEn (0.4 to 0.6) at the start of a contraction compared to a middle of contraction where ApEn has risen approximately to 0.6-0.8. The same observation can be seen at the end of contraction , where the moving ApEn (0.4 to 0.6) drops again. There is little variation before the onset of the wrist extension and wrist flexion, therefore, as expected, that ApEn is high in these area. Similar patterns of the ApEn were observed in other subjects during this task at the same speed. Some of the results of the ApEn analysis during wrist flexion/extension at other speeds (90 bpm, 120bpm and maximum speed) are included in Appendix C.

The reason for the use of the RP analysis to the SEMG signal is to explain and confirm the results from the moving ApEn analysis. Figure 5.7 shows the results from the RP analysis. The plots labeled I to VI correspond to the SEMG signal (I to VI) as shown in the top plot. Before and after the contraction (I and VI respectively), the muscles are at rest condition where the recorded SEMG signals were mainly noise. The structure of the RP pattern at these stages is interpreted as no changes in the signal or very slow changes over the 200 data point window. This non repeatable pattern confirms the high (more irregularity) ApEn values found when the muscle is relaxed. The structure of the RP at the start of a contraction (II) shows fading patterns to the upper left and lower right corners which can be interpreted as a non-stationary data that contains a trend or drift. It can be
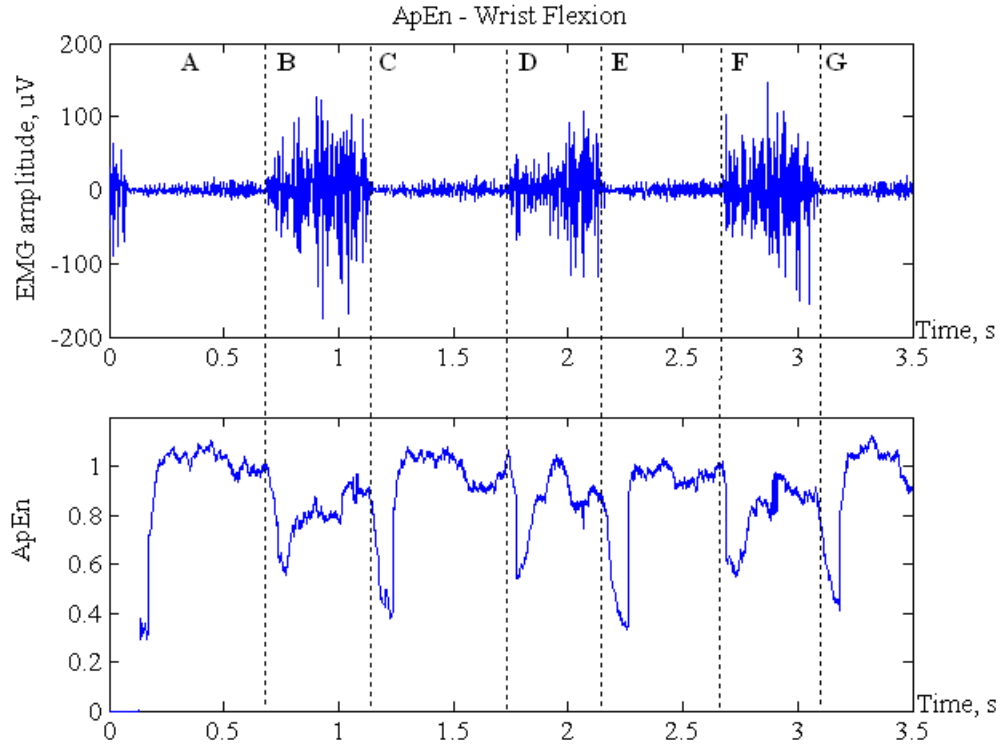
FIGURE 5.5: Top: The SEMG signal obtained from FCU during wrist flexion at 60bpm. B, D and F: during contraction; A, C and E: before contraction. Bottom: the moving ApEn analysis for the respective signal.

observed that the drops of the ApEn during the start of a contraction occur at the same time as the changes in the patterns of the RP. During the contraction (III-IV), the plots show a distribution of single isolated points that can be interpreted as a heavy fluctuation in the process of an uncorrelated random data. These plots confirm the higher ApEn values obtained during middle of both contractions, which means that there is more irregularity (less regularity) in the data at area B. At the end of contractions (V), the same patterns are observed as for the start (area A) but with opposite orientation. The plots confirm that there is a change in the pattern of the signal as the muscles stop contracting. This information has shown agreement with the results obtained from the ApEn analysis.

The average of the ApEn values from 20 subjects during the three states (start, middle and end of contraction) and also when a muscle was relaxed were calculated. The averages of the ApEn values during wrist flexion (FCU) and extension (ECR) at four different speeds are given in Figure 5.8. From the plots, the average ApEn shows differences at four states as explained earlier. From the observations, as the speed of the movement increases, the ApEn decreases during start and end of a contraction. However, during the middle of contraction there are no changes in ApEn with speed changes.
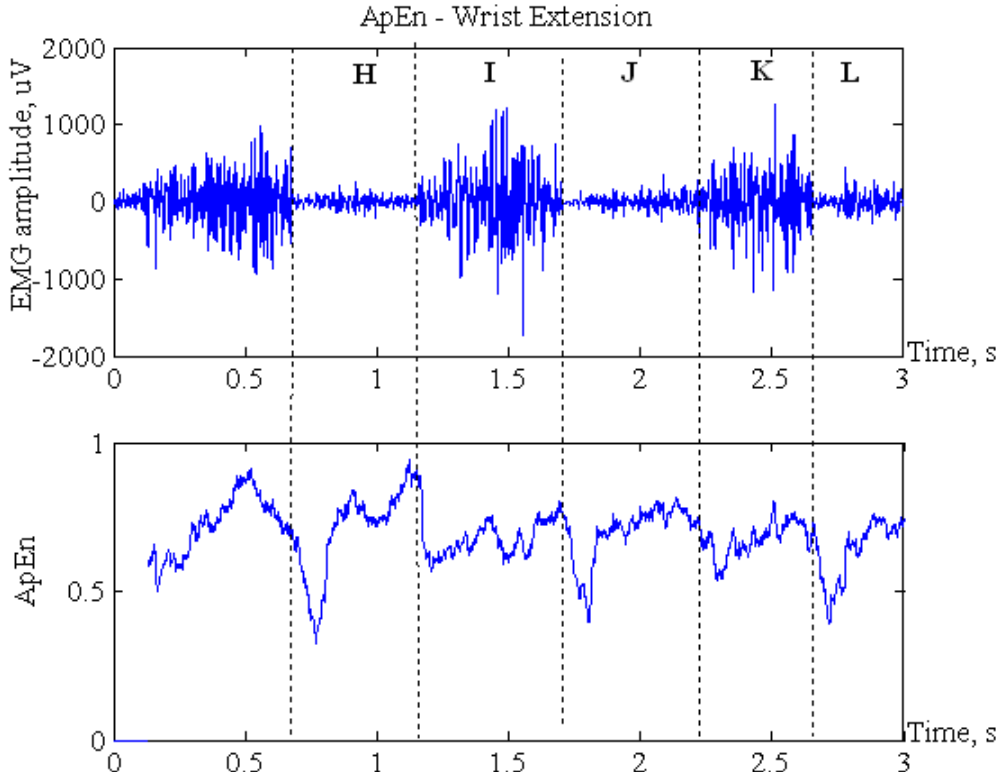
FIGURE 5.6: Top: The SEMG signal obtained from extensor carpi radialis during wrist extension at 60bpm. I and K: during contraction; H and J: before contraction. Bottom: the moving ApEn analysis for the respective signal.

The average ApEn from the FCU and ECR during co-contraction and isometric contractions at four different speeds are shown in Figure 5.9 and Figure 5.10 respectively. From the plots, they show similar pattern of the ApEn values with the wrist flexion and extension task.

From the average of moving ApEn during three tasks at four different speeds as shown in Figure 5.8, Figure 5.9 and Figure 5.10, it can be seen that the values are low and between 0.43 ($SD = 0.10$) to 0.58 ($SD = 0.12$) at the start of a contraction and are consistent for all speeds of contraction. At the end of all the contractions, the moving ApEn values drop to the range between 0.38 ($SD = 0.10$) and 0.60 ($SD = 0.06$). It also has been observed that ApEn values are lower at the end of a contraction compared to the start of a contraction. The ApEn values are higher (> 0.8, $SD \approx 0.08$) when muscle is relaxed. This is expected as there is no activity except the noise in the electronics system and also some small activity from motor units. When focusing on the speeds of the contraction at each state of a contraction, it can be seen that there are slight differences of the ApEn values at different speeds of a contraction. It has been observed that the average moving ApEn decreased when the speed of contraction increased at the start of a
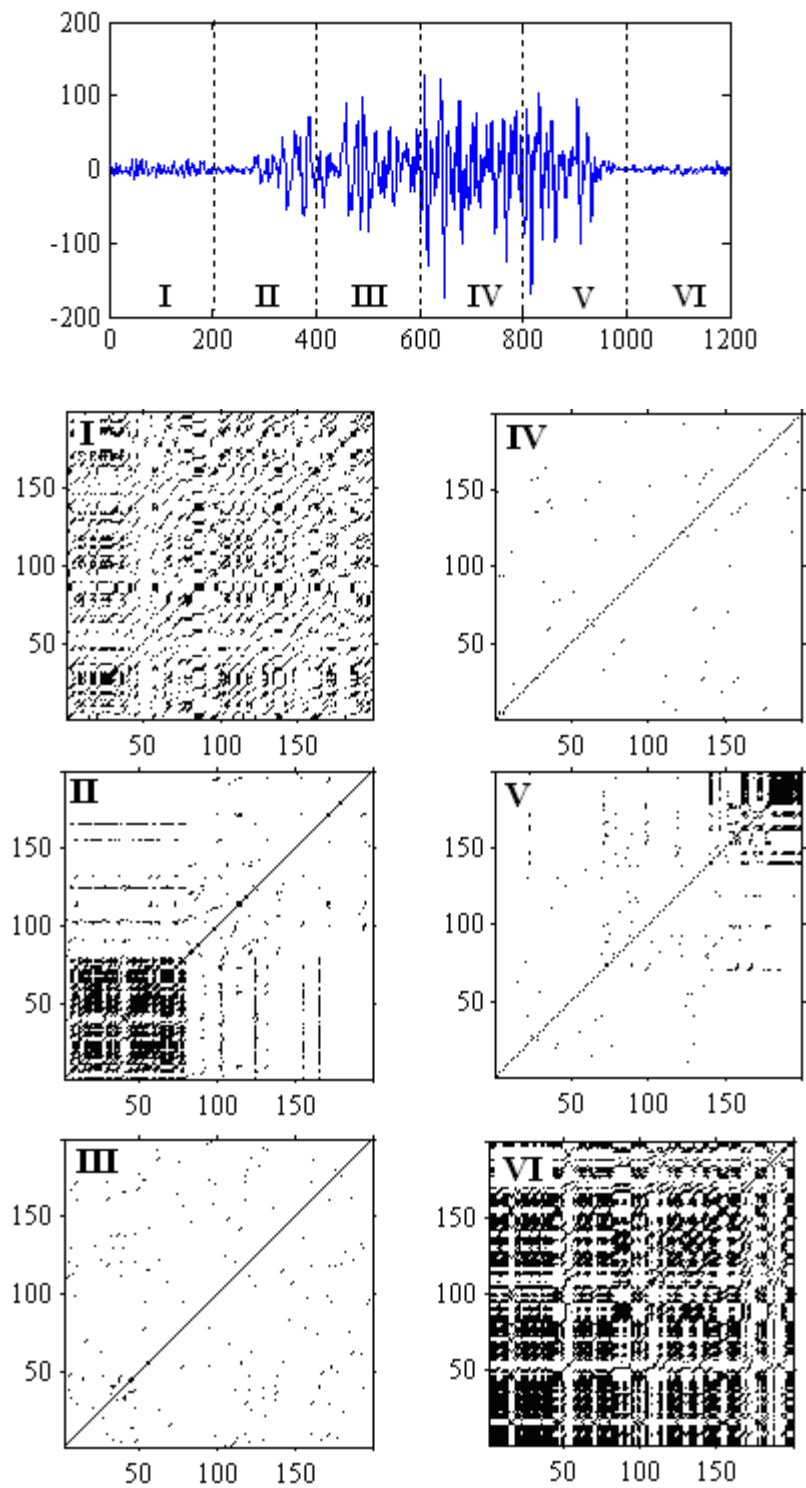
FIGURE 5.7: Top: The SEMG signal at 200 data length from before to after muscle contraction. Label I - VI in the recurrence plots correspond to the sEMG signal with embedding dimension,m = 2, delay,$\tau = 1$ and threshold,$\varepsilon = 4\sigma$
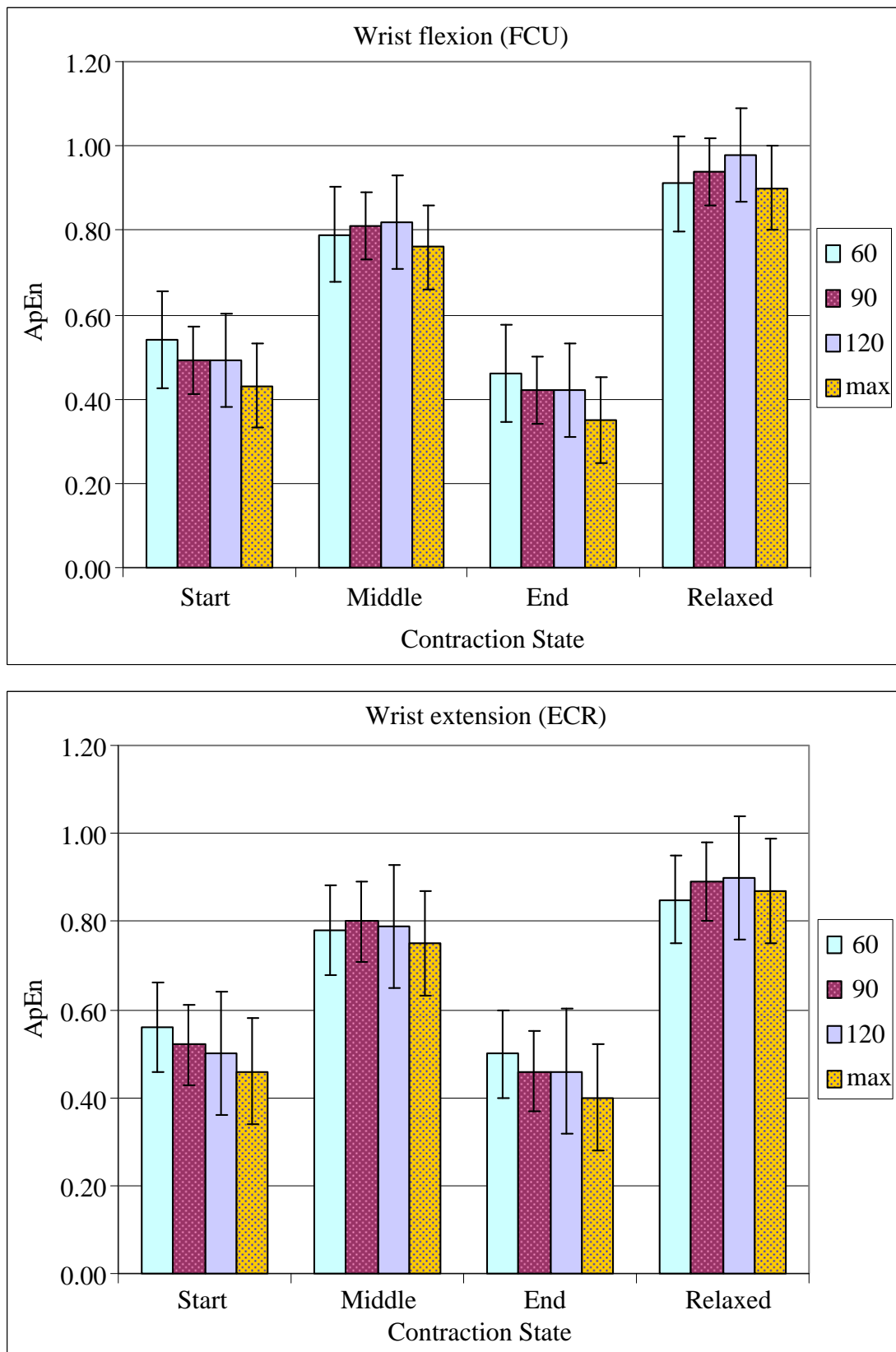
FIGURE 5.8: Average ApEn analysis from 20 subjects during wrist movement (flexion and extension)at four states and four different speeds from two muscles: FCU (top) and ECR (bottom)
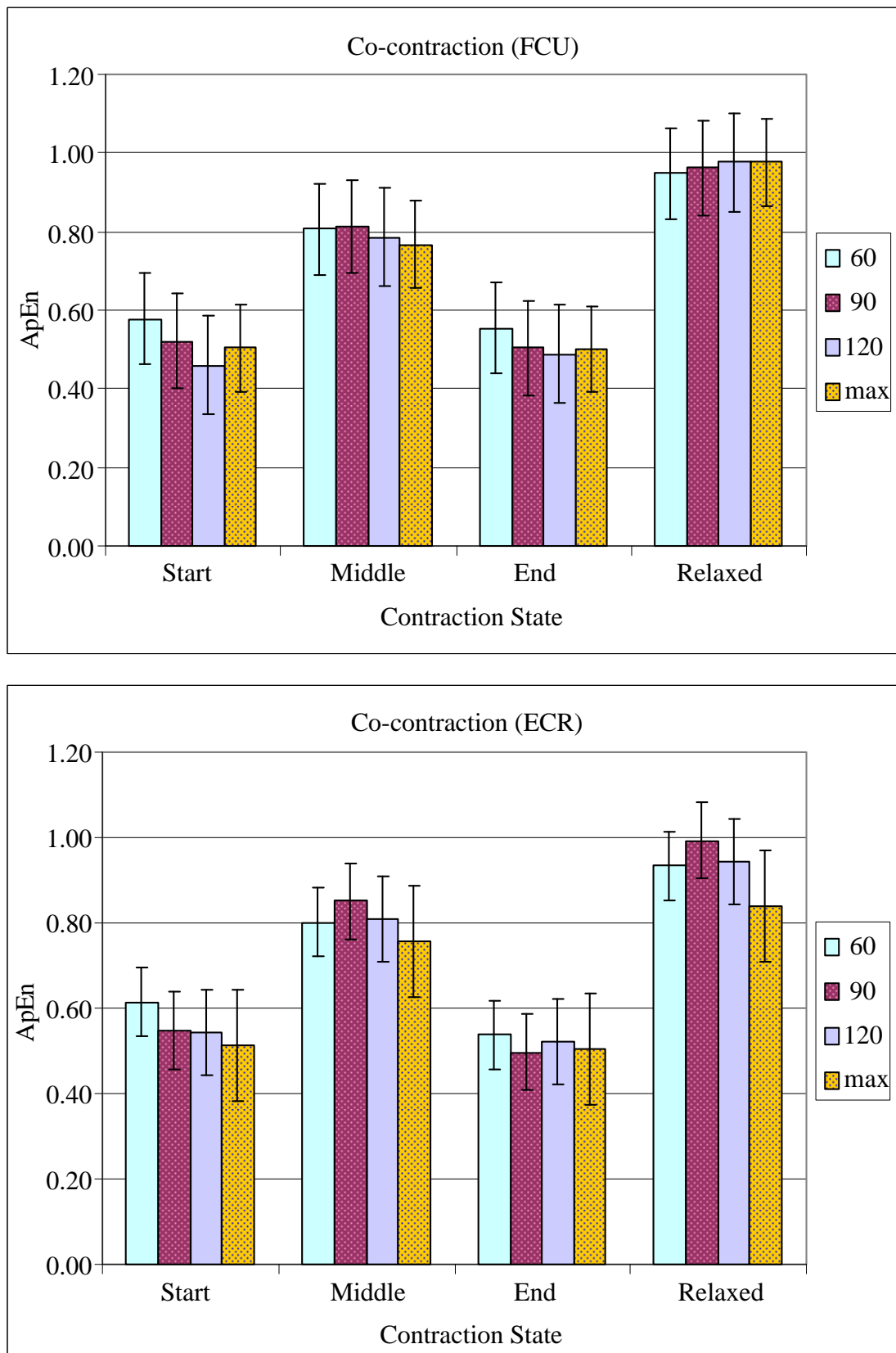
FIGURE 5.9: Average ApEn from 20 subjects during co-contraction at four states and four different speeds from FCU (top) and ECR (bottom) muscles.
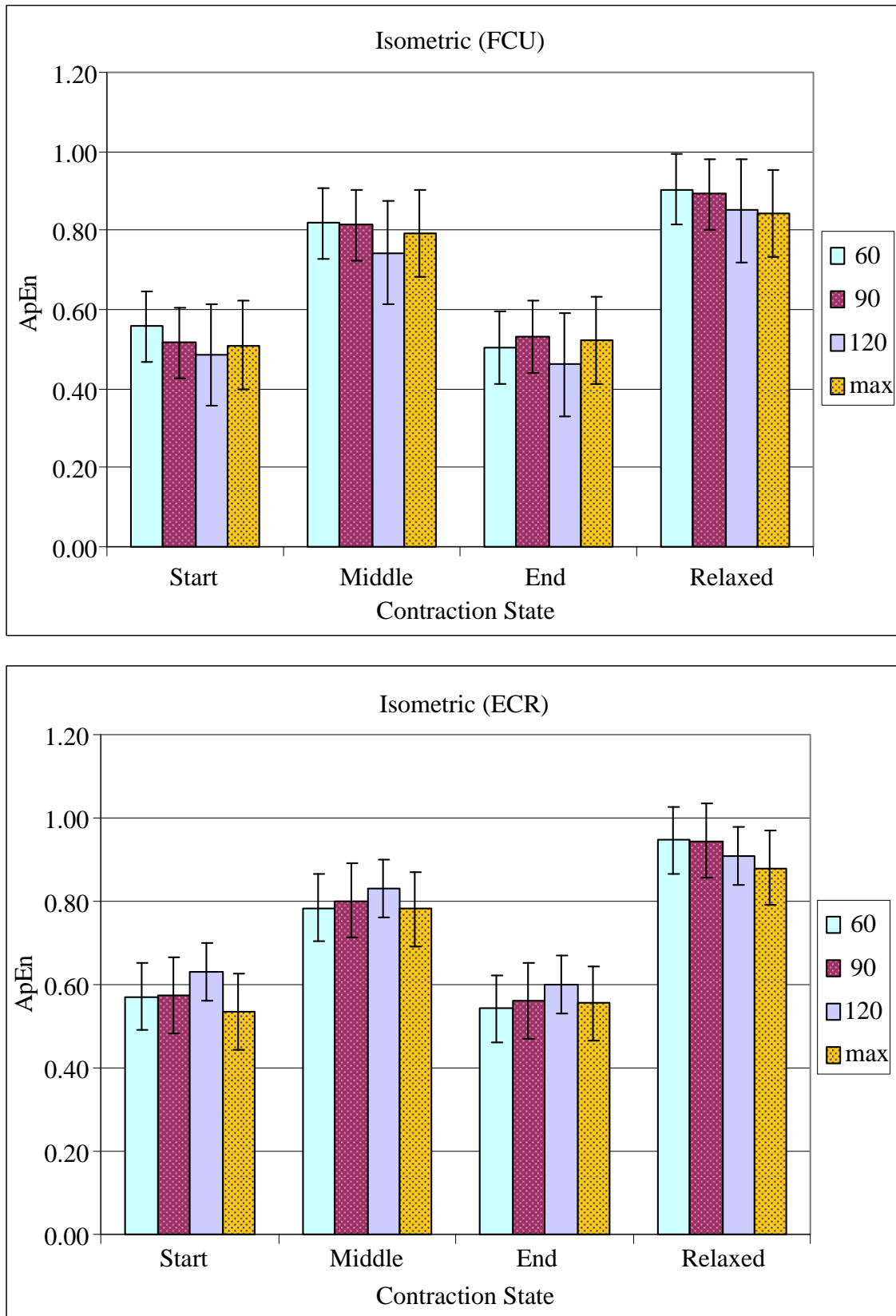
FIGURE 5.10: Average ApEn from 20 subjects during isometric contraction at four states and four different speeds from FCU (top) and ECR (bottom) muscles.

contraction during wrist extension. Also, the average moving ApEn is about the same (0.5) at the end of a contraction during wrist flexion and extension at the speed of 90bpm and 120bpm. In the middle of a contraction, the average moving ApEn gave the lowest value at the maximum speed for both wrist movements. The same observation also can be seen at the middle of a co-contraction. Differently, during isometric contraction, the moving ApEn values do not vary as the speed increases.

These average moving ApEn values at each state were then compared using un-paired 't' tests. A comparison was made between the ApEn values during relaxed condition with start, middle and end of contraction. The test was set at two tailed with 0.05 significance level. The 't' tests showed that there are significant differences between the three states of a contraction and relaxed states of the muscles ($p \ll 0.05$).

From a physiological point of view, this findings can be explained by the behaviour of recruitment/derecruitment of the motor units. As explained earlier, the SEMG signals are generated from the recruitment of the motor units, lying under the skin. Towards the middle of a contraction, motor units will recruited from smaller to larger units with random firing patterns. Towards the end of contraction, the motor units will be de-recruited until the muscle is relaxed. Van Cutsem et al. [1998] reported in their investigation on ankle muscles that there is no change in the recruitment sequence of the motor unit during ramp contraction. This may explain more regular (lower ApEn) SEMG activity at the start and end of a contraction shown by the drops that have been obtained in this study. The drops indicate there is more regularity in the recruitment of the muscle's motor units. The finding is also supported by the [Romaiguere et al., 1993] study. They reported that, even though the recruitment and de-recruitment processes undergo random fluctuation, the recruitment and de-recruitment display the same kind of fluctuation. Also, greater SEMG signal irregularity (higher ApEn) at the middle of a contraction reflects less predictable muscles firing patterns [Morrison et al., 2007]. In terms of the movement speed, Stots & Bawa [2001] had reported that no difference in the recruitment order between isometric and lengthening contractions at any speed of lengthening contraction in their investigation on wrist flexors. However, from the analysis, it could be said that the recruitment of the motor units during eccentric contraction shows more regularity as the speed increases compared to the isometric contraction.

Hudgins et al. [Hudgins et al., 1993] had shown that the SEMG signal contains information at a start of a muscle contraction in their research in prosthetics control applications. This statement is supported by the ApEn analysis presented where dip can be seen at the start of a contraction. Moreover, the analysis also show that the SEMG signals do contain information at the end of a contraction too.

5.2.1.1 Sample Entropy analysis

In this work, SampEn was used to analyze the SEMG and its performance is compared with the ApEn analysis. Figure 5.11 shows one sample the analysis of two SEMG waveforms using SampEn in comparison with the ApEn analysis. The plot on the top left is SEMG signal measured during wrist flexion from FCU. From the plots (middle and bottom), both SampEn and ApEn analysis show similar patterns where drops at the start and end of contraction can be observed before they increase in the middle of the contraction. During co-contraction, ApEn and SampEn analysis don't show a similar pattern.

From the SampEn analysis on all of the contractions at all speeds, it has been observed that it shows no repeatable pattern in the SEMG structure that could be used for pattern classification in this work. Even though the processing time was faster with SampEn, this method has been excluded for further analysis as it shows no useful findings that could be used.

5.2.2 MAV, skewness and kurtosis's analysis

The analysis of the SEMG signal using other methods mentioned in section 5.1.3 had been carried out and some of the results are shown in Figure 5.12. From a visual inspection of the presented and un-presented results, NoZc is excluded from further analysis as it had shown no useful results where no pattern structures can be seen from the analysis. SD analysis shows a same pattern with MAV, it is also been excluded. Also, SD is used in ApEn calculation and by excluding it, extra processing can be avoided. Skewness and kurtosis show interesting spikes that occur at the start and end of contraction.

From the findings, MAV, skewness and kurtosis have been considered for further analysis as they've shown interesting outcomes. MAV is a technique normally used as smoothing operation. In this work, rectified values were used and from
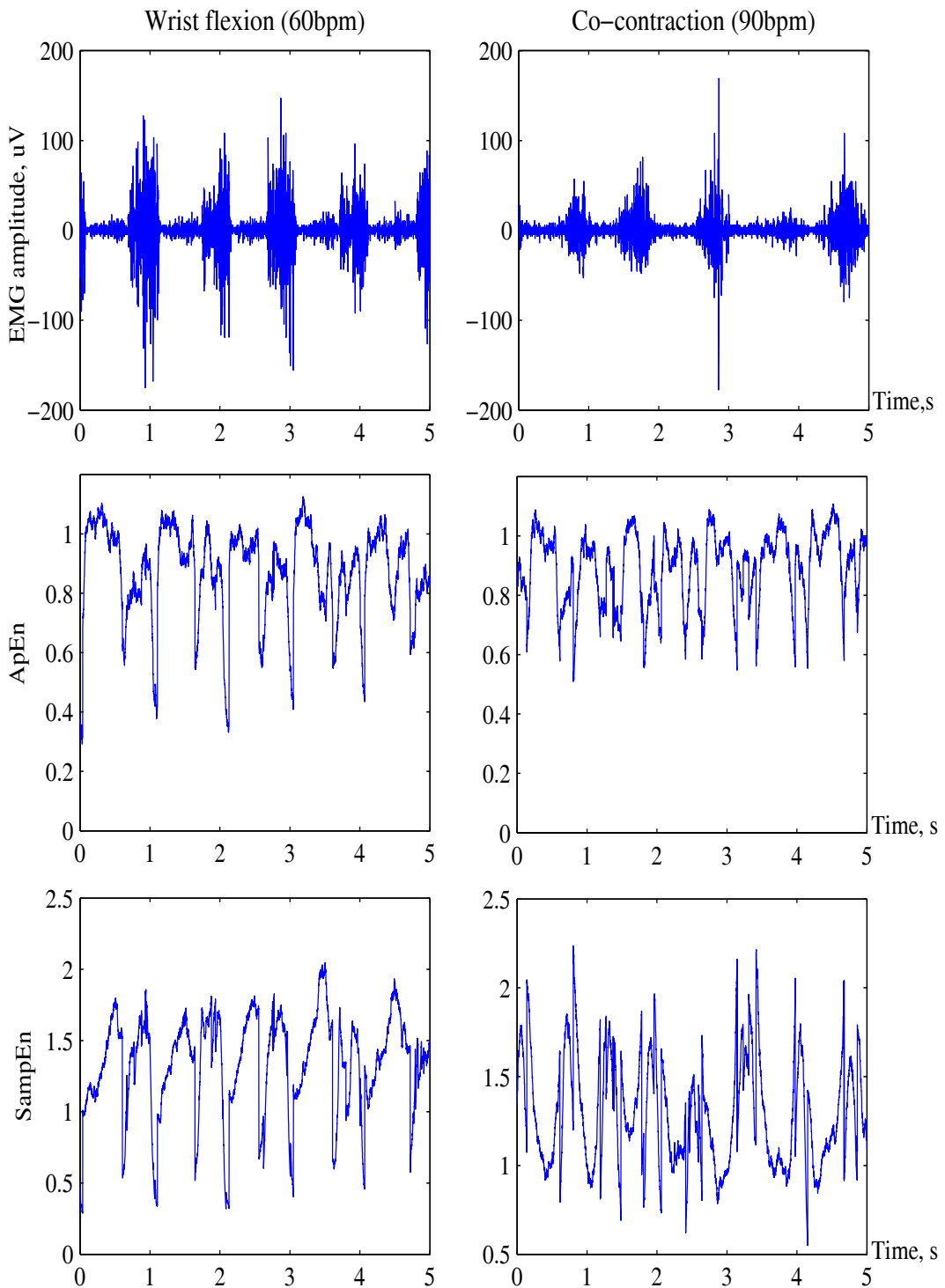
FIGURE 5.11: SampEn and ApEn analysis during wrist flexion(left) and co-contraction (right) from FCU muscle
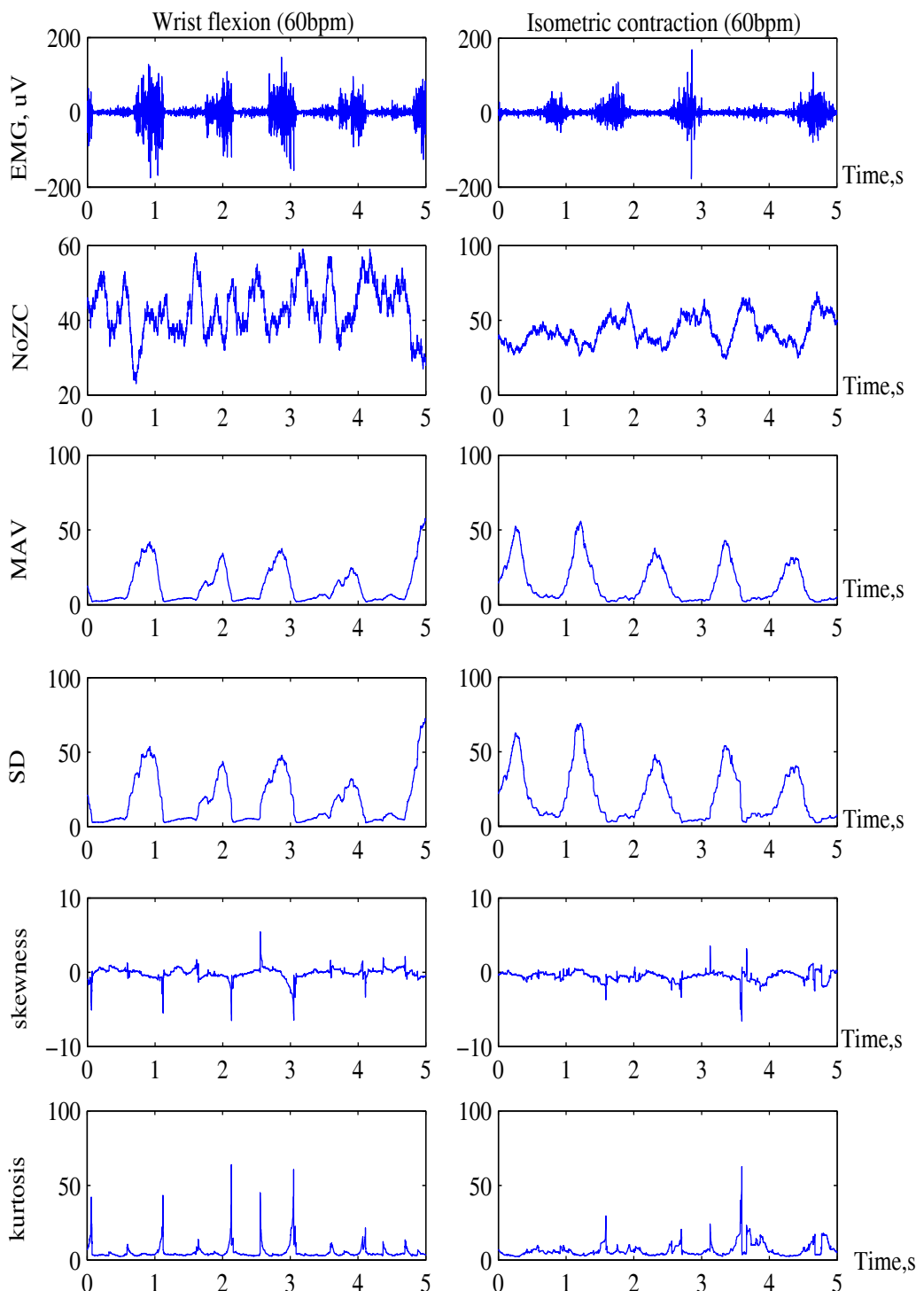
FIGURE 5.12: From top to bottom: the SEMG signal measured during wrist flexion (left) and isometric (right), NoZc, SD, MAV, skewness and kurtosis.

the analysis repeatable structures where it shows the envelope of the rectified signal during muscle contractions can be seen at all speed of contraction. As expected, the MAV show a rise and fall across all contractions. Kurtosis and skewness are methods to study the data distribution of the signal. Kurtosis analysis shows that the SEMG signals have positive kurtosis. The analysis from 20 subjects show that higher kurtosis occurred at the start and end of a contraction, compared to the middle of a contraction; which shows that the distribution of the data has more acute peak at these states.

The average of these three features from 20 subjects during four states at different speeds of a contraction were calculated and the results during wrist flexion and extension are shown in Figure 5.13. From the plots, differences can be observed at four different states in MAV and kurtosis, but not in skewness. In MAV, at the speed of 60 bpm , the values are low (0 to 40) at the start and end of contraction and increase to >60 in the middle of contraction. The MAV return to lower (<10) value that during start (and end) of contraction. These patterns are also follow at other speeds. The average kurtosis shows consistent differences at the four states where high kurtosis is seen at the start, drops in the middle of contraction before it increases to higher kurtosis at the end of contraction. However, it appears that no pattern for skewness at the start, middle end and muscle relaxed (Figure 5.13, middle plots) and it will be excluded from the ECS development.

The findings from the kurtosis analysis could be used to explain the behaviour of muscles contraction relative to the recruitment orders in motor units, but not from MAV and skewness analysis. A possible explanation for the spikes at the start and end of a contraction from kurtosis analysis is that the recruitment is changed from small to large and large to small motor units respectively causing a peak at the data distribution.

5.3   Summary

In this investigation, three movements at four different speeds related to wrist muscles were investigated. Moving approximate entropy was employed as the main method to investigate the SEMG signals whether any significant pattern exist in the structure of the signal. SEMG signals were acquired from the wrist muscles from twenty subjects. The analysis shows that moving ApEn gave a distinct pattern during the start, middle and end of a contraction. These important outcomes could be extended to the feature extraction technique for the ECS based
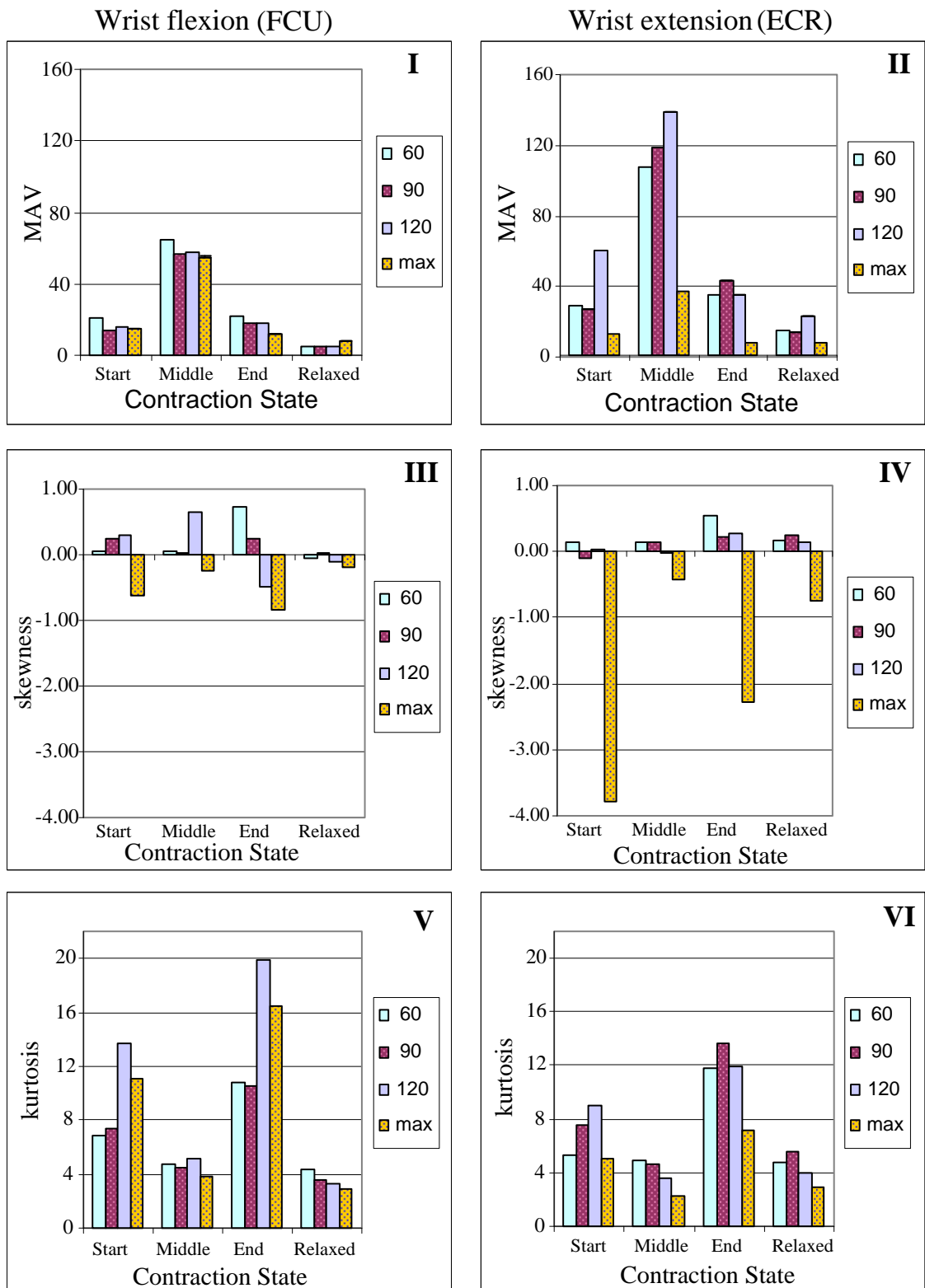
FIGURE 5.13: Average MAV, skewness and kurtosis from 20 subjects during wrist flexion and extension at four states and four different speeds from FCU (left) and ECR (right) muscles.

on pattern recognition where each state of the contraction can be used to classify one grip posture. The findings also showed that there are small differences at the magnitude of each features at different speed of contraction, which also can be used for the classifier design.

To increase the performance and the accuracy of the control system, more that one feature is preferable during the feature extraction process. Besides moving approximate entropy, MAV and kurtosis features will be adopted in the pattern classification of the SEMG signal as they have shown potential in the investigation.

Chapter 6

Development and Testing of the Electromyographic Control System

This chapter discusses the development of the electromyographic control system in detail. The same data used in the investigation of the SEMG signal (Chapter 5) was used in this work. The development process involved in several stages and this chapter emphasizes the classifier design process where fuzzy logic classifier is used. Two main approaches have been used in the classifier design which are based on the state and speed of a contraction. The design process and the findings are presented and discussed in this chapter.

6.1 Overview of the electromyographic control system

The aim of the electromyographic control system (ECS) development is to have a simple system that should be able to select one of four different grip postures with the SEMG as the control channel and could be implemented in a microcontroller in the future.

The acquired SEMG signals will be fed to the ECS where it will do all the processes before deciding the final output.The ECS consists of two main stages which are feature extraction and classification process as shown in Figure 6.1. The SEMG signals will be acquired from the wrist's flexor(FCU) and extensor (ECR) muscles

during wrist flexion, wrist extension and co-contraction. The SEMG acquisition setup follows the same procedures as described in Chapter 5, section 5.1.2. The control system should select one from four different hand grip postures where at this stage, the grip postures will be represented by states (e.g. STATE1, STATE2, STATE3 and STATE4).

The feature extraction process follows the same procedure as discussed in Chapter 5. Three main conclusions have been drawn from the investigation which are;

1. Three from seven features used in the feature extraction process will be used and they are moving ApEn, MAV and kurtosis.

2. Differences between these three features can be seen at different speeds of contraction; 60, 90 and 120 bpm.

3. Repeatable patterns can be seen at the start, middle and end of a contraction

These information are then used to design the classification system for the ECS which will be discussed further in the following section.

6.2   Design of the fuzzy logic classifier

A classifier function is to map the pattern and match them appropriately in determining the final output. In this work, the classifier will be used to discriminate different output states from the extracted features. These output states represent different hand grip postures. Fuzzy logic (FL) is used as the classifier and it is well known in providing a simple way to arrive at a definite conclusion just based upon imprecise input information. The theoretical background of the FL system will not be discussed in detail. There are many references on the FL operation and also specifically on pattern recognition application [Bezdek & Pal, 1992; Zadeh, 1965].

In the development process, there are two approaches that have been used in designing the classifier which are:

1. The contraction speed based

   This classifier will use the speeds of the contraction information: slow (S), medium (M) and high (H) to determine the final output state of the system.
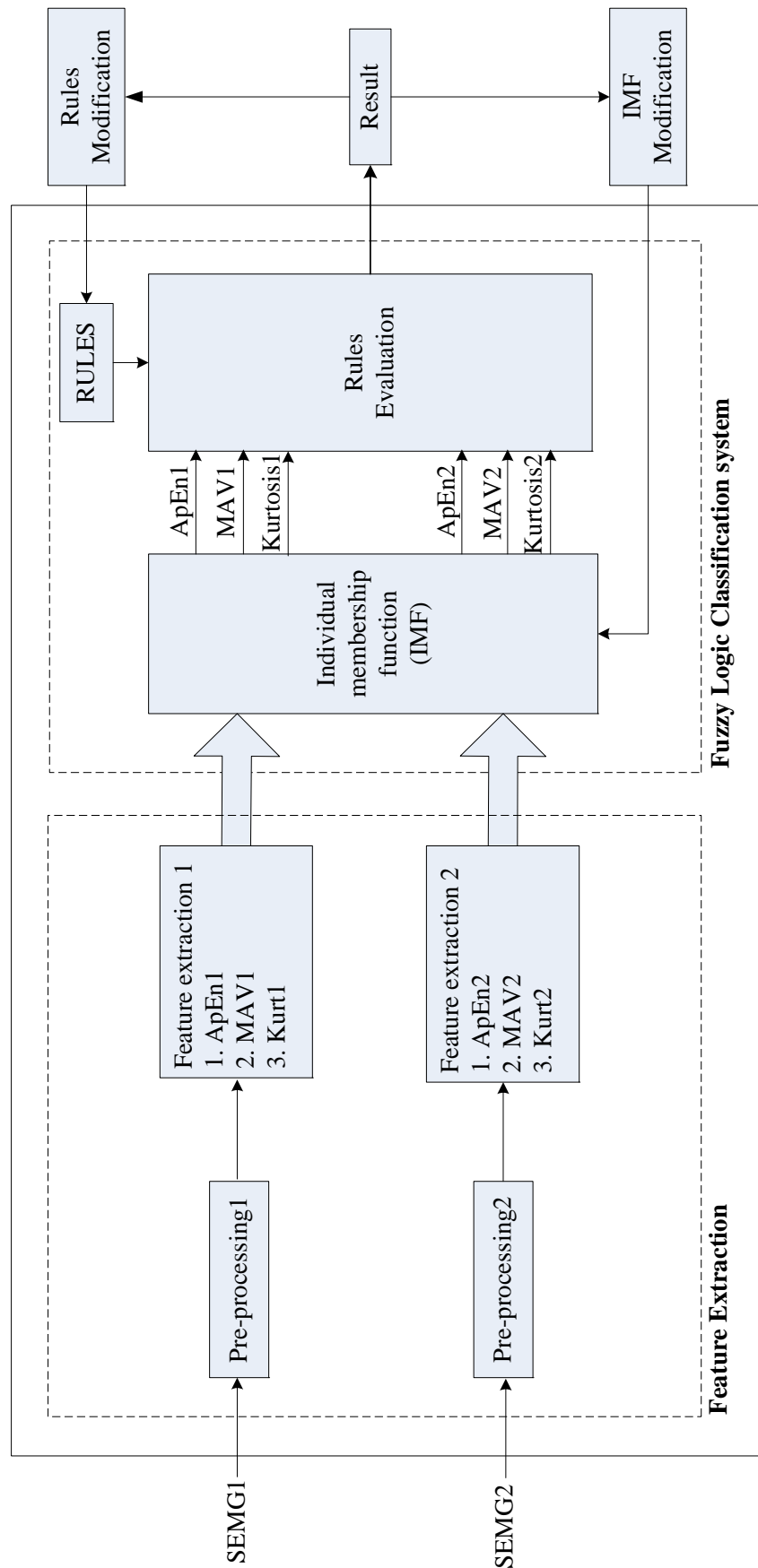
FIGURE 6.1: The flow diagram of the ECS with the feature extraction and the FL classification components

2. The contraction state based

   This classifier will use the states of the contraction information: start (S), middle (M) and end (E) to determine the final output state of the system.

In general, the FL classifier has six inputs generated from the feature extraction process of the SEMG signals and one output which is the state. Figure 6.2 shows the diagram of the FL system which used the Mamdani type FL system [Mamdani & Assilian, 1999]. The rules are created depend upon which way is used. Triangular and trapezium shapes are used for the membership function (MF) of the inputs and triangular shape is used for the output's MF. For the defuzzification, the centroid method is used. The FL classification is developed using Matlab Fuzzy Logic Toolbox and tested using Simulink.
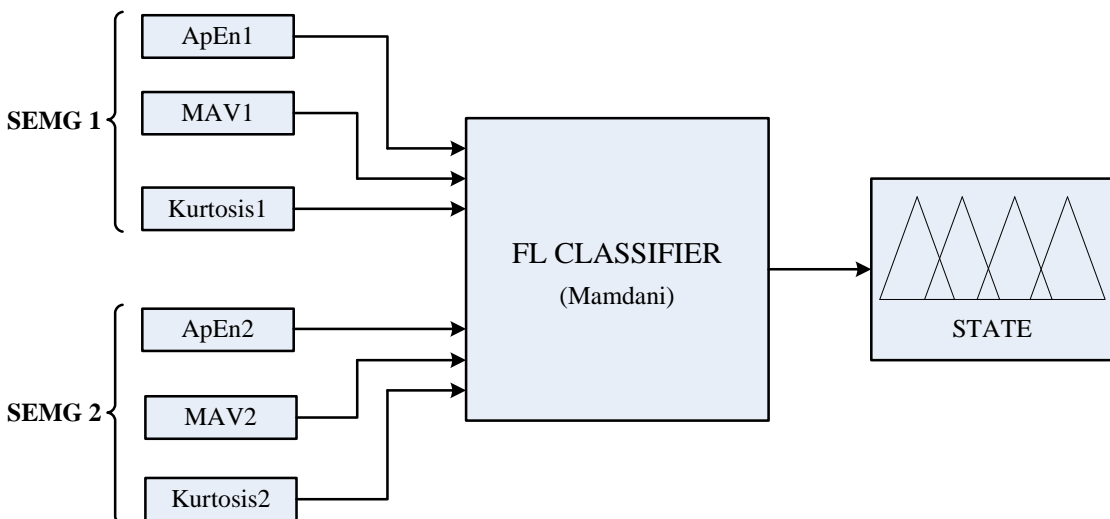
FIGURE 6.2: The block diagram of the Mamdani type FL classification system

6.2.1 Classification based on the speeds of a contraction

This classifier is built using the information on the contraction speed where earlier investigation has shown that moving ApEn, MAV and kurtosis show differences of their magnitudes at different speeds of contraction. For this type of classifier, the dip that can be observed at the start and end of a contraction in ApEn analysis will be used to trigger and stop the classification process respectively. With this method, the processor power consumption could be saved as the system doesn't need to do continuous classification.

Several different approaches for this type of classifier have been tried and the following sections will give detail explanations on each approach.

6.2.1.1 Four state system

The four state classifier system is to classify the extracted information from wrist movements and co-contraction at different speeds in selecting one of the four outputs. The operation of the system is as follows:

1. Wrist flexion at a speed of 60bpm (SLOW)	STATE1
2. Wrist flexion at a speed of 90bpm (MEDIUM)	STATE2
3. Wrist flexion at a speed of 120bpm (HIGH)	STATE3
4. Wrist extension at a speed of 60bpm (SLOW)	STATE1
5. Wrist extension at a speed of 90bpm (MEDIUM)	STATE2
6. Wrist extension at a speed of 120bpm (HIGH)	STATE3
7. Co-contraction at a speed of 60bpm (SLOW)	STATE4

The subject has to do two movements which are wrist flexion/extension at the speed of 60 bpm (SLOW, S), 90 bpm (MEDIUM, M) and 120bpm (HIGH, H) and co-contraction only at 60bpm (C). The feature extraction of two SEMG signals gives six features: ApEn1 (A1), MAV1 (B1), kurtosis1 (C1) from the FCU and ApEn2 (A2), MAV2 (B2) and kurtosis2 (C2) from ECR. For the MF of the inputs, the speed of the contraction is used for the fuzzy set where they can be grouped into four which are SLOW (S), MEDIUM (M) and HIGH (H) speeds for the wrist flexion/extension. While for the co-contraction, it applies only at a speed of 60bpm and will be labeled as C. This classifier will discriminate the information from the feature extraction process into four different states namely STATE1 (S1), STATE2 (S2), STATE3 (S3) and STATE4 (S4).

The MF for the inputs and the output of the system are shown in Figure 6.3. In the top left plot of Figure 6.3 is the MF of the input A1. In order from left to right: co-contraction (C), HIGH (H, 120bpm), MIDDLE (M, 90bpm), SLOW (S, 60bpm) and RELAX (R). These functions are derived from a non-Gaussian distribution data obtained in each speed of the contraction. The differences between the means at different speeds of contraction are small. However despite these small differences, they can be used in a practical system.

The rules of the classifier are given in Table 6.1. The first three rules are applied during wrist flexion, rule 4 to rule 6 during wrist extension movement and the last rule applied to the co-contraction at any speeds.
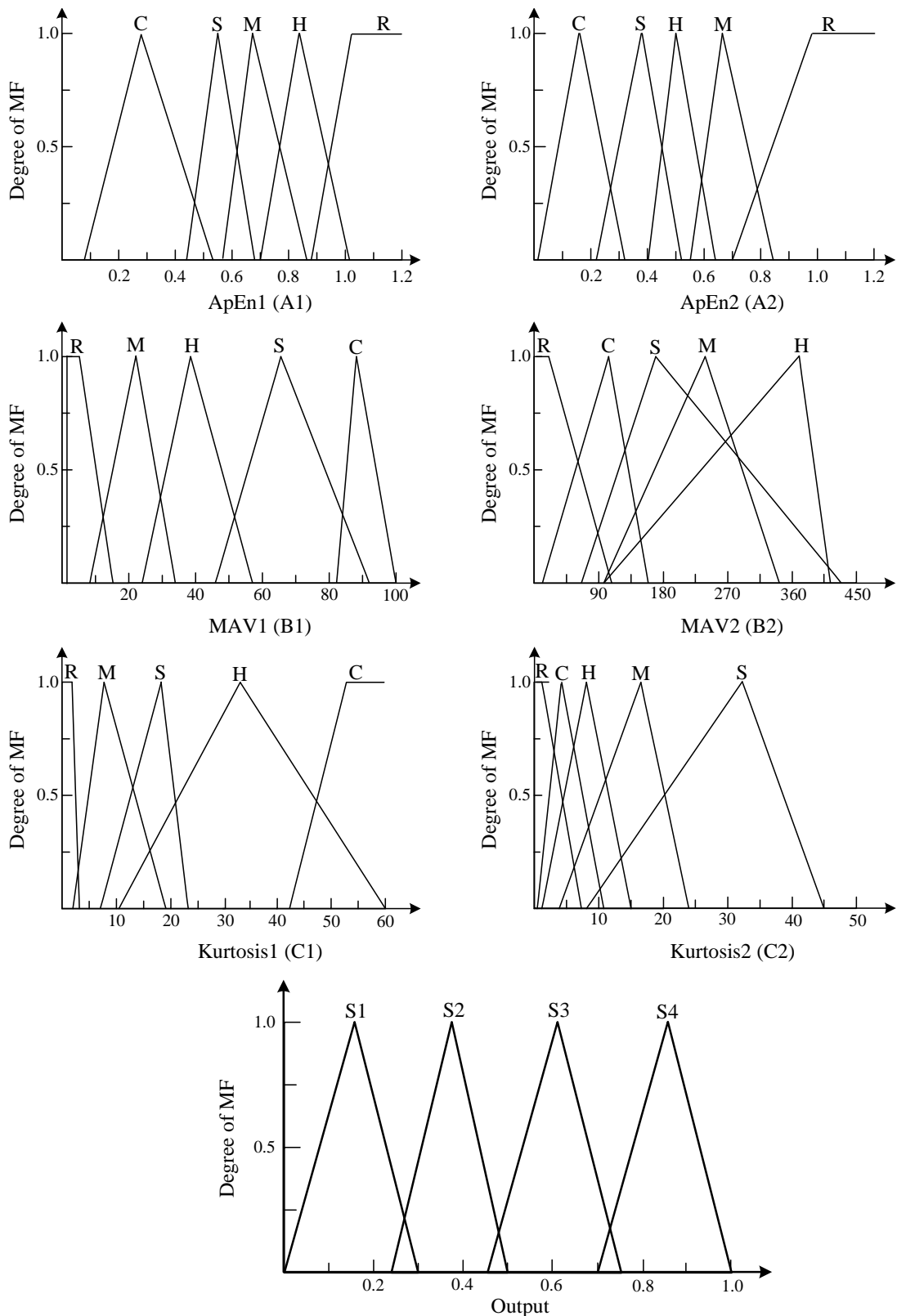
FIGURE 6.3: The membership function for the inputs and the output of the four state system. Inputs A1, B1 and C1 are from FCU and A2, B2 and C2 are from ECR. S: SLOW, M:MEDIUM, H:HIGH, C:Co-contraction, R: RELAX

TABLE 6.1: IF-THEN rules for the four states system

Rule	A1		B1		C1		A2		B2		C2		State
1	S	&	S	&	S	&	R	&	R	&	R	THEN	S1
2	M	&	M	&	M	&	R	&	R	&	R	THEN	S2
3	H	&	H	&	H	&	R	&	R	&	R	THEN	S3
4	R	&	R	&	R	&	S	&	S	&	S	THEN	S1
5	R	&	R	&	R	&	M	&	M	&	M	THEN	S2
6	R	&	R	&	R	&	H	&	H	&	H	THEN	S3
7	C	&	C	&	C	&	C	&	C	&	C	THEN	S4

Figure 6.4 shows the results of the simulation of the ECS during wrist flexion/extension at 60bpm. Region A1 and A2 are during wrist flexion, while region B1 and B2 are during wrist extension. Figure 6.4 shows that the classifier is able to select the correct state outputs during wrist flexion almost correctly but not during wrist extension. It can be seen clearly that during wrist extension (top plot - region B1 and B2), the classification output is 0.5 (shown in the bottom plot). This output indicates that the classifier cannot determine any output at the given inputs. For a correct classification, the outputs values are shown in Figure 6.5. The results obtained follows at other speeds of contraction where a poor classification result is obtained during wrist extension. The same result is obtained during co-contraction.

After several cycles of testing, possible changes of the MF for each input were explored. The changes included modification of the MF shape and range of values of the inputs but the same results were obtained. It has been found that poor classification results are due to the kurtosis input from both SEMG channels. These tests have led to the exclusion of kurtosis for further analysis in the ECS's development for this type of classifier. Modifications were done to the MF in Figure 6.3 and the revised MFs is shown in Appendix D, Figure D.1 and also the rules of the system. In the revised MF, inputs C1 and C2 were removed from the system. Also, co-contraction was removed from the fuzzy set on inputs A1 and A2. The modified rules of the revised four states system is shown in Table 6.2 below.

Figure 6.6 shows the results of the revised ECS during wrist flexion/extension at 60bpm when kurtosis is removed. The expanded views for the classification results labeled (*a*) and (*b*) are shown in Figure 6.7 and it can be seen clearly the classifier is able to select the correct output, which in this case is STATE1 (S1), labeled (a) and (b), where from the output MF, the range is between 0 to 0.3. Even though
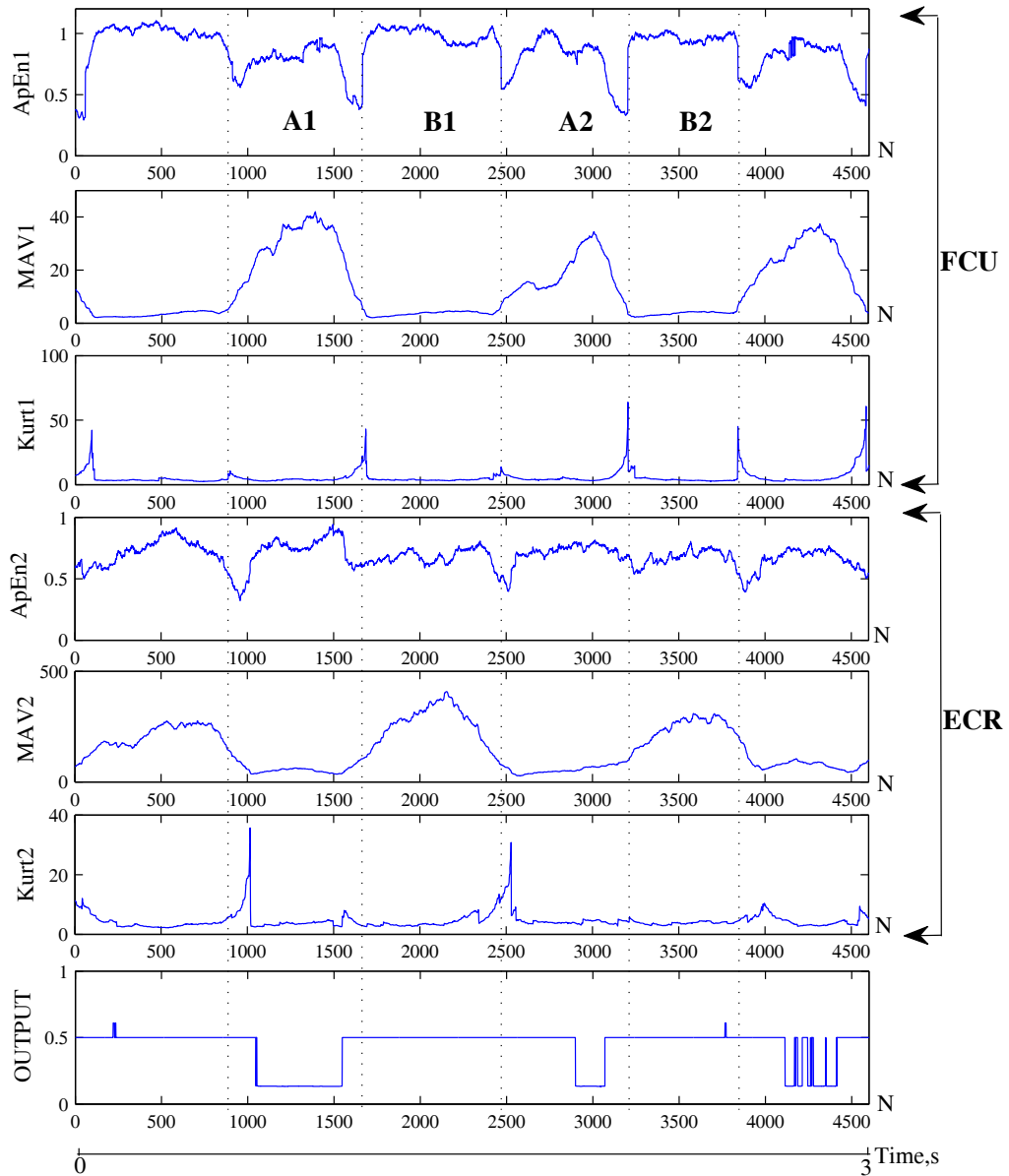
FIGURE 6.4: The result of the classification during wrist flexion/extension at 60bpm for the four states system

there are glitches during the classification result in one contraction, the average of the values produces the correct output state.

Some of the classification results during other movements and speeds for this type of classifier are included in Appendix E.

The analysis of the accuracy of the revised system is carried out and shown in Figure 6.8. The accuracy (in percentage, %) of the system is measured by the
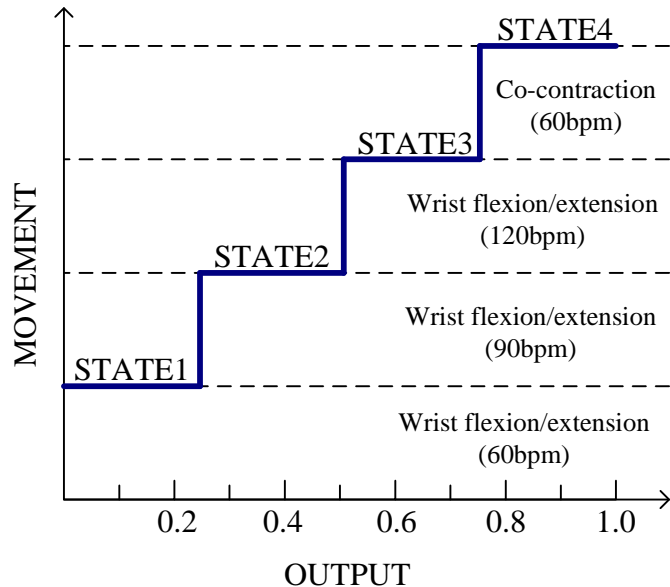
FIGURE 6.5: The movements vs. correct output for four states system

TABLE 6.2: IF-THEN rules for the revised four states system

Rule	A1		B1		A2		B2		State
1	S	&	S	&	R	&	R	THEN	S1
2	M	&	M	&	R	&	R	THEN	S2
3	H	&	H	&	R	&	R	THEN	S3
4	R	&	R	&	S	&	S	THEN	S1
5	R	&	R	&	M	&	M	THEN	S2
6	R	&	R	&	H	&	H	THEN	S3
7	S	&	C	&	S	&	C	THEN	S4
8	M	&	C	&	M	&	C	THEN	S4
9	H	&	C	&	H	&	C	THEN	S4

following equation:

$$\% = \frac{\text{number of correct classification in one contraction}}{\text{number of total classifications}} \times 100\% \quad (6.1)$$

From the speeds of contraction perspective, during wrist flexion/extension, the classifier was able to select STATE1 (S1) and STATE2 (S2) accordingly but not at STATE3 (S3) which is when the contraction is performed at the speed of 120 bpm. A further investigation has been carried out on this HIGH speed and it's been found that the classifier is not able to select the output state correctly at this speed. Most of the times, at 120bpm contractions, the classifier selects S1.
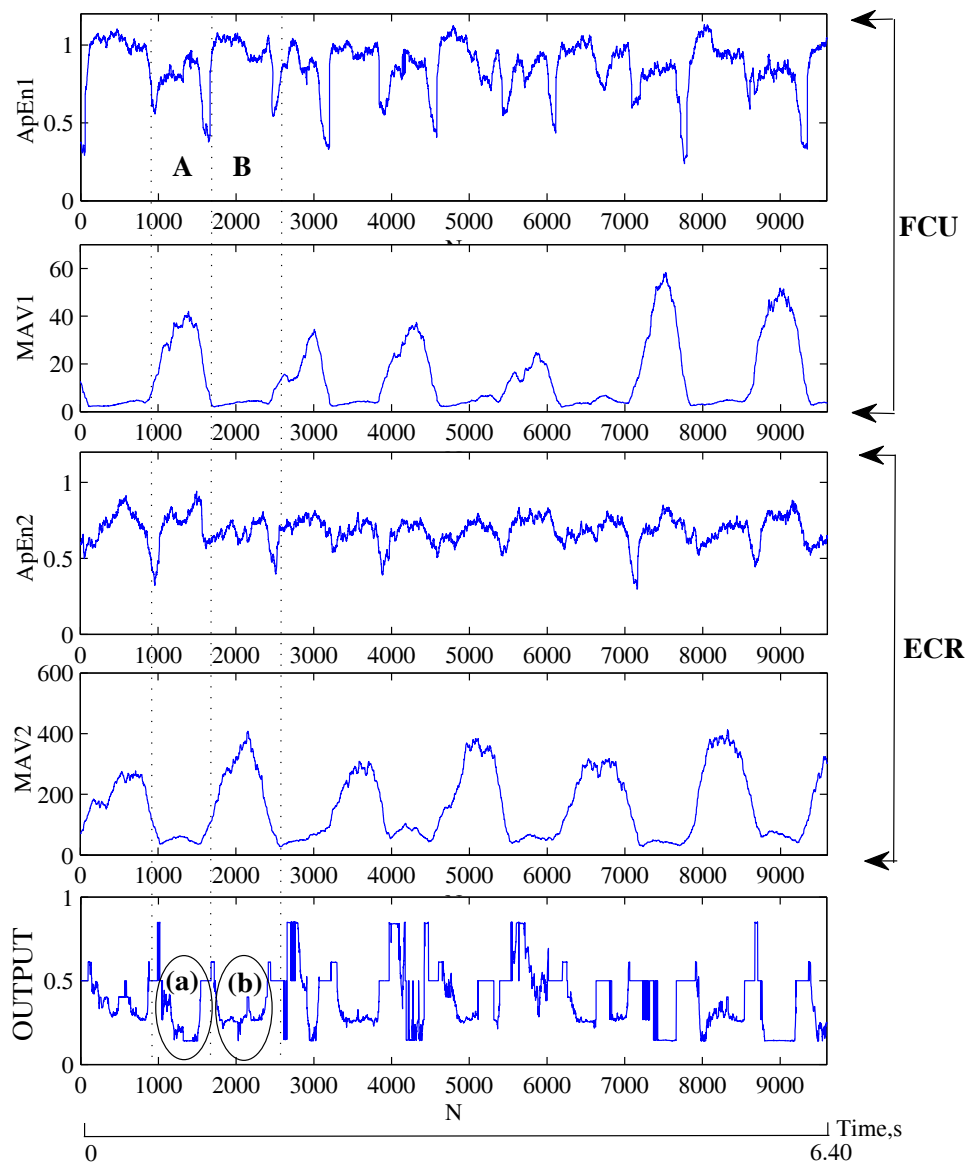
FIGURE 6.6: The result of the classification system for wrist flexion (A) and wrist extension (B) at 60bpm for the revised four states system
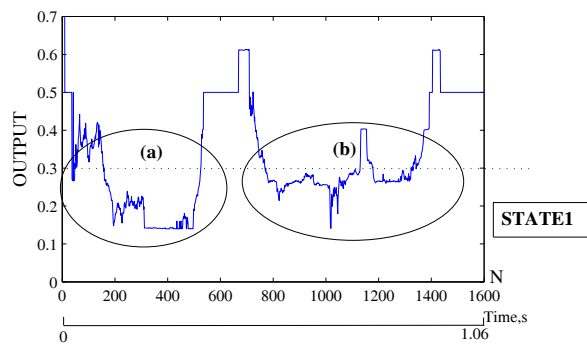
FIGURE 6.7: The expanded view of the classification result (label (a) and (b) in Figure 6.6)
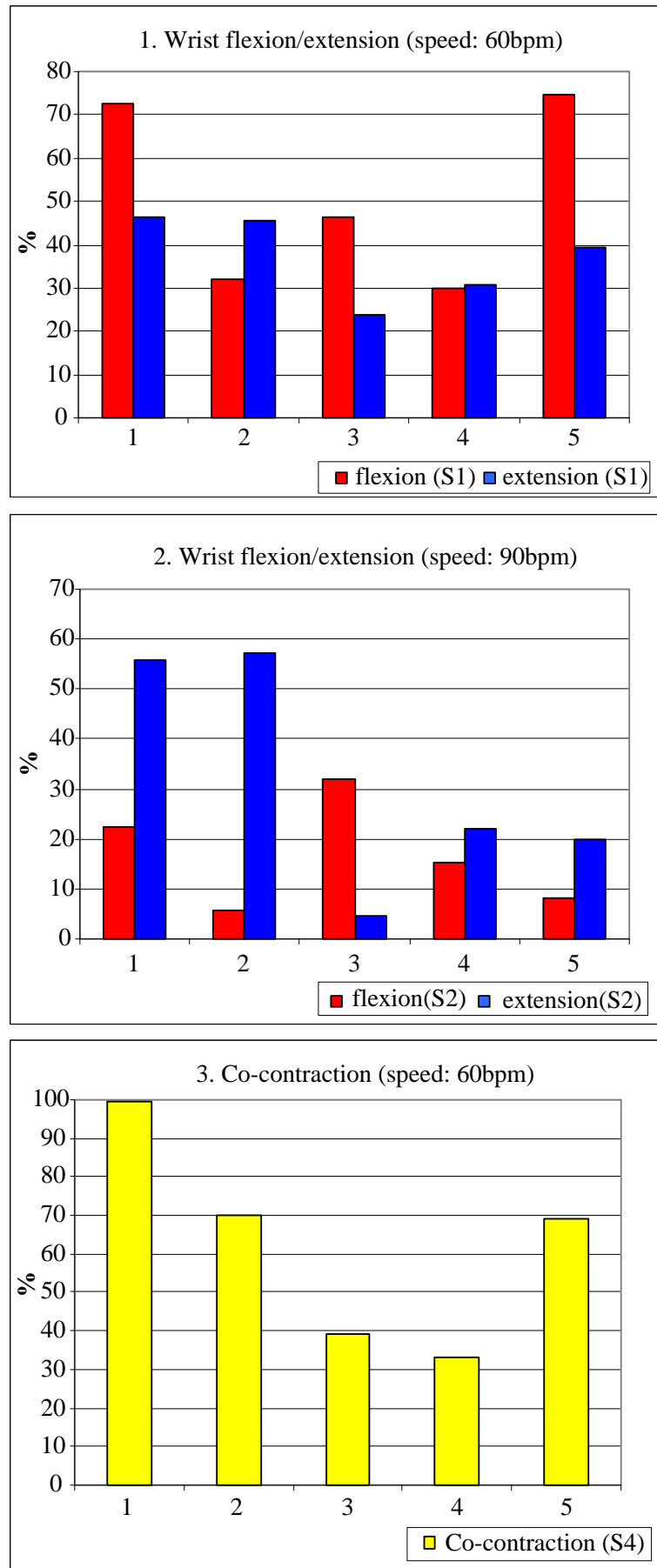
FIGURE 6.8: The accuracy (in %) of the ECS during wrist flexion/extension at 60bpm (SLOW) - top, wrist flexion/extension at 90bpm (MEDIUM) - middle and co-contraction at 60bpm - bottom, for the revised four state system

6.2.1.2 Three state system

The results obtained in the four states system led to a little modification of the classifier design and to develop a three states classifier. The main change is the exclusion of the HIGH speed contraction in the classification system. Using almost the same principles as the previous system, the output states is reduced to three and the operation is as follows:

1. Wrist flexion at a speed of 60bpm	STATE1
2. Wrist flexion at a speed of 90bpm	STATE2
3. Wrist extension at a speed of 60bpm	STATE1
4. Wrist extension at a speed of 90bpm	STATE2
5. Co-contraction at a speed of 60bpm	STATE3

The subject has to do the same procedures as in four states system but only at two speeds which are 60 bpm (SLOW, S) and 90 bpm (MEDIUM, M). The FL classifier has two inputs from the feature extraction of each SEMG signals: ApEn1 (A1) and MAV1 (B1) from the FCU , and ApEn2 (A2) and MAV2 (B2) from ECR. This classifier will discriminate the information from the feature extraction process into three different states namely STATE1 (S1), STATE2(S2)and STATE3 (S3). The MF for the inputs and outputs of the three states system is shown in Figure 6.9.

The rules of the classifier is given in Table 6.3. The first two rules are applied during wrist flexion, rule 3 to rule 4 applied to the wrist extension and the last rule applied to the co-contraction.

TABLE 6.3: IF-THEN rules for the three states system

Rule	A1		B1		A2		B2		State
1	S	&	S	&	R	&	R	THEN	S1
2	M	&	M	&	R	&	R	THEN	S2
3	R	&	R	&	S	&	S	THEN	S1
4	R	&	R	&	M	&	M	THEN	S2
5	C	&	C	&	C	&	C	THEN	S3

Figure 6.10 shows the results of the three states ECS system when a continuous SEMG signals from FCU and ECR during wrist flexion/extension movement at 60bpm were fed to the ECS. The extraction features (ApEn1, MAV1, ApEn2 andMAV2) from both SEMG signals are shown in the first four rows of the plot. The dotted lines with label A is the wrist flexion region and label B is the wrist
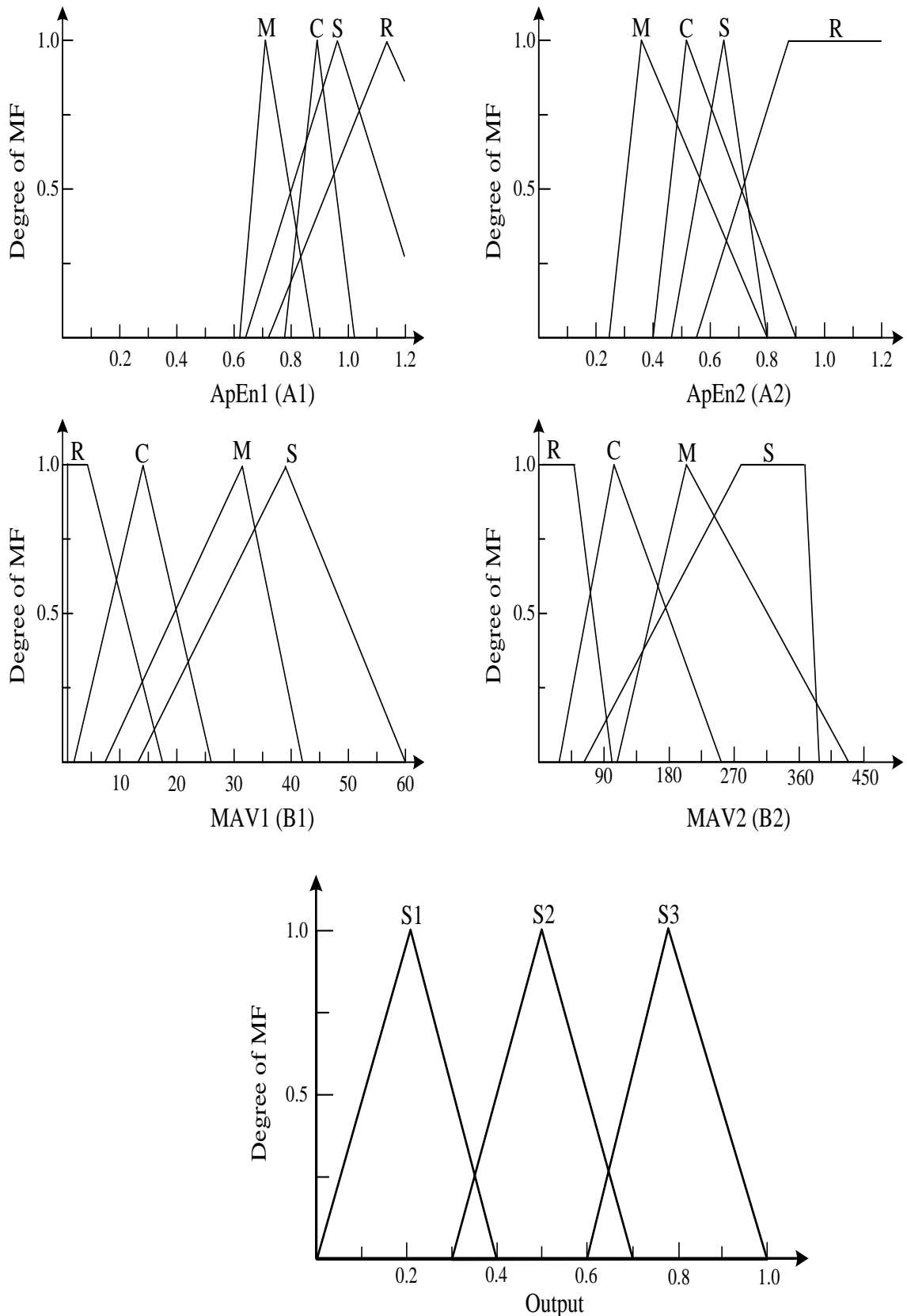
FIGURE 6.9: The input membership function for ApEn1(A1), MAV1(B1), ApEn2(A2), MAV2(B2) and the output for the three states FL classifier.S: SLOW, M:MEDIUM, H:HIGH, C:Co-contraction, R: RELAX

extension region. The ellipses with label (a) and (b) (in the OUTPUT plot) are the classification results corresponding to the wrist flexion and wrist extension respectively. From visual observation, it can be seen that $S1$ was selected during both contractions.

The expanded views for the classification results labeled (a) and (b) are shown in Figure 6.11 and it can be seen clearly that $S1$ (output $= 0 - 0.4$) is selected. Even though glitches can be seen at classification result 2, but the average of the area will still be selecting $S1$.

Some of the classification results during other movements and speeds for this type of classifier are included in Appendix F.

The analysis of the accuracy of the three states system for wrist flexion/extension at 60bpm and 90bpm, and also during co-contraction at 60bpm is shown in Figure 6.12. The same method as the four states ECS system used in the calculation of the accuracy (in %) of the system (see Equation 6.1). At a speed of 60bpm, both wrist flexion and wrist show higher classification accuracy where S1 are selected. The classification rate for both movements is more than 80% except during one analysis where the accuracy is about 42%. However, at a speed of 90bpm, the classification accuracy during wrist extension is much lower compared to during flexion. From the analysis, it shows that better classification is achieved at SLOW speed compared to MEDIUM speed. As for the co-contraction, the average for the accuracy is about 60% and is lower in comparison with the wrist flexion/extension movement.

6.2.1.3   Five state system

The five state system uses a different approach in its design, in comparison with the four and three states system. Unlike the four and three states system that use information during wrist flexion/extension at certain speed in selecting one output state, the five states ECS system uses information from each movement at different speeds to select one output state. The two extracted variables (moving ApEn and MAV) from the two SEMG signals are used as the inputs to the classifier. The same movements and speeds used in the three states system is used in this classifier design. By classifying the extracted features, the system will discriminate one of five different output states namely STATE1(S1), STATE2(S2), STATE2(S3), STATE4(S4) and STATE5(S5). The operation can be explained as follows:
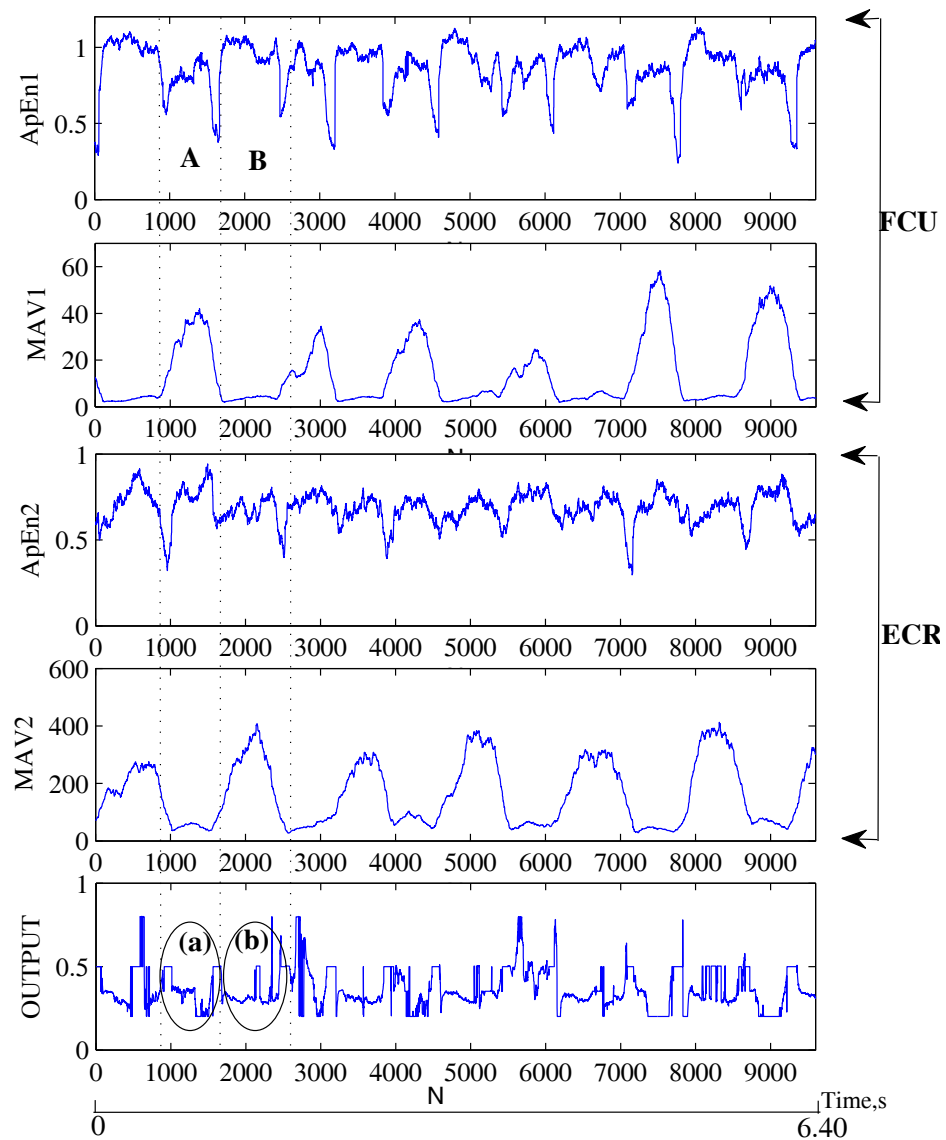
FIGURE 6.10: The classification result of the three states ECS system during wrist flexion (A) and wrist extension (B) at 60bpm
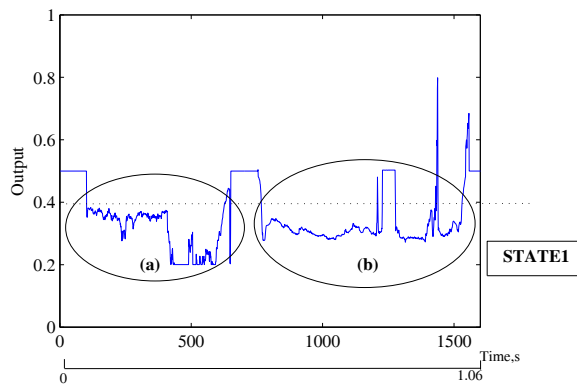

FIGURE 6.11: The expanded view of the classification result (labeled (*a*) and (*b*) in Figure 6.10)
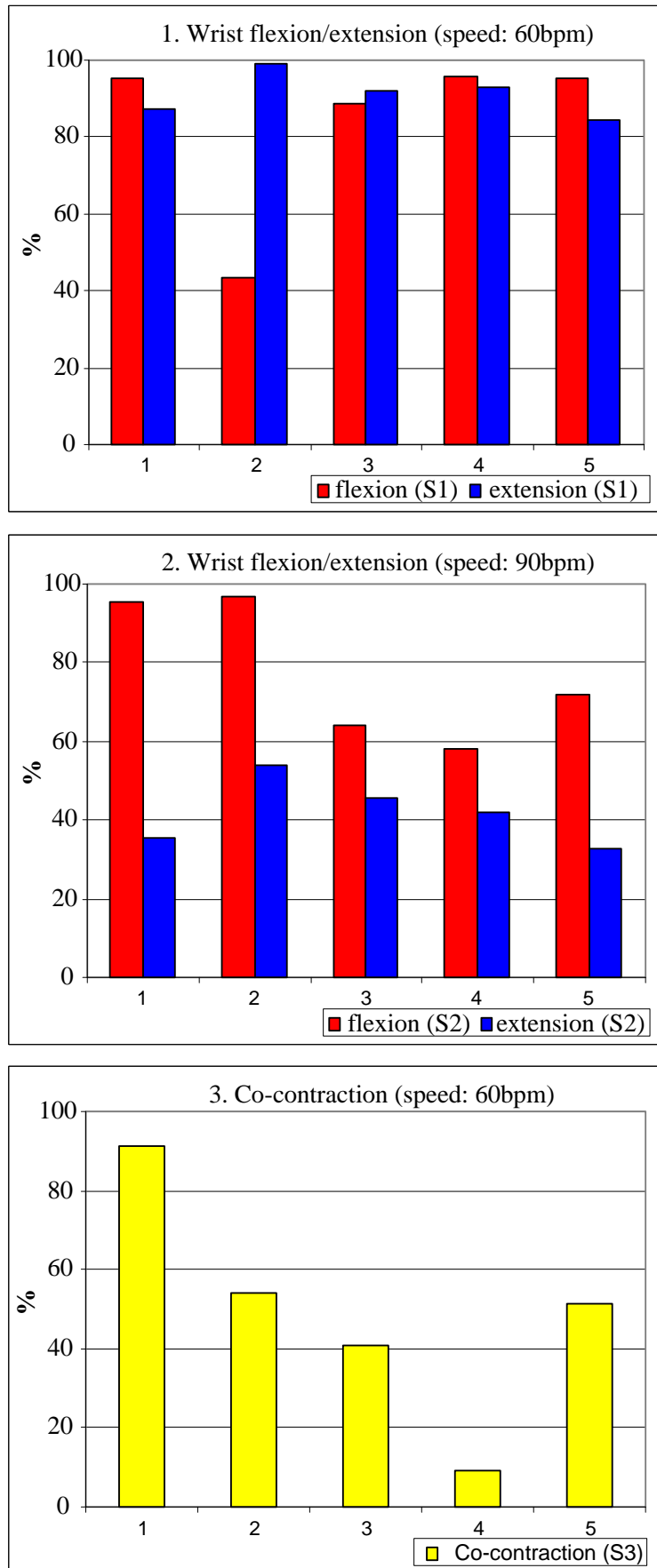
FIGURE 6.12: The accuracy (in %) of the ECS during wrist flexion/extension at a speed of 60bpm (SLOW) - top and 90bpm (MEDIUM) - middle, and co-contraction at a speed of 60bpm - bottom for the three state system

1. Wrist flexion at a speed of 60bpm	STATE1
2. Wrist flexion at a speed of 90bpm	STATE2
3. Wrist extension at a speed of 60bpm	STATE3
4. Wrist extension at a speed of 90bpm	STATE4
5. Co-contraction at a speed of 60bpm	STATE5

The MF for the inputs and outputs of the three states system is shown in Figure 6.13. Table 6.4 shows the rules for the system. Rule 1 and rule 2 will be applied during wrist flexion at speeds of 60bpm and 90bpm respectively. Rule 3 and rule 4 will be applied during wrist extension at 60bpm and 90bpm respectively, the last rule will be applied during co-contraction at 60bpm.

TABLE 6.4: IF-THEN rules for the five states system

Rule	A1		B1		A2		B2		State
1	S	&	S	&	R	&	R	THEN	S1
2	M	&	M	&	R	&	R	THEN	S2
3	R	&	R	&	S	&	S	THEN	S3
4	R	&	R	&	M	&	M	THEN	S4
5	C	&	C	&	C	&	C	THEN	S5

Figure 6.14 shows the classification's result of the five states system when continuous SEMG signals obtained during wrist flexion/extension at a speed of 60bpm were fed to the ECS. The classification results demonstrated that the ECS is able to select two different output states from two different movements. For instance, the dotted lines in the plot shows the processes during wrist flexion (labeled A) and wrist extension (labeled B) and the classification result (label (a) - (S1) and (b) - (S3) respectively) is shown in the bottom plot.

The closed up view of the classification result for label (a) and (b) are shown in Figure 6.15. The plot shows that $STATE1$ (output range: 0 - 0.27) is selected during wrist flexion and $STATE3$ (output range: 0.48 - 0.78) is selected during wrist extension at a SLOW speed. The averages of both areas were calculated and gave one final number which is the correct output of the system.

Some of other classification results during other movements and speeds for this type of classifier are included in Appendix G.

The accuracy of the ECS is then determined using the same method (see Equation 6.1) as mentioned in the previous systems. Figure 6.16 shows the performance of the system during wrist flexion/extension at SLOW speed (top plot), MIDDLE speed (middle plot) and co-contraction at SLOW speed (bottom plot). In comparison for the wrist flexion at two different speeds, more robust selection is made
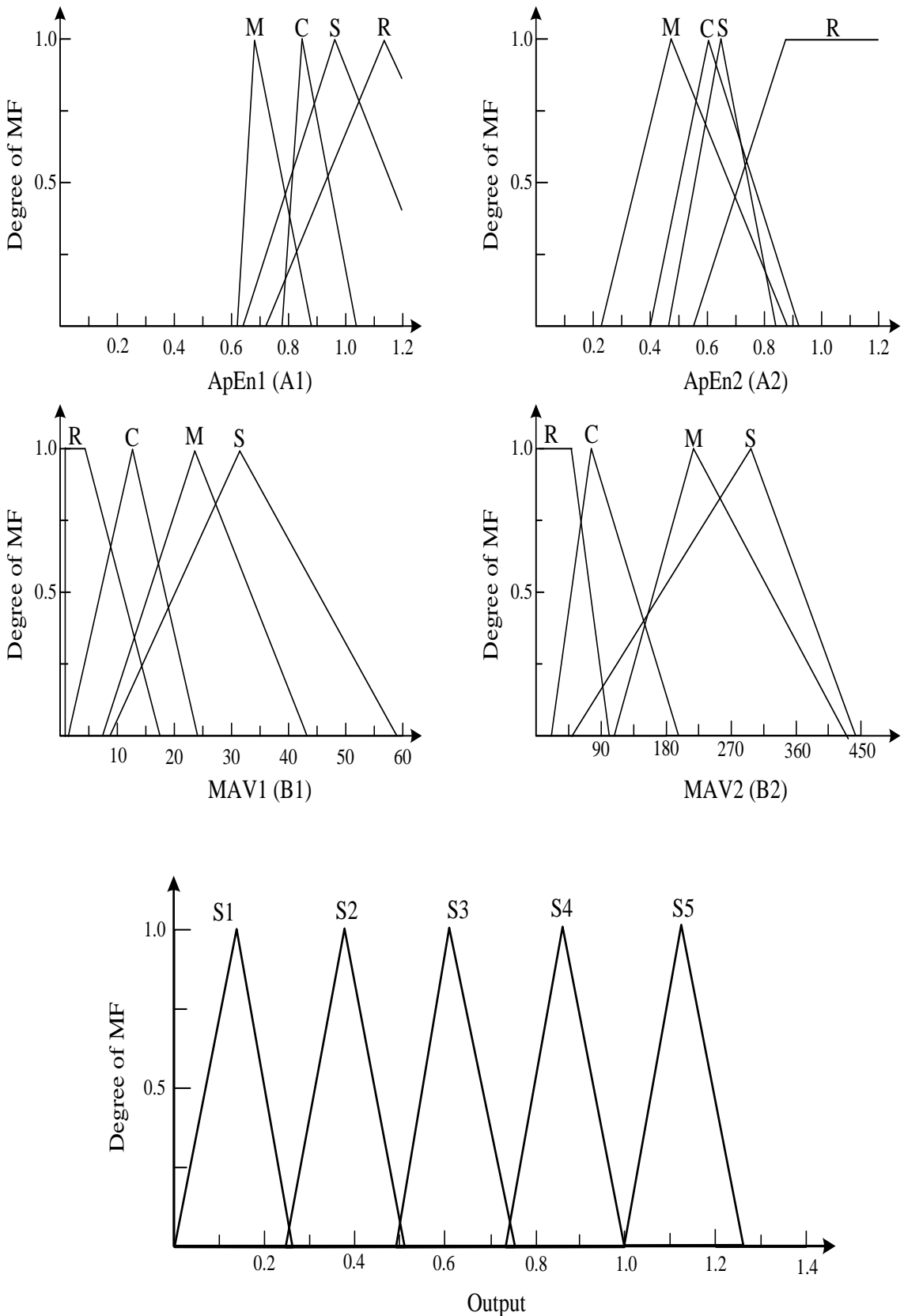
FIGURE 6.13: The input membership function for ApEn1(A1), MAV1(B1), ApEn2(A2), MAV2(B2) and the output for the five states FL classifier. S: SLOW, M:MEDIUM, H:HIGH, C:Co-contraction, R: RELAX
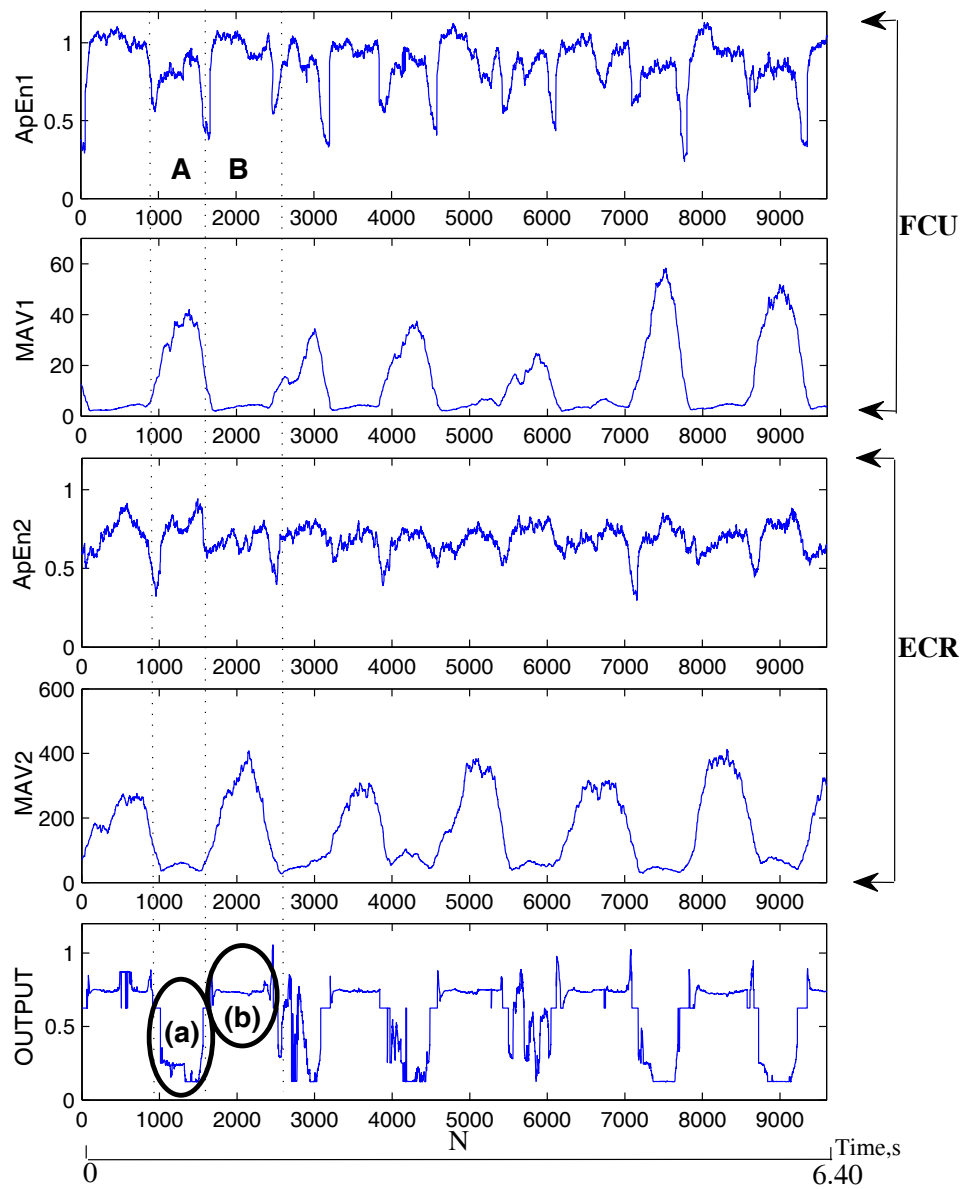
FIGURE 6.14: The classification result of the five states ECS system during wrist flexion (*A*) and wrist extension (*B*) at 60bpm
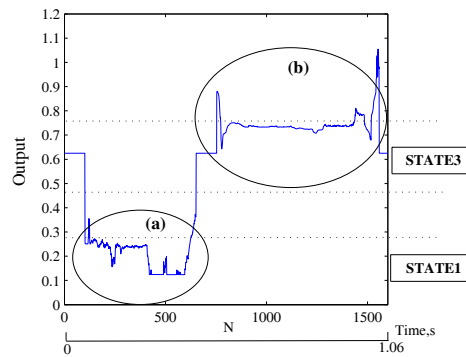

FIGURE 6.15: The expanded view of the classification result (labeled (*a*) and (*b*)) in Figure 6.14

during the MEDIUM speed where the classification rate is between 65% to 100% and 39% to 88% in SLOW speed. The classification rate during wrist extension and wrist flexion movement at the SLOW speed is about the same where the range is from 40% to 90%. At MEDIUM speed, the classification rate during wrist extension is much low compared to wrist flexion which is about half of it. The analysis shows that the five states system could perform better classification during wrist flexion/extension compared to during co-contraction.

6.2.2 Classification based on the contraction state

As can be seen in the moving ApEn analysis, distinct pattern can be seen at different states of contraction where dips can be seen at the start and end of a contraction. The classifier uses the information on the contraction's state which are start, middle and end of a contraction to discriminate four different grip postures.

Still using the information from two SEMG signals, the subject has to do the same two movements which are wrist flexion/extension and co-contraction except that, the movements can be performed at their convenience as this classifier type is not based on the contraction speed. The operation of the system is as follows:

1. Wrist flexion at the START of a contraction	STATE3
2. Wrist flexion at the MIDDLE of a contraction	STATE2
3. Wrist flexion at the END of a contraction	STATE1
4. Wrist extension at the START of a contraction	STATE1
5. Wrist extension at the MIDDLE of contraction	STATE2
6. Wrist extension at the END of a contraction	STATE3
7. Co-contraction at the START of a contraction	STATE4

The feature extraction of the two SEMG signals gives six features: ApEn1 (A1), MAV1 (B1), kurtosis1 (C1) from the FCU and ApEn2 (A2), MAV2 (B2) and kurtosis2 (C2) from ECR. For the inputs MF, the states of a contraction is used as the fuzzy set which are START(S), MIDDLE (M) and END (E) of a contraction and also when the muscle is relaxed (R). This classifier will discriminate the information from the feature extraction process into four different states namely STATE1 (S1), STATE2 (S2), STATE3 (S3) and STATE4 (S4). Figure 6.17 shows the MF for the inputs and the output of the system.

The rules are given in Table 6.5. The first rule is applied to wrist flexion (only FCU contracts), rule 2 to rule 5 apply to wrist flexion/extension (both FCU and ECR contract alternately), rule 6 apply to wrist extension (only ECR contracts)
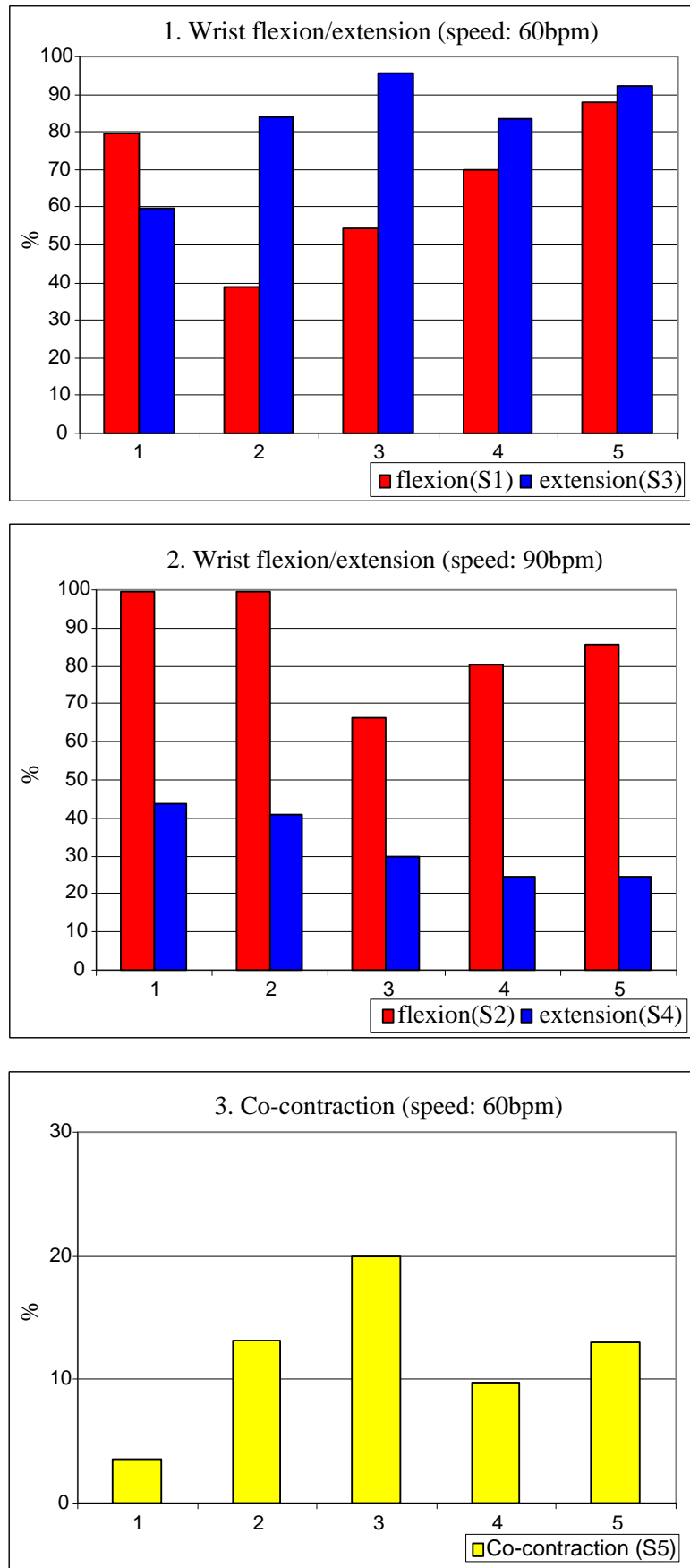
FIGURE 6.16: The accuracy (in %) of the ECS during wrist flexion/extension at a speed of 60bpm (SLOW)- top and 90bpm (MEDIUM)- middle, and co-contraction at a speed of 60bpm - bottom for the five state system
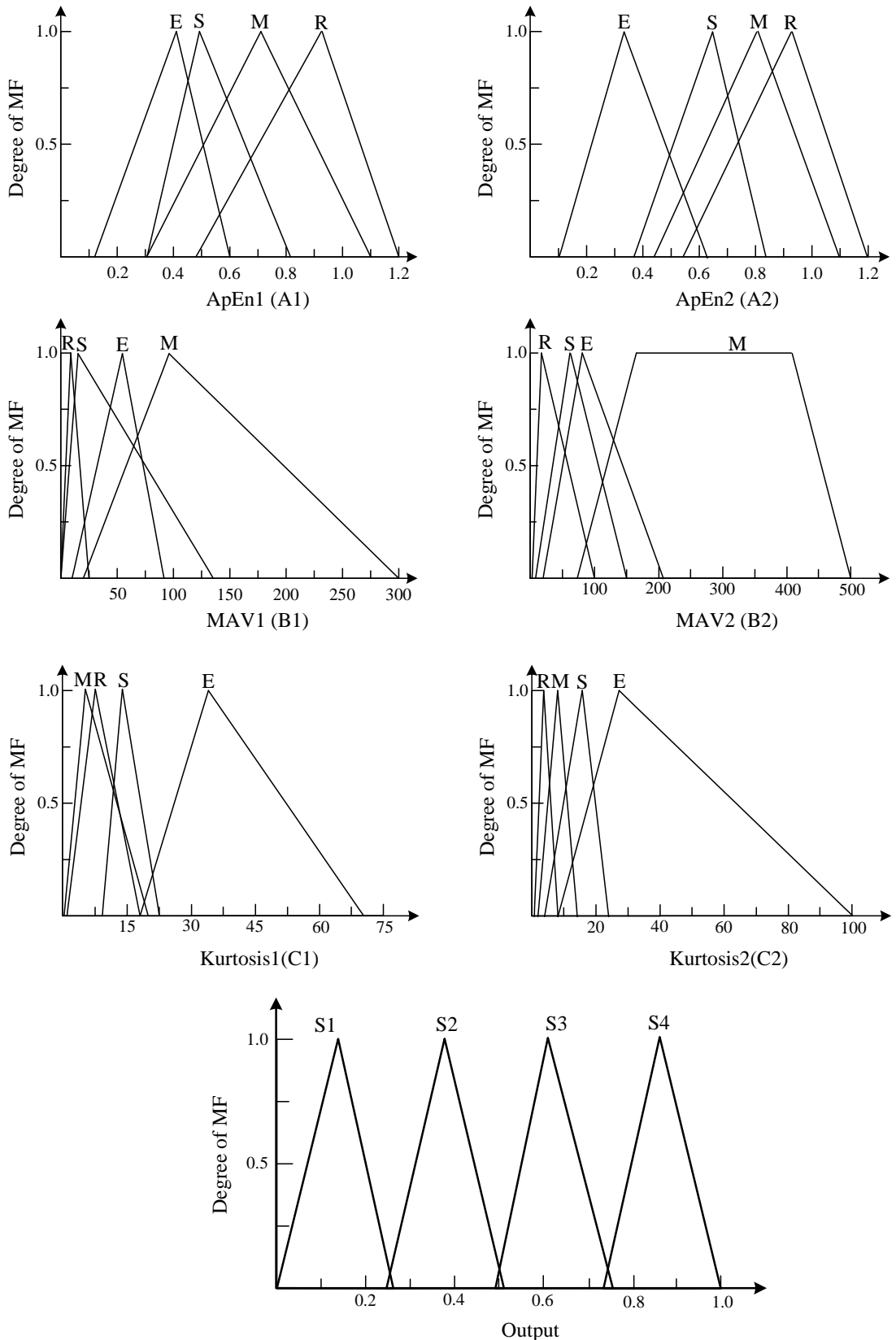
FIGURE 6.17: The membership function for the inputs and output of the four states system for the state based classifier. The first top three rows are the MF inputs and the bottom row is the output.

TABLE 6.5: IF-THEN rules for the state based classifier

Rule	A1		B1		C1		A2		B2		C2		State
1	S	&	S	&	S	&	R	&	R	&	R	THEN	S3
2	S	&	S	&	S	&	E	&	E	&	E	THEN	S3
3	M	&	M	&	M	&	R	&	R	&	R	THEN	S2
4	R	&	R	&	R	&	M	&	M	&	M	THEN	S2
5	E	&	E	&	E	&	S	&	S	&	S	THEN	S1
6	R	&	R	&	R	&	S	&	S	&	S	THEN	S1
7	S	&	S	&	S	&	S	&	S	&	S	THEN	S4

and the last rule applies to the co-contraction (both FCU and ECR contract on the same time).

Figure 6.18 shows the classification result when continuous SEMG signals from FCU and ECR during wrist flexion/extension were applied to the ECS. Three features were extracted for each signal (row 1 to row 6) and the classification result is shown in the bottom plot. Region A and B shown in the plot are the analysis during wrist flexion and label (*a*) and (*b*) are the classification results respectively. From the plots, it can be seen that the classifier is able to discriminate three states (S1 to S3) based on the contraction's state. Appendix H shows some of the classification results during other movements.

Figure 6.19 shows the expanded view of the classification result for the first and second contraction (labeled (*a*) and (*b*) respectively in Figure 6.18). It can be seen clearly that different output are selected at different states of a contraction during wrist flexion where at the start (S) of a contraction, S3 (output range: 0.5 to 0.76) is selected, S2 (output range: 0.25 to 0.52) is selected at the middle of a contraction and S1 (output range: 0 to 0.26) is selected at the end of a contraction.

The accuracy of the classification during wrist flexion/extension is calculated as shown in Figure 6.20. The same method used in calculating the accuracy in speed based classifier is also used for this type of classifier. From the plots, they show that the classifier could select the right output state during middle of a contraction very accurately during wrist flexion and wrist extension, where the accuracy is between 95% to 100%. Lower accuracy can be seen in the start and end of a contraction for both movements and the percentage range from 20% to 80%.
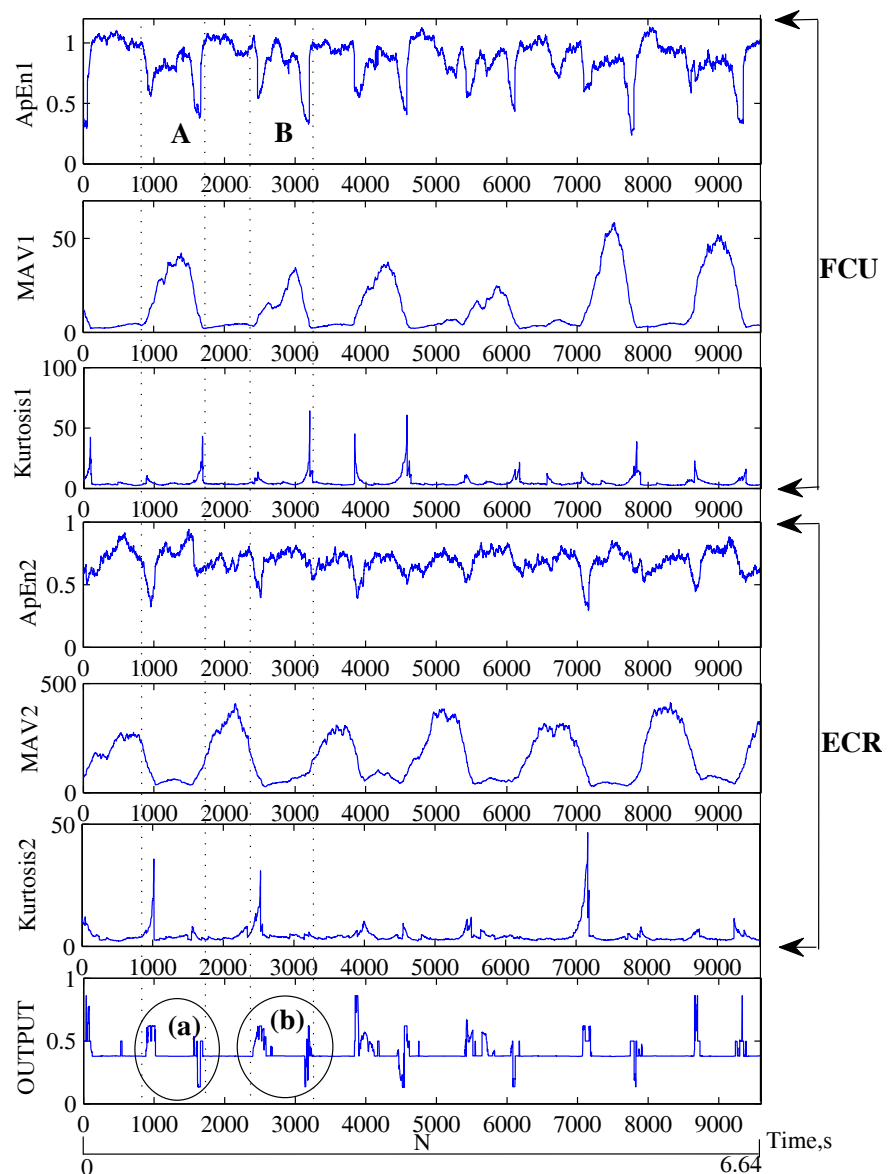
FIGURE 6.18:   The classification result of the state based ECS during wrist flexion extension
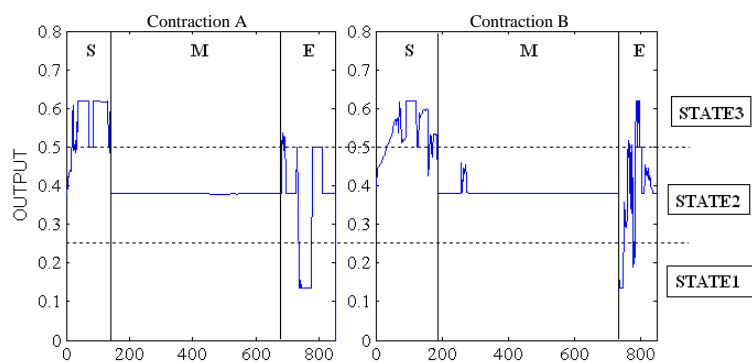
FIGURE 6.19:   The expanded view of the classification results labeled (*a*) and (*b*) in Figure 6.18
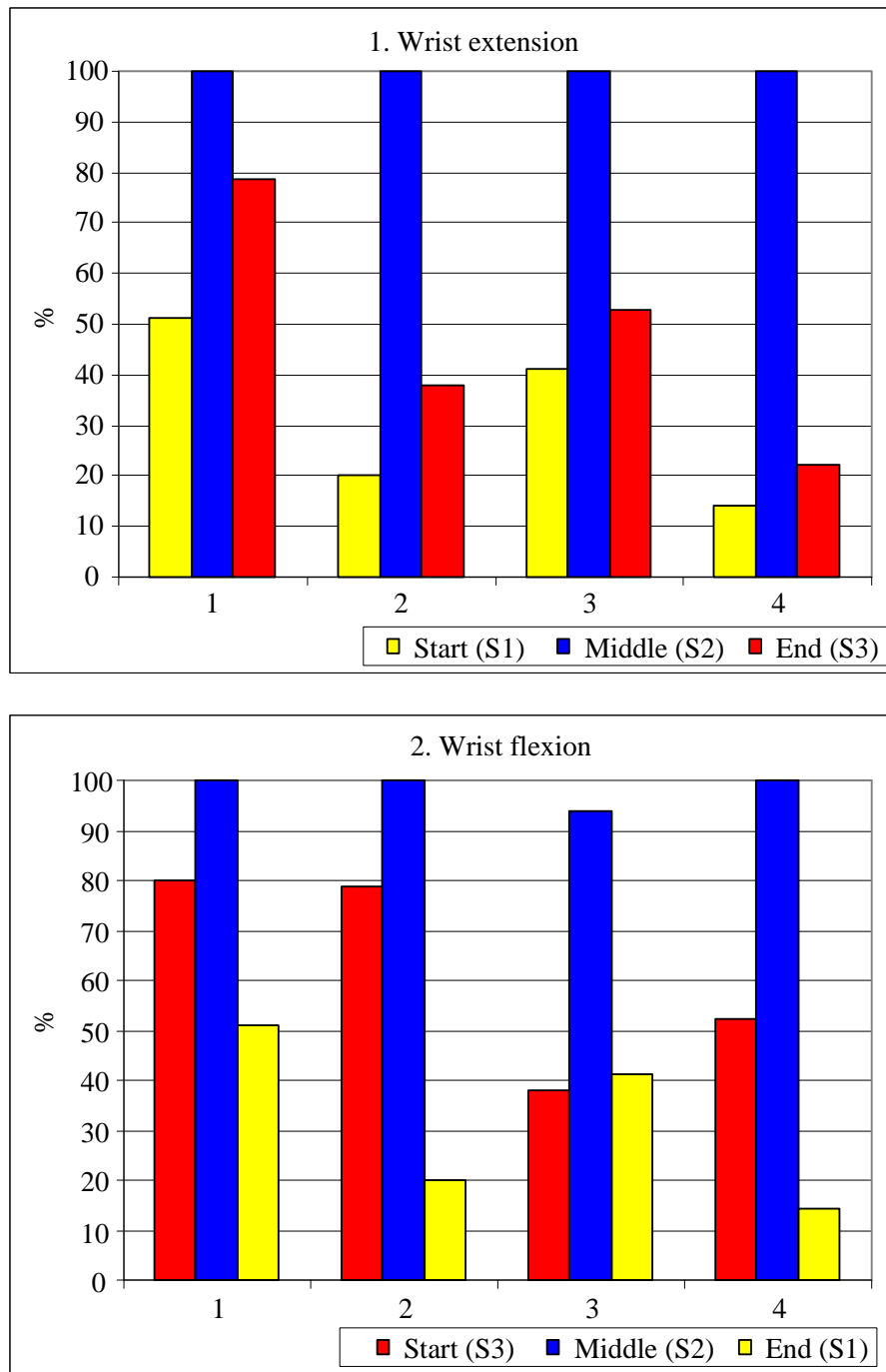
FIGURE 6.20: The accuracy (in %) of the ECS during wrist extension (top) and wrist flexion (bottom) at three states of a contraction; start (S), middle (M) and end (E)

6.3 Discussion

The development of the ECS is discussed and the findings from the development are presented. Two SEMG channels are used as the control channel where there are three different movements; wrist flexion, wrist extension and co-contraction. Even though four movements were investigated as discussed in Chapter 5, only these three movements are used in the ECS development process as they are easier, requiring just a little training by a person.

There are two main components in the ECS which are feature extraction and classification. In the first component, three main methods are used to extract information from the raw SEMG signal and they are moving ApEn, MAV and kurtosis. Three features were extracted from each SEMG signal and two SEMG signals will generate six features. The extracted information are then will be fed to the the second part of the ECS which is the classifier. Two approaches have been tried in designing the classifier for the ECS, which are based on the speed of muscle contraction and based on the state of a contraction.

6.3.1 Speed based classifier

The speed based classifier used the extracted information from different speeds of contraction in determining the final output of the ECS. It focuses on the three speeds of contraction, which are 60bpm (SLOW,S), 90bpm (MEDIUM, M) and 120bpm (HIGH, H). As co-contraction is more difficult to perform in comparison to wrist flexion/extension, it has been set that, a person only needs to do the co-contraction at one speed which is 60bpm. Even though it might be difficult for a person to perform different speeds of contraction, it can be done by carrying out a little training to do the movement at different speeds at the initial stage. With minimal training, they could learn how to control their speed of contraction.

Three different (three, four and five states) systems were being tested for this classifier where the difference between each system is how many output states can be selected. The three feature extractions methods were used in the initial stage of the test. However after several cycles of testing, the kurtosis was excluded as it appeared to be little changes for the classifier. Furthermore, for the three states and five state system, the HIGH speed contraction has been excluded in the classifier design as it has shown poor classification results at this speed in the four state system.

Notably, in comparison between wrist flexion/extension and co-contraction, the three, four and five state systems gave robust performance during the first movement at both SLOW and MEDIUM speeds. The average classification rate for the wrist flexion/extension is about 80% and just 50% for co-contraction. However, between wrist flexion and wrist extension, the later movement gives lower classification rate. Also, wrist flexion at SLOW speed give better classification compared to the MEDIUM speed.

With two SEMG control channels, this contraction speed based classifier could select from three to five different output states. From the analysis of the accuracy of the system, it shows that the three states system gives the highest accuracy compared to the other two systems. This is as expected because better selection can be achieved for a system with less functions to be achieved.

6.3.2   State based classifier

The state based classifier used the information from states of contraction to determine the final output state for the system. The states are start, middle and end of contraction. Like the speed based classifier design, this classifier uses two SEMG signals as the control channel where the amputees have to do wrist flexion, wrist extension and co-contraction, and all these movements can be performed at their convenience.

The classification results indicate that this classifier could discriminate different output based on the states of contraction. From the accuracy percentage shown in Figure 6.20, it can be seen that, this type of classifier could give a more robust classification result especially in the middle of a contraction, compared to the start and end of a contraction. In comparison between speed and state based classifier, the later classifier gave better classification rate.

6.4   Summary

The aim of this work is to develop the ECS that is simple in operation and also implementable for real time application. Two methods have been tried in designing the classifier of the ECS, the contraction's speed and state based. It has been found that both methods are able to classify the extracted information in determining

the final output of the system. With two SEMG signals as the control channel, the system is able to select from three to five different grip postures.

Chapter 7

Discussion

7.1 Overview

This thesis is concerned with the development of an ECS based on pattern recognition for prosthetic hands application, emphasizing on a new method, moving ApEn in processing the SEMG signal. By using SEMG signals as control channels, the ECS should able to discriminate one of four different hand grip postures. The system consists of two main components which are feature extraction and classification.

Feature extraction is where information is determined from the SEMG signal and represented in a feature vector. Various methods have been used for this purpose. The research has established a new method, moving ApEn in extracting information from a SEMG signal produced from the wrist muscles. The analysis is looking for any significant patterns that can be observed in the structure of the signal. An investigation of this method has shown new outcomes that are used in the next stage of the ECS development. Apart from moving ApEn, other methods are also used to increase the performance of the system which are MAV and kurtosis.

In the classification stage, the extracted features will be discriminated accordingly to determine the final output of the system. A FL classifier has been used in this work and two types of classifier (contraction's state based and contraction's speed based) are designed based on the findings in the feature extraction stage.

The developed ECS has shown practical and useful results using the methods described above.

7.2 Discussion

7.2.1 Moving Approximate Entropy

Approximate entropy (ApEn) is a method to quantify the regularity of data and has proved useful in other biomedical signal analysis. For example, an investigation of heart rate had shown that a healthy heart has more irregularity in its action than a less healthy heart [Pincus, 1991]. However, this method has not been used widely in SEMG analysis and not in the application for prosthesis control .

Based on the original ApEn algorithm, a new method called moving ApEn has been developed. Moving ApEn is applied to the SEMG signals and the results demonstrated significant patterns at different states of a contraction. Distinct dips can be seen at the start and end of contraction, and higher ApEn values in the middle of contraction. Hudgins et al. [1993] had also reported in the same research field that the SEMG signal contains information at the start of a contraction. The results from the moving ApEn have confirmed their findings analytically.

Besides prosthesis control, this useful information can be used in movement analysis studies to define the onset and end of contraction. A standard method is to measure a SEMG signal at maximum voluntary contraction (MVC) and then to establish a threshold at some low percentage value of this maximum. On exceeding this threshold the start of a contraction is deemed to have taken place. Deciding a value for MVC is subjective since some criterion has to be established, for example averaging over a specified time or using one or several peak values in the SEMG signal. With this method, it finds the start and end of a contraction based on a chosen set of criteria and not on an analytical basis. Differently with moving ApEn, it is very useful as it automatic and unbiased which makes it a good method for the determination of muscle activation pattern that could be used in clinical studies by physiologists and other clinical personnel.

In addition, the investigation on the SEMG signals of healthy people shows that the moving ApEn return values ranging from 0.3 to 1.0 with low SD (≈ 0.1) from one subject to another. A glance at the signal waveform shows that the data varies widely so it would be expected that the ApEn values would also have a wide variation. This is not the case however and is an advantage of using moving ApEn in this field as it provides a very small variation between subjects.

7.2.2   The electromyographic control system

Researchers at the Institute of Biomedical Engineering, University of New Brunswick have work actively in developing signal processing algorithms prosthetics and control system field [New Brunswick University, 2009]. For example, Hudgins et al. [1993] used a single SEMG signal to select five different states. Several methods were used to represent the SEMG patterns and one of them was MAV. ANN was used as the classifier for the control system where the data needed to be trained prior in testing the system. A disadvantage of this system is that use of ANN requires training of a network to extract parameters that are particular to an individual.

In this work, two SEMG signals from the wrist muscles are used as the control channels to the system in selecting different hand grip postures. With the objective to select one of four different grip postures, two muscle signals are sufficient in controlling the system. Moreover, there is a trade off between the number of control channels used and the complexity of the system. For example, more grip postures can be achieved with bigger number of control channels, but this will cause more complexity in implementing the system. On the other hand, one control channel will give simpler system implementation but with limited functionality.

The success of an ECS based on pattern recognition depends on the appropriate selected feature used to extract information from the SEMG signals. Moving ApEn has shown that it is useful for prosthesis control application. In moving ApEn calculation, the value is obtained in a 200 samples data window and the next value is obtained in the next window (same data length). The adjacent window is delayed by one point ($0.7ms$) and gives high data rate of ApEn. This arrangement make the changes of ApEn values can be tracked easily and respond very quickly. This gives a good transient performance as the controller could respond quickly to the changes. Also, this is another advantage on the developed system as the response time is critical to the acceptance of an ECS to the user of artificial hand.There are several factors that may affect the performance of the extraction process. This includes the electrode placement and the muscle strength during the SEMG signal acquisition.

The classifier function is to map different patterns of the extracted features and match them appropriately in determining the final output of the system. A FL classifier is used in this work. Even though ANN has been the most widely used method for this purposes, FL system is chosen because it provides simple and

robust operation. Furthermore, FL requires no training in its operation and this is an advantage of the developed system as it fits with the behavior of ApEn that has a small SD. This means, the transferable of the system between one person to another is easier to be done with a little adjustment needed. However, the use of neuro-fuzzy or ANN might improve the classifier performance as appropriate information from the individual is used but adopting one of these methods would result in a loss of the generic nature of ApEn.

The whole ECS was implemented on a personal computer (2.00GHz Intel$^{\circledR}$ Pentium, 2.00GB memory) using Matlab 7.5 and Simulink 2.2 to simulate the algorithm. For 200 samples of SEMG data, the processing time until the final decision is made takes about $16ms$. This time is within the acceptable time frame for prosthetic hand control application and this value is small compared to the maximum acceptable delay of about $200ms$. Furthermore, the processing time is also depends upon the system used and this can be improved in order to have a faster processing time.

In the developed ECS, with moving ApEn values that have low variance and simple and robust operation of the FL classifier, the ECS performance is good in selecting the correct output state during wrist flexion and wrist extension movement. For example, 100% classification rate is achieved in the contraction state based classifier and an average of 90% classification rate is achieved in the three state contraction speed based system. A lower classification rate is obtained during co-contraction which is range from 10% to 99% for both types of classifier design. Due to the large variation of the classification rate, it is not recommended to use this movement in the control system.

One immersing question is what is the acceptable classification rate to a user of the system? An example is how many times is it acceptable for the system to misclassify the selection of a power grip when carrying out an activity of daily living such as pouring water into a bottle. Out of ten trials, for a normal person, is one failure acceptable? Naturally a person will occasional 'malfunction' and grasp an object in a posture that is not appropriate to its shape, size and texture. The rate that this happens will vary. However from the user point of view, there is an acceptable level for the classification rate of the system. This can be seen in the projection plot of number of misclassification verses the number of trials carried out shown in Figure 7.1 for classification rate between 90% to 99%. Both x- and y- axes are in log scale with multiple ranges in one segment. It can be seen that for up to $100,000$ trials, the system might misclassify the inputs up to

$10,000$ times at a 90% classification rate. With this number of misclassification, most probably the users will not be happy with the system as they expect a much better rate. 4. There is no study to judge on the acceptable classification rate for the ECS. However, for this work, it aims for a classification rate more than 90% which has been achieved.
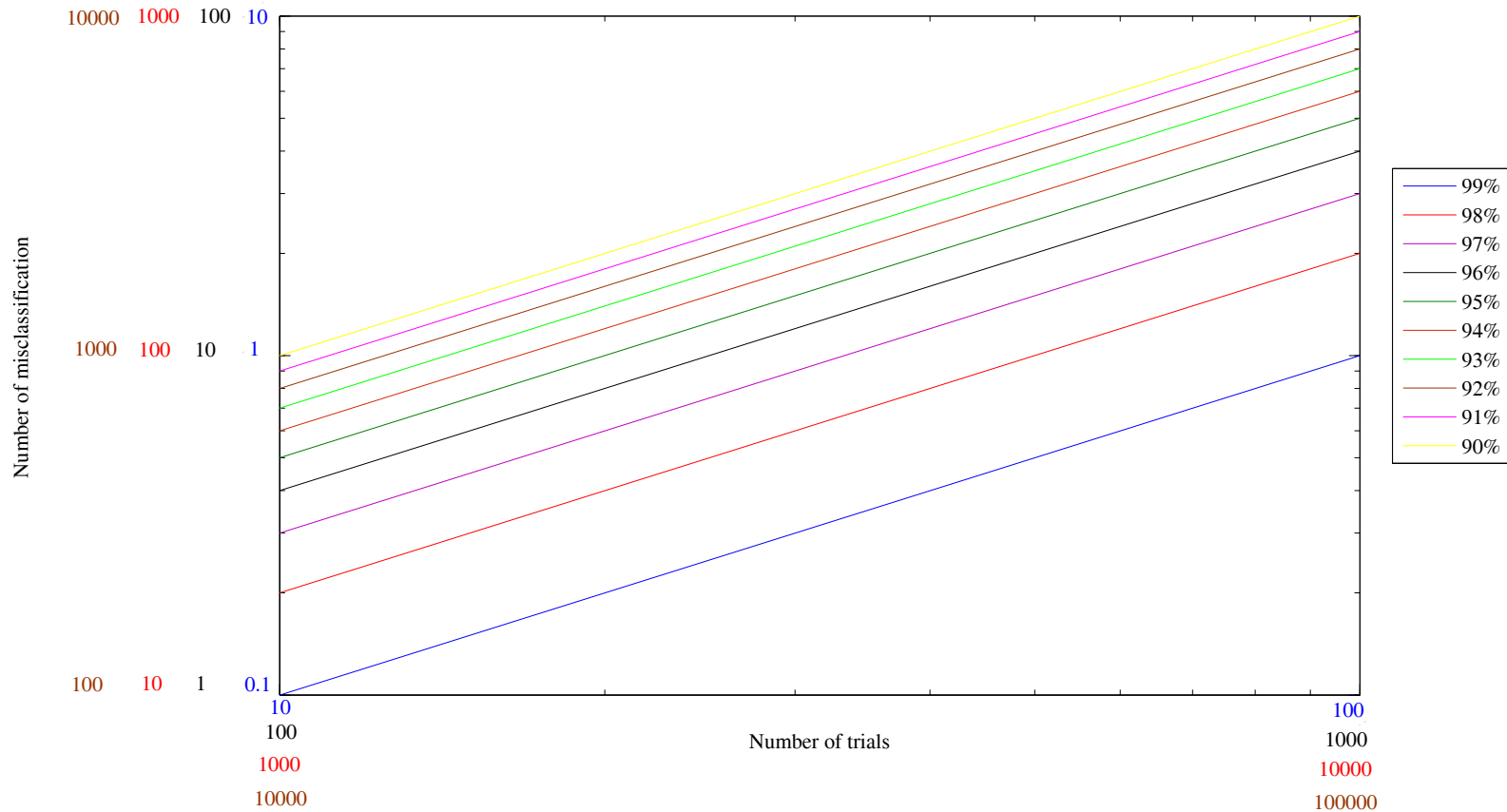
FIGURE 7.1: The misclassification error projection for numbers of trial for classification accuracy between 90% to 99%

Chapter 8

Conclusions and Future Work

8.1 Conclusions

The control algorithm for an upper limb prosthesis is one of the the most important factors in its design. There has been continuous research where the main aim is to mimic the functionality and control of the natural human hand. Since the 1970s, the EMG signal has became the most robust control method in controlling a prosthesis.

This research highlighted the development of the ECS for prosthetic hand application, specifically the Southampton Hand. Dual SEMG signals, used as the control channels, can be derived from normal contraction and can be performed with little training. The signals are acquired during wrist flexion, wrist extension and co-contraction. It emphasizes the new developed method, moving ApEn, that is used to extract information from the SEMG signal and then used with a FL classifier to select the final output. The developed control system aims to be simple and fast which would allow an amputee to select at least four different hand grip postures.

By employing moving ApEn as the main method, an investigation of the SEMG from the wrist muscles (FCU and ECR) of twenty healthy participants was carried out. Several other methods were investigated namely SampEn, MAV, NoZC, SD, skewness and kurtosis. The main conclusion drawn from the investigation was, moving ApEn, MAV and kurtosis have shown distinct patterns in the SEMG structure, while other methods had shown no significant findings and were excluded for further analysis. These three methods were used in the classification stage of the ECS.

The main finding from the moving ApEn analysis on normal healthy subjects is that the values range from 0.3 to 1.0. Furthermore, significant patterns can be seen at three states of contraction, namely start, middle and end. These were also detected using recurrence plots. Moving ApEn returns a value between 0.43 ($SD = 0.10$) and 0.58 ($SD = 0.12$) at the start of a contraction and this is consistent for all movements and speeds of contraction. This shows that the SEMG is more regular (lower ApEn) at this state compared to the middle of a contraction where moving ApEn increases to above 0.7 ($SD = 0.09$), which shows less regularity in this state. At the end of all the contractions, the moving ApEn values drop again to the range between 0.35 ($SD = 0.10$) and 0.60 ($SD = 0.06$) for all movements and speeds of contractions which show there is regular SEMG activity in the flexor/extensor muscles. As expected, when the muscles are relaxed, there is very minor muscle contraction activity except noise from the acquisition system, where moving ApEn gave a value greater than 0.8 ($SD \approx 0.08$). This shows that the ApEn analysis of an SEMG signal does not depend on an individual subject and has low SD between subjects. MAV and kurtosis are also used in processing the SEMG signal at the feature extraction stage to strengthen the performance of the ECS.

Furthermore, except for the MAV analysis, the findings from the ApEn and kurtosis analysis maybe explained by the behavior of muscle contraction relative to the recruitment order of motor units. This idea is supported by evidence from experiments found in the literature on the physiology of muscles [Van Cutsem et al., 1998; Morrison et al., 2007; Stots & Bawa, 2001; Romaiguere et al., 1993].

A FL classifier is used in selecting the final output of the system. Two methods have been used to design the classifier, which are speed based and state based system. The state based classifier used the information of the states of contraction in selecting the final output of the ECS. The states are start, middle and end of a contraction. With this type of classifier, three output states can be selected from one contraction. It has been shown that this type of classifier could produce the final output accurately and gave robust performance, especially at the middle state of contractions. The highest classification rate is achieved during the middle of a contraction where it produced an accuracy of 100% with only one state (see Figure 6.20) producing 98%. The classification rate at the start and end of a contraction produced a wide range from 15% to 80%.

For the speed based classifier design, outputs with three, four and five states

have been investigated. The difference between these three systems is the number of output states (grip postures) that can be achieved. All these systems used speed of contraction information in discriminating the final output of the system. They used information in the wrist movement at SLOW, MEDIUM and HIGH speeds, and three features: ApEn, MAV and kurtosis. However, as the development progressed, it was determined that moving ApEn and MAV are sufficient in determining the final output of the system. Also, better classifications were achieved at SLOW and MEDIUM speeds but not at HIGH speed. Hence, the HIGH speed movement was excluded in the three and five states system. The investigation shows that a better selection can be achieved on the three states system (98% classification rate), slightly degraded performance can be seen in five states system (93%) and the four system gave a classification rate about 85%.

From the investigation of both speed based and state based classifier, both are able to discriminate the features accordingly using a fuzzy logic system. For both types of classifier, the classification accuracy is between 85% and 100%, where 98% classification rate was achieved in the three states system of the speed based and for the state based, a classification rate 100% was achieved. The same rate of 98% was achieved by Englehart et al. [2001] which is the highest rate cited in the literature.

Using a standard personal computer, the time taken to calculate one ApEn value is $16ms$. It is conjectured that the implementation of this algorithm using a modest microcontroller will take a similar time. The ApEn algorithm can be executed in a standard 8-bit microcontroller. For example, Microchip PIC16F688 microcontroller is a 8-bit architecture with 5.00MHz clock speed, 256KB memory and has all the instruction sets required for the ApEn algorithm implementation.

This research has demonstrated the development of an electromyographic control system using a new method, moving ApEn. A FL classifier can select at least four different grip postures in a robust manner and most importantly, requires no training. The basic system operation has been successfully developed and tested. Upon applying the system to amputees, only simple adjustments will need to be made for each person. The long term objective of this research is to design and build the Southampton Hand System which consists of the artificial hand and a robust control system.

8.2   Future Work

Some areas can be explored in improving the developed control system performance and are described as follows:

1. Further evaluation of the ECS.

   The following is a brief description of what can be done in evaluating the performance of the system:

   - Use of different types of classifier.

     As previously discussed, ANN is the most used method in classifying the features. Even though the developed ECS has shown its usefulness in classifying the data, a further evaluation, using ANN is needed and may improve the system performance. In addition to that, a neuro-fuzzy classifier could also be investigated as it is a combination of ANN and fuzzy logic. Both of these methods would require training data from the individual user of the system which is a disadvantage.

   - Use of different data sets.

     In this work, the system was tested with SEMG data from normal healthy people. It is expected that there will be not much difference in the system performance between healthy people and people with amputation. Further study on the ECS that uses amputee's SEMG data from their remnant muscle is needed.

   - Effect of the electrode placement.

     For this evaluation, the sensitivity of the electrodes placement could be investigated on how it will effect the system performance. This can be done by displacing the electrodes by few *cm* from the correct location. From the investigation, a guideline document on acceptable electrodes placement could be made.

2. Implementation of the ECS into a microcontroller

   A complete algorithm of the ECS has been developed, tested and simulated. It is very important to implement the system in a microcontroller for a real time application to provide a practical and small system.

   The most crucial part is to implement the moving ApEn algorithm into a microcontroller. As for the FL classifier, it can be implemented on a standard microprocessor or a dedicated FL integrated circuit which may make the implementation easier.

3. Investigation of the automatic control feedback between the ECS and the artificial hand

   Before the developed ECS is integrated with the actual artificial hand, it can be tested with a model of the hand to investigate the closed loop feedback control operation to securely grip the object.

   A preliminary investigation using a test rig that represent a pinch grip had been built. Appendix I describes the operation of the test rig that consist of three sensing elements; force, acceleration and vibration that represent the main sensors found in a natural human hand. An algorithm to provide force to securely grip the object is also included.

   For future investigations, a slip sensor based on piezoelectric technology developed by the group could be integrated into the system. The slip sensor could work together with the cartridge to detect the vibration when the object starts to slip and prevent it from slipping. Another interesting aspect to explore is using a different shaped objects. For example an object that can move upward when more force is applied. It is anticipated that the experimental tests will present some resemblance to the prehensile processes of human grasping.

4. Integration of the ECS and the Southampton artificial hand

   The integration of the Southampton Hand and the control mechanism is a long term objective as previously discussed. Future work areas should be explored successfully in order to ensure the completion of the integration process. Upon integration of the system, an interfacing mechanism is required to provide the communication between these two structures.

Appendix A

Calculation of ApEn

The example is on random numbers and illustrated in figure A.1.
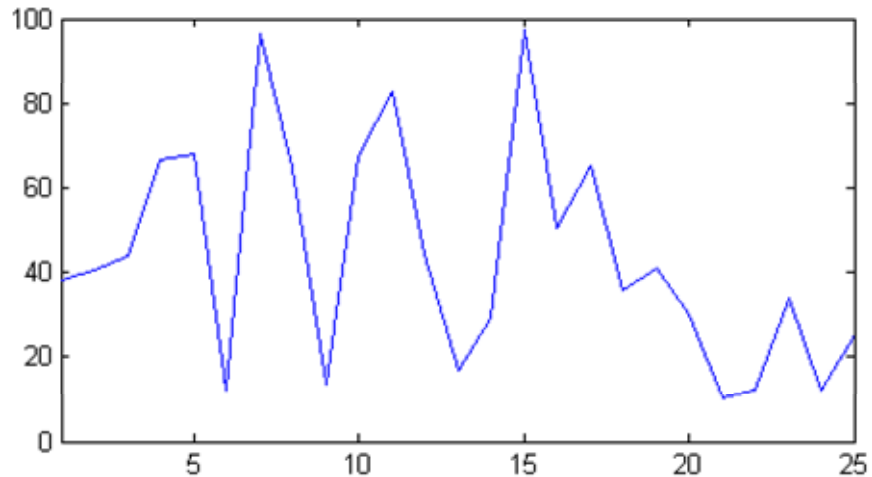
FIGURE A.1: Random numbers for ApEn computation

Given that N = 25, and the sequence X_N consists of 25 samples as follows:

$X_N = \{$ 38.36, 40.58, 43.78, 66.74, 68.15, 12.19, 96.60, 64.53, 13.69, 67.42, 82.92, 44.44, 16.61, 29.35, 97.6, 50.52, 65.4, 35.61, 40.96, 30.29, 10.11, 12.05, 33.9, 12.29, 25.55 $\}$

Let's choose $m = 2$ and $r = 0.2SD$. The SD of the data is 26.2 and this give $r = 5.24$. The m-vectors (Equation 4.1) of $X(i)$ are formed and gave:

Also, $X_i = X_j$.

The most time consuming step in the ApEn computation is the calculation of $C_r^m(i)$. The following steps show how to find $C_r^m(i)$.

107

$$X(1) = \{38.36, 40.58\}$$
$$X(2) = \{40.58, 43.78\}$$
$$X(3) = \{43.78, 66.74\}$$
$$.$$
$$.$$
$$X(24) = \{12.29, 25.55\}$$

The next thing to determine is how many of $X(i)$ that is similar to $X(j)$. By using Equation 4.2 and $r = 5.24$, each of the 2 components in $X(i)$ must be within ± 5.24 of the corresponding component of $X(j)$. For example, $X(1)$ is similar to $X(2)$ but not similar to $X(3)$, since the last component in $X(3)$ (66.74) is different by more than 5.24 units with both components in $X(1)$.

The distance between X_i and X_j, $(d(i,j))$ are obtained using Equation 4.2 and the results are entered in Figure A.2 according to the following rule, $s(i,j) = 0$ if $d(i,j) > r$; $s(i,j) = 1$ if $d(i,j) < r$.

The number of $d[X(i), X(j)] \leq$ r, $N_m(i)$ can be determined from Figure A.2 and an example on how to obtain $N_m(1)$ is shown below:

$N_m(i) = [X(1,1) \cap X(2,2)] + [X(1,2) \cap X(2,3)] + [X(1,3) \cap X(2,4)] + [X(1,4) \cap X(2,5)] + [X(1,5) \cap X(2,6)] + [X(1,6) \cap X(2,7)] + [X(1,7) \cap X(2,8)] + [X(1,8) \cap X(2,9)] + [X(1,9) \cap X(2,10)] + [X(1,10) \cap X(2,11)] + [X(1,11) \cap X(2,12)] + [X(1,12) \cap X(2,13)] + [X(1,13) \cap X(2,14)] + [X(1,14) \cap X(2,15)] + [X(1,15) \cap X(2,16)] + [X(1,16) \cap X(2,17)] + [X(1,17) \cap X(2,18)] + [X(1,18) \cap X(2,19)] + [X(1,19) \cap X(2,20)] + [X(1,20) \cap X(2,21)] + [X(1,21) \cap X(2,22)] + [X(1,22) \cap X(2,23)] + [X(1,23) \cap X(2,24)] + [X(1,24) \cap X(2,25)]$

By referring to Figure A.2:

$N_m(1) = 1+1+0+0+0+0+0+0+0+0+0+0+0+0+0+0+0+1+0+0+0+0+0+0$
$N_m(1) = 3$

Then $C_r^m(1)$ from Equation 4.3 is determined:

$$C_r{}^m(1) = \frac{N_m(1)}{24} = 0.125$$

The above 2 steps are performed over all i for $i = 1, N - m + 1$. Table A.1 shows the $C_r^m(i)$, $N_m(i)$ and their natural logarithm for all i.

Equation 4.4 is performed and gives:

X(i) \ X(j)	38.36	40.58	43.78	66.74	68.15	12.19	96.6	64.53	13.69	67.42	82.92	44.44	16.61	29.35	97.6	50.52	65.4	35.61	40.96	30.29	10.11	12.05	33.9	12.29	25.55
38.36	1	1	0	0	0	0	0	0	0	0	0	0	0	0	0	0	0	1	1	0	0	0	1	0	0
40.58	1	1	1	0	0	0	0	0	0	0	0	1	0	0	0	0	0	1	1	0	0	0	0	0	0
43.78	0	1	1	0	0	0	0	0	0	0	0	1	0	0	0	0	0	0	1	0	0	0	0	0	0
66.74	0	0	0	1	1	0	0	1	0	1	0	0	0	0	0	0	1	0	0	0	0	0	0	0	0
68.15	0	0	0	1	1	0	0	1	0	1	0	0	0	0	0	0	1	0	0	0	0	0	0	0	0
12.19	0	0	0	0	0	1	0	0	1	0	0	0	1	0	0	0	0	0	0	0	1	1	0	1	0
96.6	0	0	0	0	0	0	1	0	0	0	0	0	0	0	1	0	0	0	0	0	0	0	0	0	0
64.53	0	0	0	1	1	0	0	1	0	1	0	0	0	0	0	0	1	0	0	0	0	0	0	0	0
13.69	0	0	0	0	0	1	0	0	1	0	0	0	1	0	0	0	0	0	0	0	1	1	0	1	0
67.42	0	0	0	1	1	0	0	1	0	1	0	0	0	0	0	0	1	0	0	0	0	0	0	0	0
82.92	0	0	0	0	0	0	0	0	0	0	1	0	0	0	0	0	0	0	0	0	0	0	0	0	0
44.44	0	1	1	0	0	0	0	0	0	0	0	1	0	0	0	0	0	0	1	0	0	0	0	0	0
16.61	0	0	0	0	0	1	0	0	1	0	0	0	1	0	0	0	0	0	0	0	0	1	0	1	0
29.35	0	0	0	0	0	0	0	0	0	0	0	0	0	1	0	0	0	0	0	1	0	0	1	0	1
97.6	0	0	0	0	0	0	1	0	0	0	0	0	0	0	1	0	0	0	0	0	0	0	0	0	0
50.52	0	0	0	0	0	0	0	0	0	0	0	0	0	0	0	1	0	0	0	0	0	0	0	0	0
65.4	0	0	0	1	1	0	0	1	0	1	0	0	0	0	0	0	1	0	0	0	0	0	0	0	0
35.61	1	1	0	0	0	0	0	0	0	0	0	0	0	0	0	0	0	1	0	0	0	0	1	0	0
40.96	1	1	1	0	0	0	0	0	0	0	0	1	0	0	0	0	0	0	1	0	0	0	0	0	0
30.29	0	0	0	0	0	0	0	0	0	0	0	0	0	1	0	0	0	0	0	1	0	0	1	0	1
10.11	0	0	0	0	0	1	0	0	1	0	0	0	0	0	0	0	0	0	0	0	1	1	0	1	0
12.05	0	0	0	0	0	1	0	0	1	0	0	0	1	0	0	0	0	0	0	0	1	1	0	1	0
33.9	1	0	0	0	0	0	0	0	0	0	0	0	0	1	0	0	0	1	0	1	0	0	1	0	0
12.29	0	0	0	0	0	1	0	0	1	0	0	0	1	0	0	0	0	0	0	0	1	1	0	1	0
25.55	0	0	0	0	0	0	0	0	0	0	0	0	0	1	0	0	0	0	0	1	0	0	0	0	1

FIGURE A.2: The distance between X_i and X_j according to the following rule, $s(i,j) = 0$ if $d(i,j) > r$; $s(i,j) = 1$ if $d(i,j) < r$

TABLE A.1: The $C_r{}^m$(i),N_m(i) and their ln for m

i	N_m(i)	C_r^m(i)	$\ln(C_r^m(i))$
1	3	0.1250	-2.0794
2	3	0.1250	-2.0794
3	1	0.0417	-3.1781
4	1	0.0417	-3.1781
5	2	0.0833	-2.4849
6	1	0.0417	-3.1781
7	1	0.0417	-3.1781
8	2	0.0833	-2.4849
9	1	0.0417	-3.1781
10	1	0.0417	-3.1781
11	1	0.0417	-3.1781
12	1	0.0417	-3.1781
13	3	0.1250	-2.0794
14	1	0.0417	-3.1781
15	1	0.0417	-3.1781
16	1	0.0417	-3.1781
17	1	0.0417	-3.1781
18	3	0.1250	-2.0794
19	1	0.0417	-3.1781
20	2	0.0833	-2.4849
21	1	0.0417	-3.1781
22	2	0.0833	-2.4849
23	2	0.0833	-2.4849
24	2	0.0833	-2.4849

$$\phi^m(\text{r}) = -2.8217$$

All the above steps are repeated for $m+1$. $C_r{}^{m+1}(1)$ and $\phi^{m+1}(\text{r})$ are determined. Table A.2 shows the values of both parameters for $i = N - m$, and also their natural logarithm.

Equation 4.4 is performed again and give:

$$\phi^{m+1}(\text{r}) = -3.1355$$

ApEn is finally obtained from:

$$\text{ApEn} = \phi^m(\text{r}) - \phi^{m+1}(\text{r})$$

$$\text{ApEn} = 0.3138$$

TABLE A.2: The $C_r{}^m$(i),N_m(i) and their ln for $m+1$

i	N_{m+1}(i)	$C_r^{m=1}$(i)	$\ln(C_r^{m+1}(i))$
1	1	0.0435	-3.1355
2	1	0.0435	-3.1355
3	1	0.0435	-3.1355
4	1	0.0435	-3.1355
5	1	0.0435	-3.1355
6	1	0.0435	-3.1355
7	1	0.0435	-3.1355
8	1	0.0435	-3.1355
9	1	0.0435	-3.1355
10	1	0.0435	-3.1355
11	1	0.0435	-3.1355
12	1	0.0435	-3.1355
13	1	0.0435	-3.1355
14	1	0.0435	-3.1355
15	1	0.0435	-3.1355
16	1	0.0435	-3.1355
17	1	0.0435	-3.1355
18	1	0.0435	-3.1355
19	1	0.0435	-3.1355
20	1	0.0435	-3.1355
21	1	0.0435	-3.1355
22	1	0.0435	-3.1355
23	1	0.0435	-3.1355

Appendix B

ApEn Evaluation for Different m and r
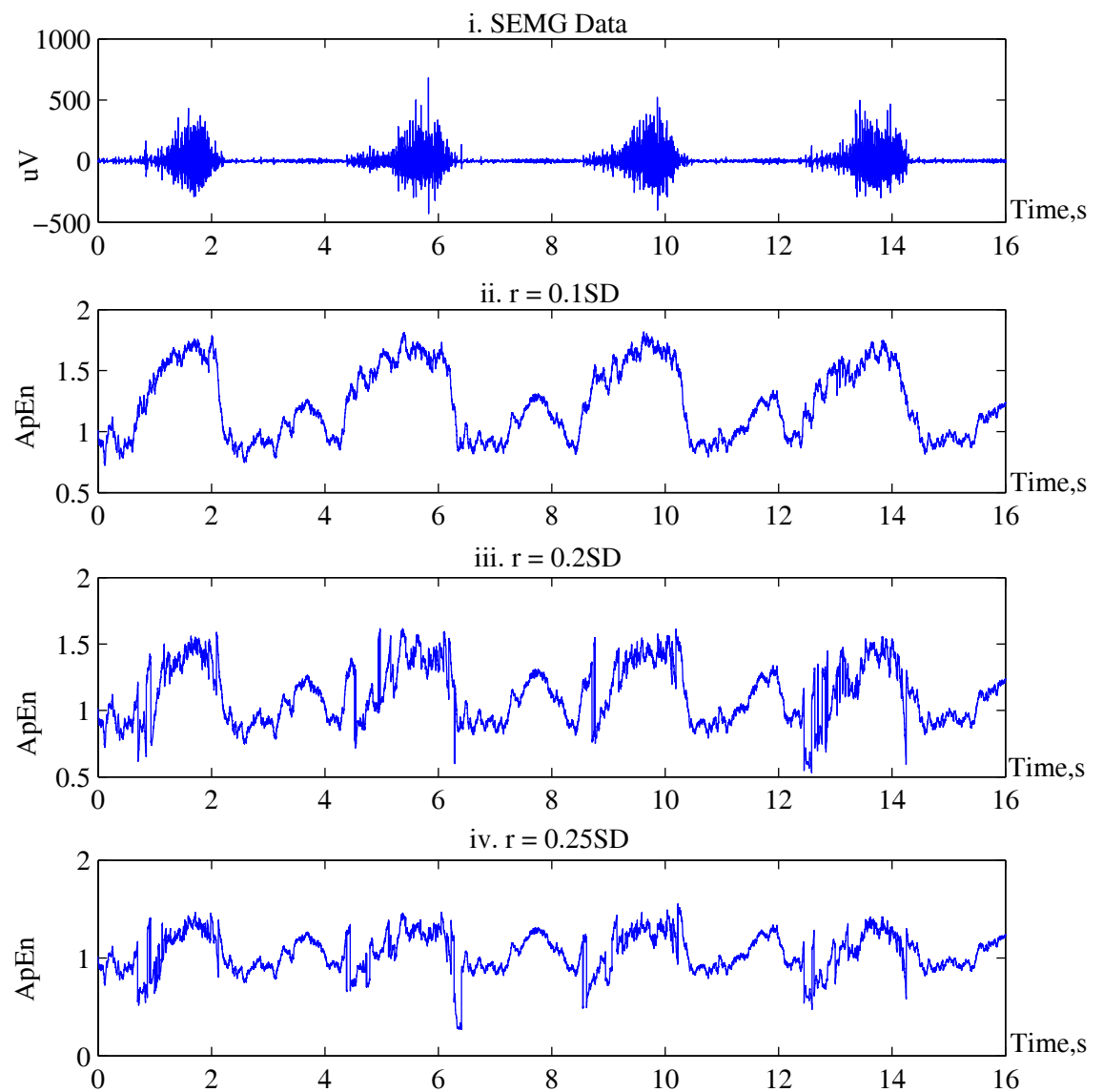
FIGURE B.1: The ApEn evaluation during wrist extension for $m = 1$ and different r; (ii)$r = 0.1SD$, (iii)$r = 0.2SD$ and (iv)$r = 0.25SD$
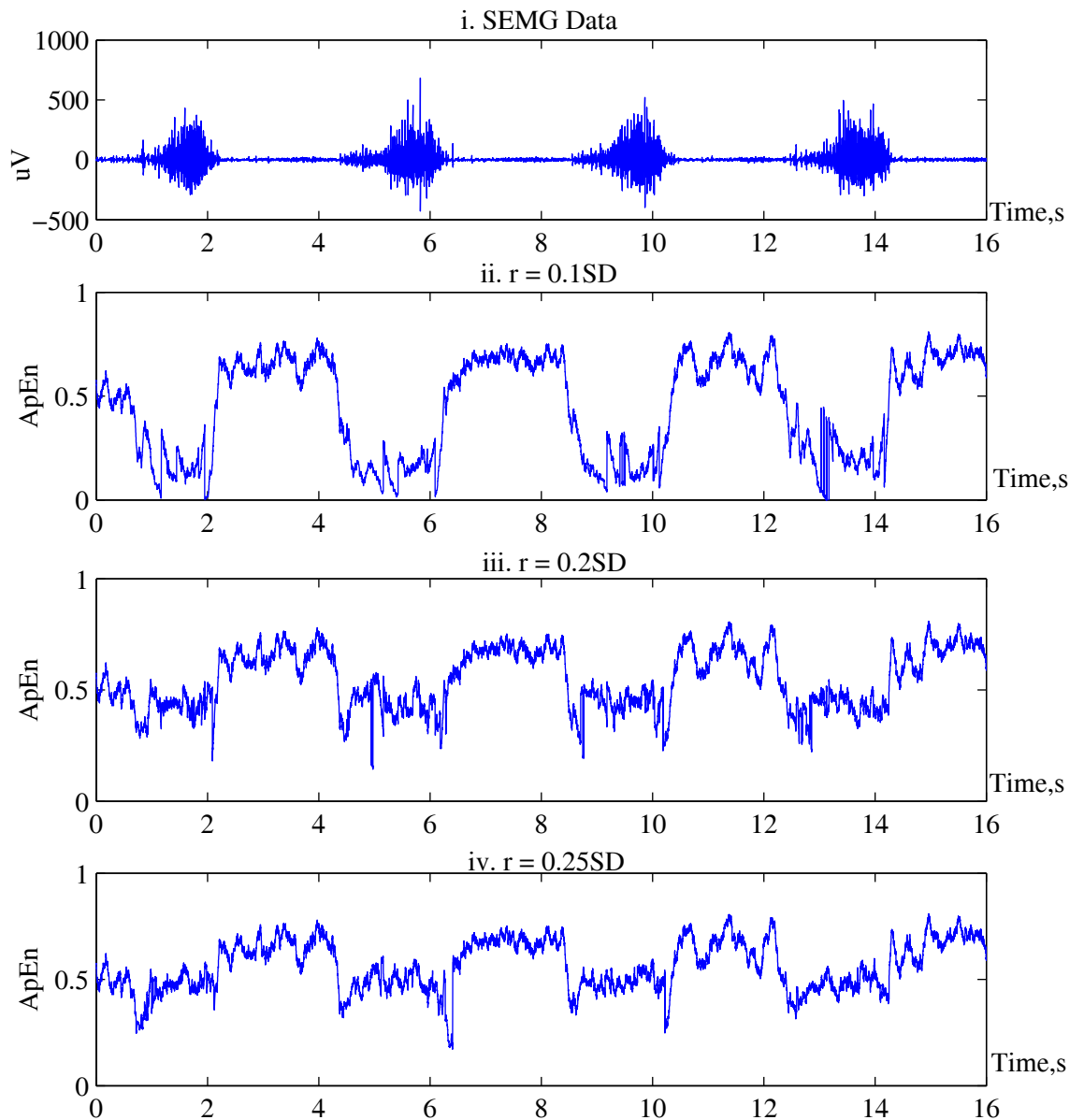
FIGURE B.2: The ApEn evaluation during wrist extension for $m = 3$ and different r; (ii)$r = 0.1SD$, (iii)$r = 0.2SD$ and (iv)$r = 0.25SD$

Appendix C

Results of the feature extraction of the SEMG signals
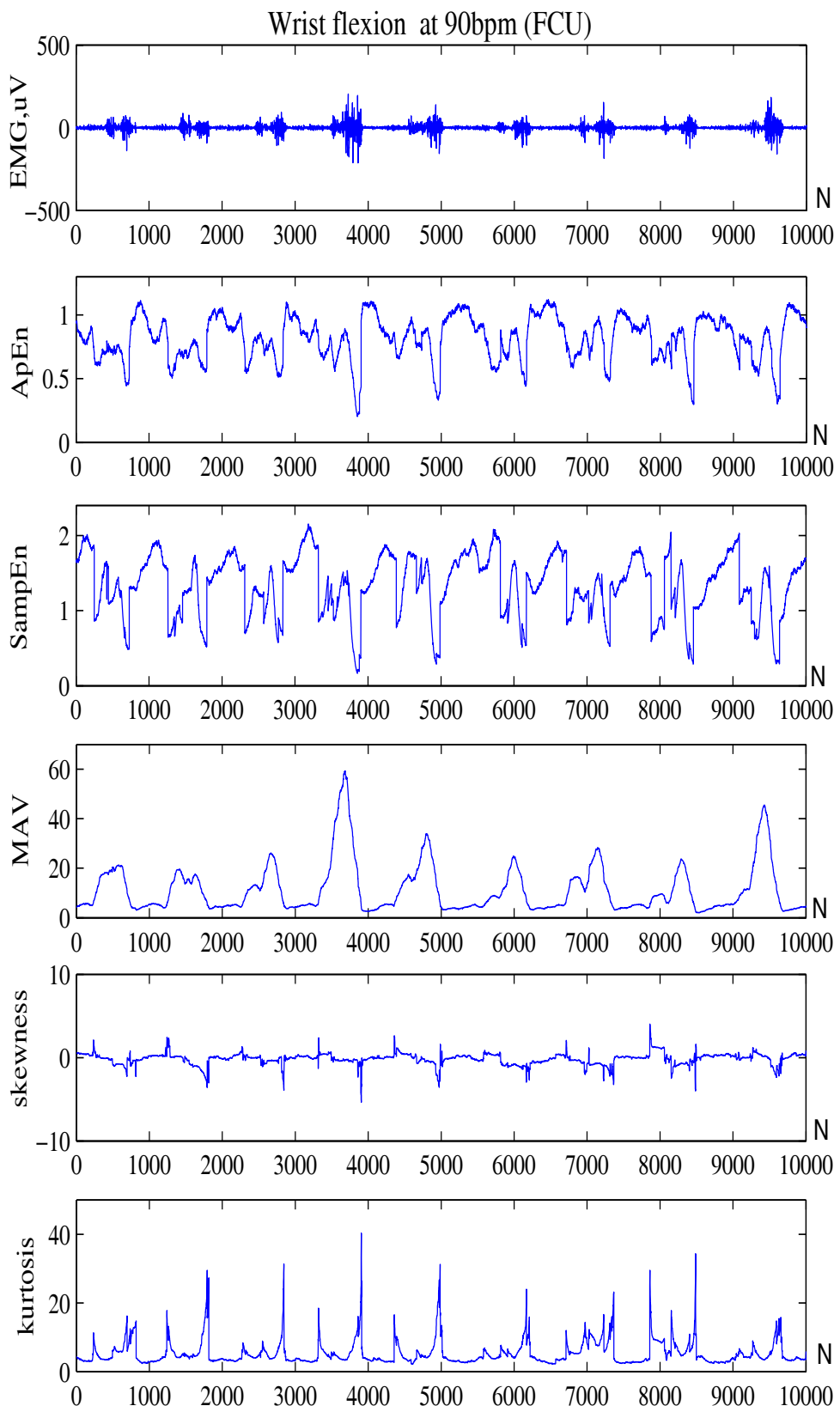
FIGURE C.1: Feature extraction of the SEMG signal during wrist flexion from FCU muscle at 90bpm. From top to bottom: the SEMG signal, ApEn, SampEn, MAV, skewness and kurtosis.
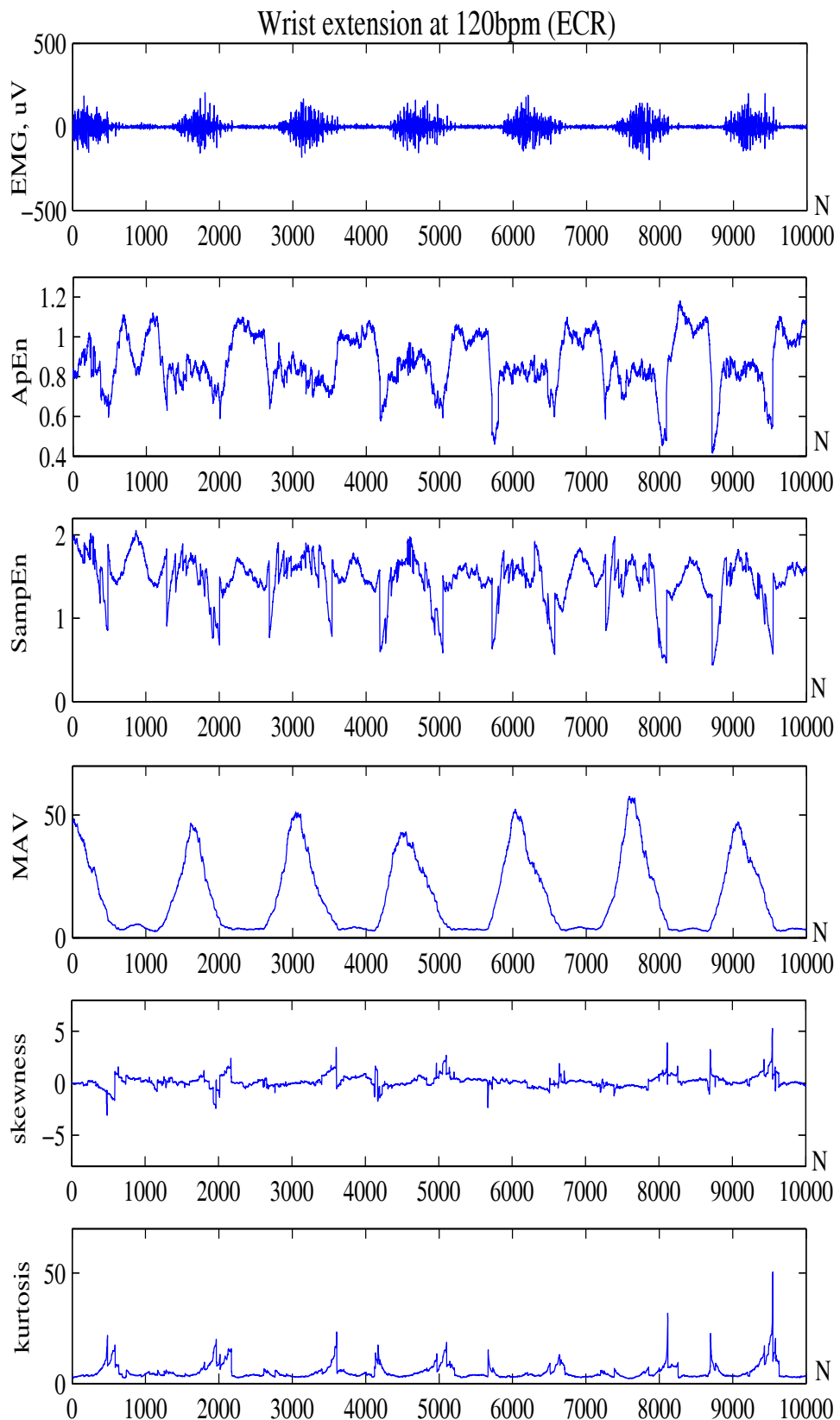
FIGURE C.2: Feature extraction of the SEMG signal during wrist extension from ECR muscle at 120bpm. From top to bottom: the SEMG signal, ApEn, SampEn, MAV, skewness and kurtosis.
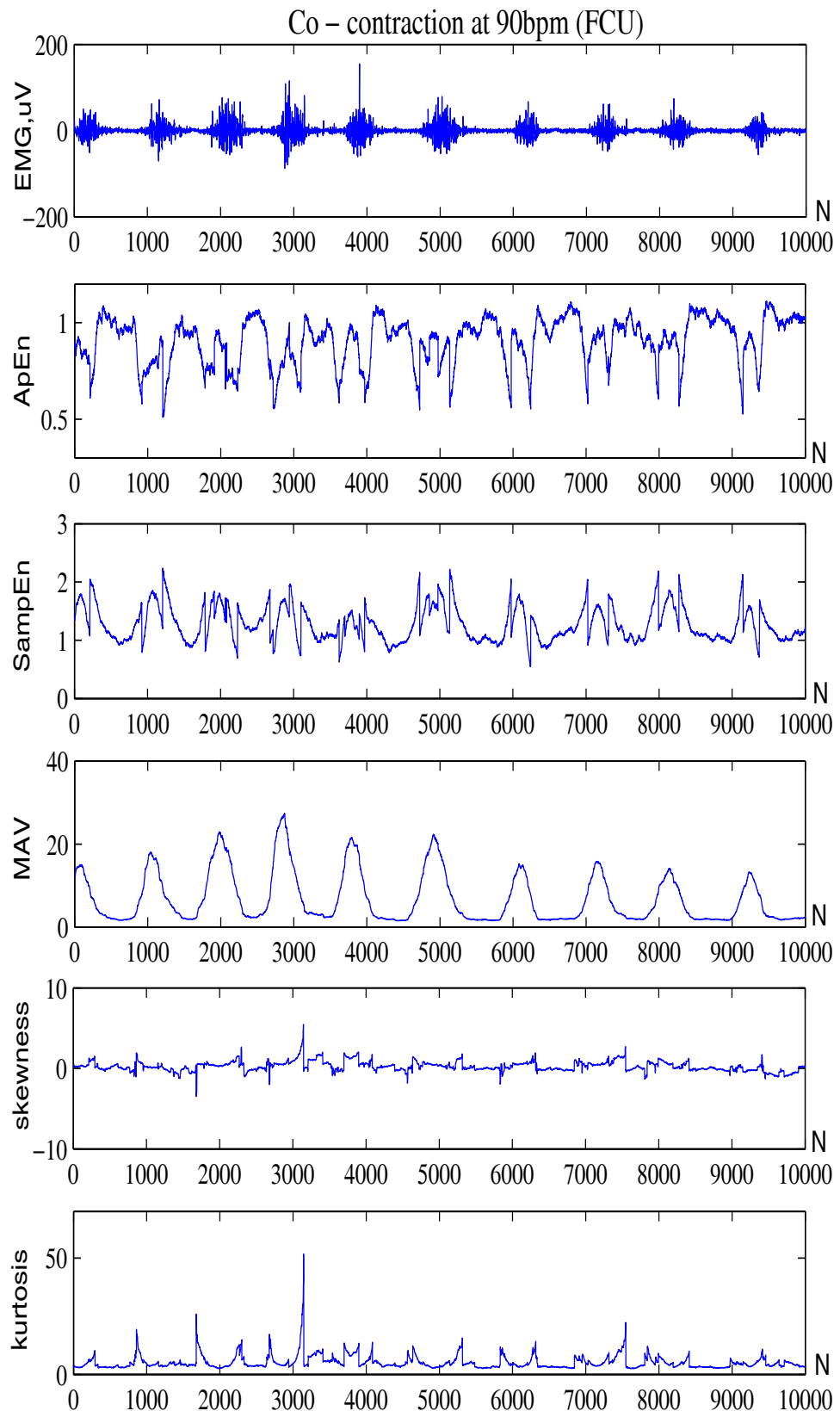
FIGURE C.3: Feature extraction of the SEMG signal during co-contraction from FCU muscle at 90bpm. From top to bottom: the SEMG signal, ApEn, SampEn, MAV, skewness and kurtosis.
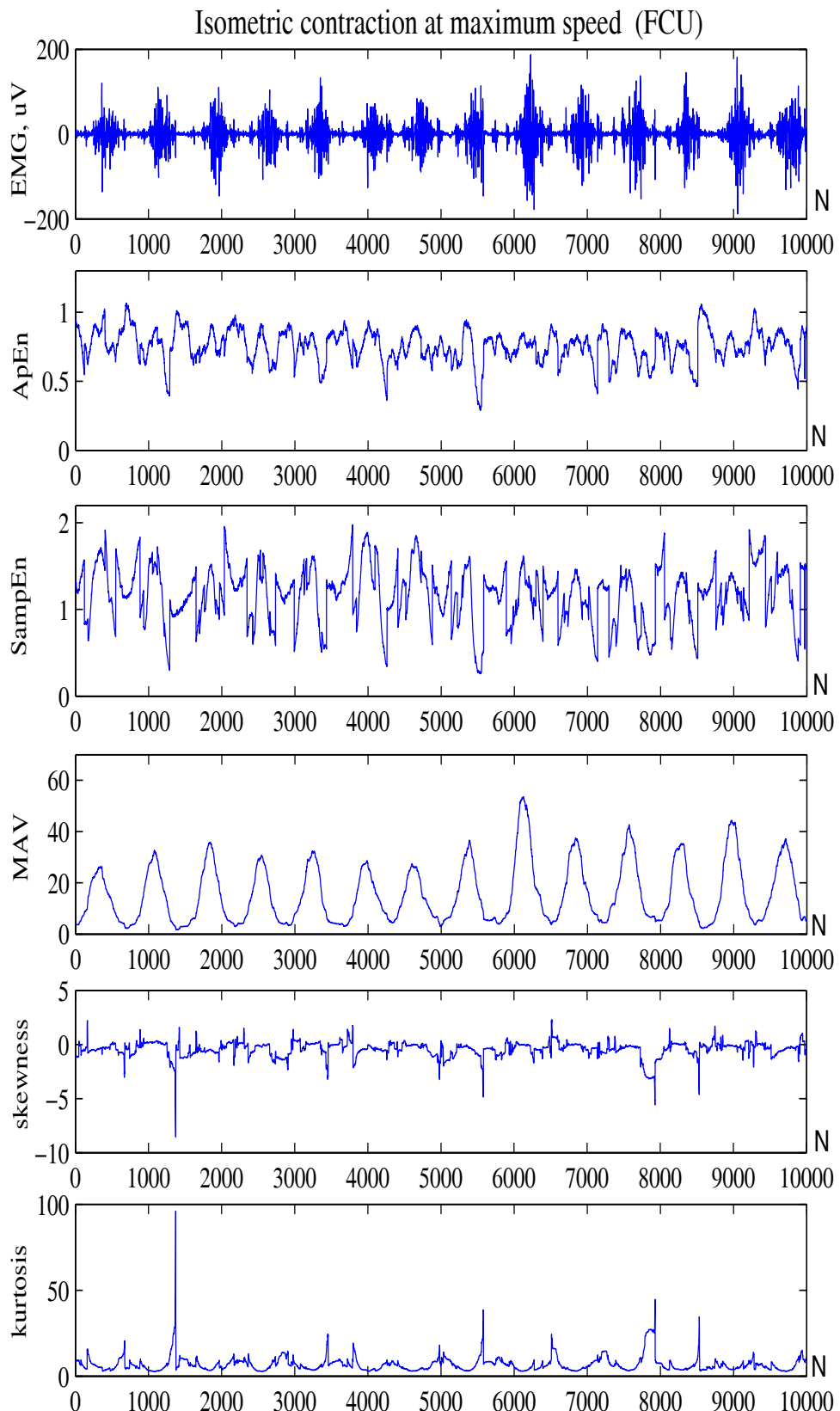
FIGURE C.4: Feature extraction of the SEMG signal during isometric contraction from FCU muscle at maximum speed. From top to bottom: the SEMG signal, ApEn, SampEn, MAV, skewness and kurtosis.

Appendix D

The membership function for the revised four states FL classifier system
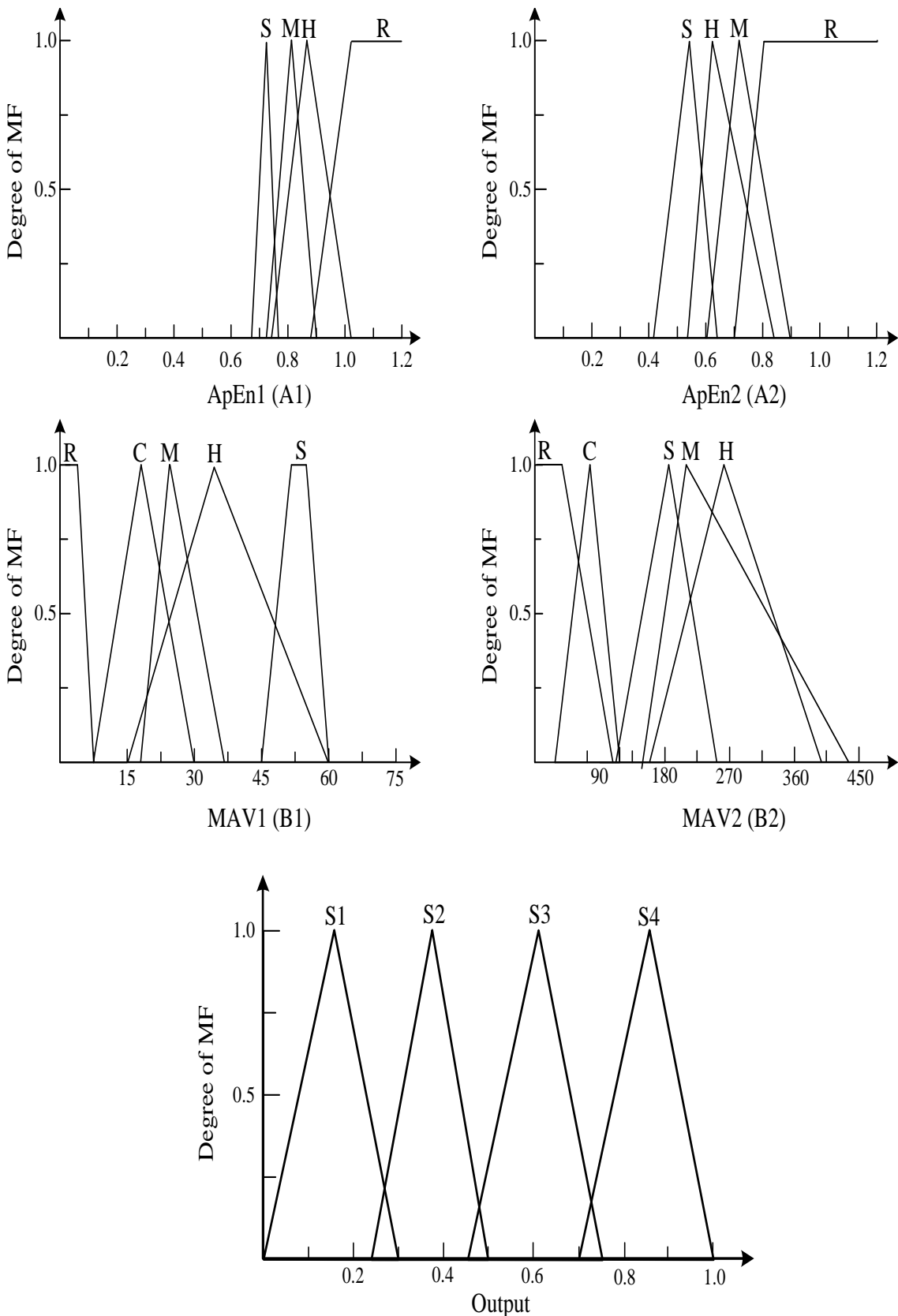
FIGURE D.1: The input membership function for ApEn1(A1), (MAV1B1), ApEn2(A2), MAV2(B2) and the output for the revised four state FL classifier. Inputs A1 and B1 are from FCU; A2 and B2 are from ECR. S: SLOW, M:MEDIUM, H:HIGH, C:Co-contraction, R: RELAX

Appendix E

The classification results - four states ECS system
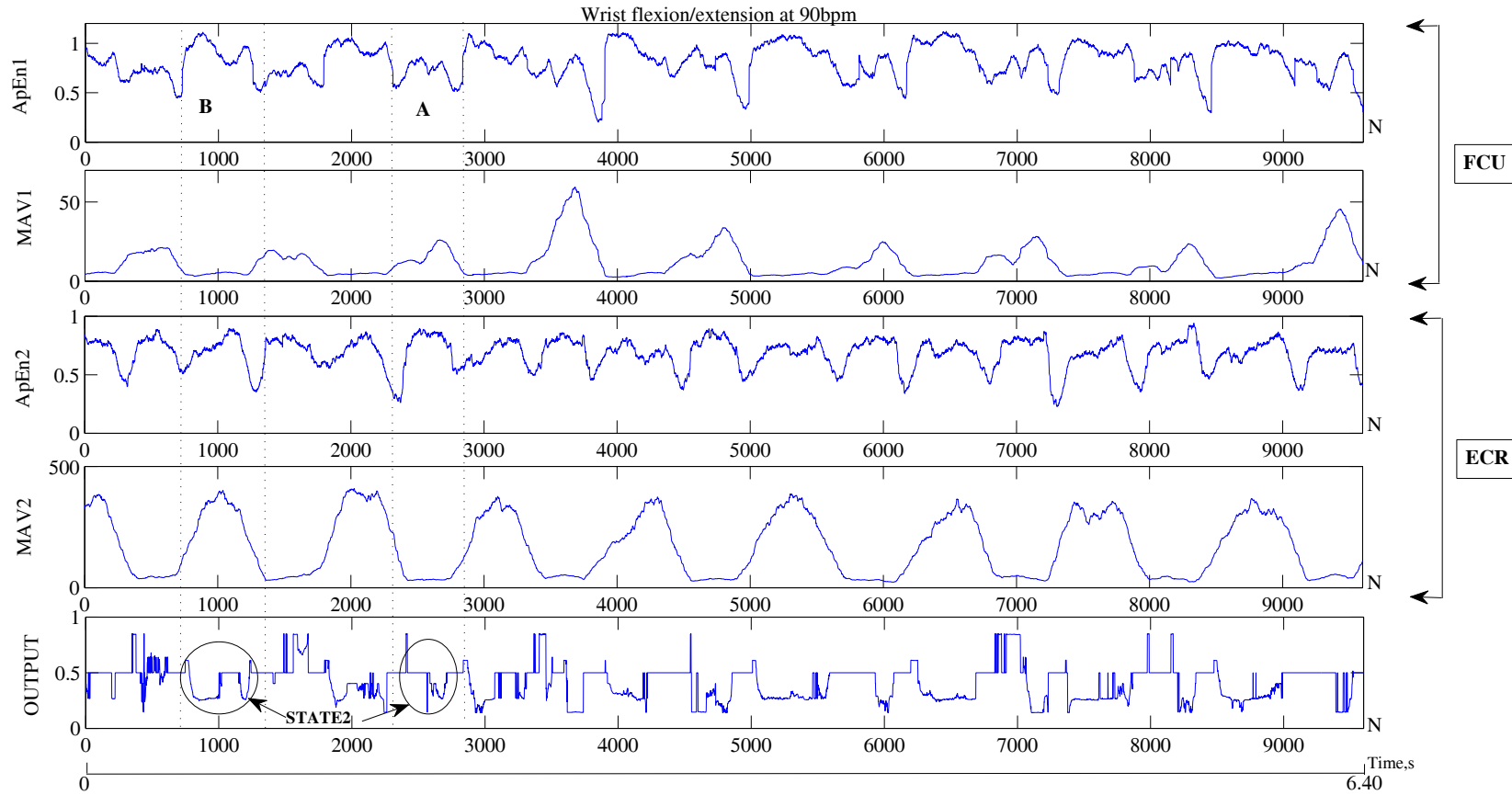
FIGURE E.1: The result of the revised four states classification system during wrist flexion/extension at 90bpm. Label STATE1 (0.00 - 0.30) is the classification result during wrist flexion (region A) and wrist extension (region B).
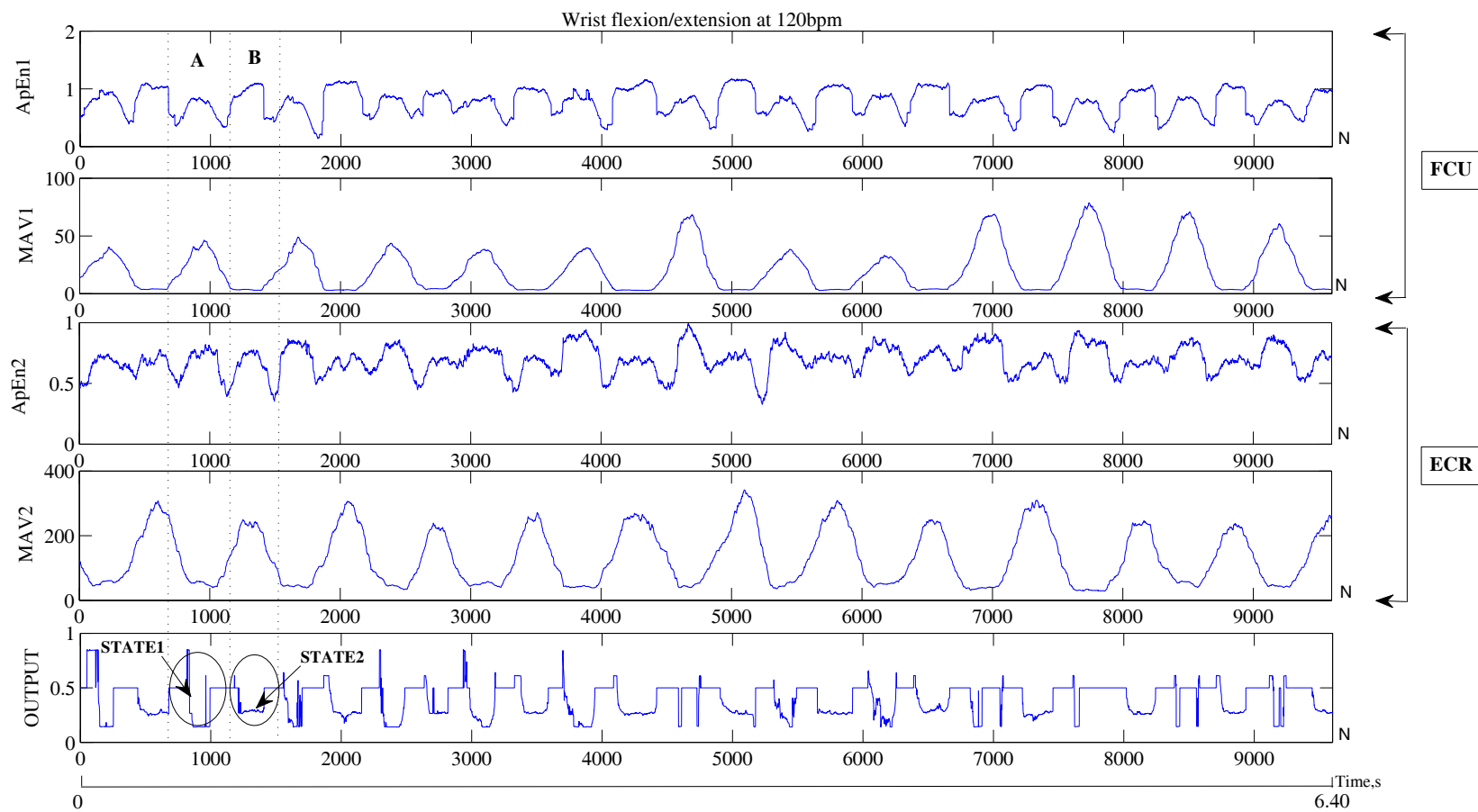
FIGURE E.2: The result of the revised four states classification system during wrist flexion/extension at 120bpm. Label STATE1 (0.00 - 0.30) is the classification result during wrist flexion (region A) and label STATE2 (0.25 - 0.50) is the classification result during wrist extension (region B). However, the results obtained were inaccurate as the system should select STATE3 (0.45 - 0.78).
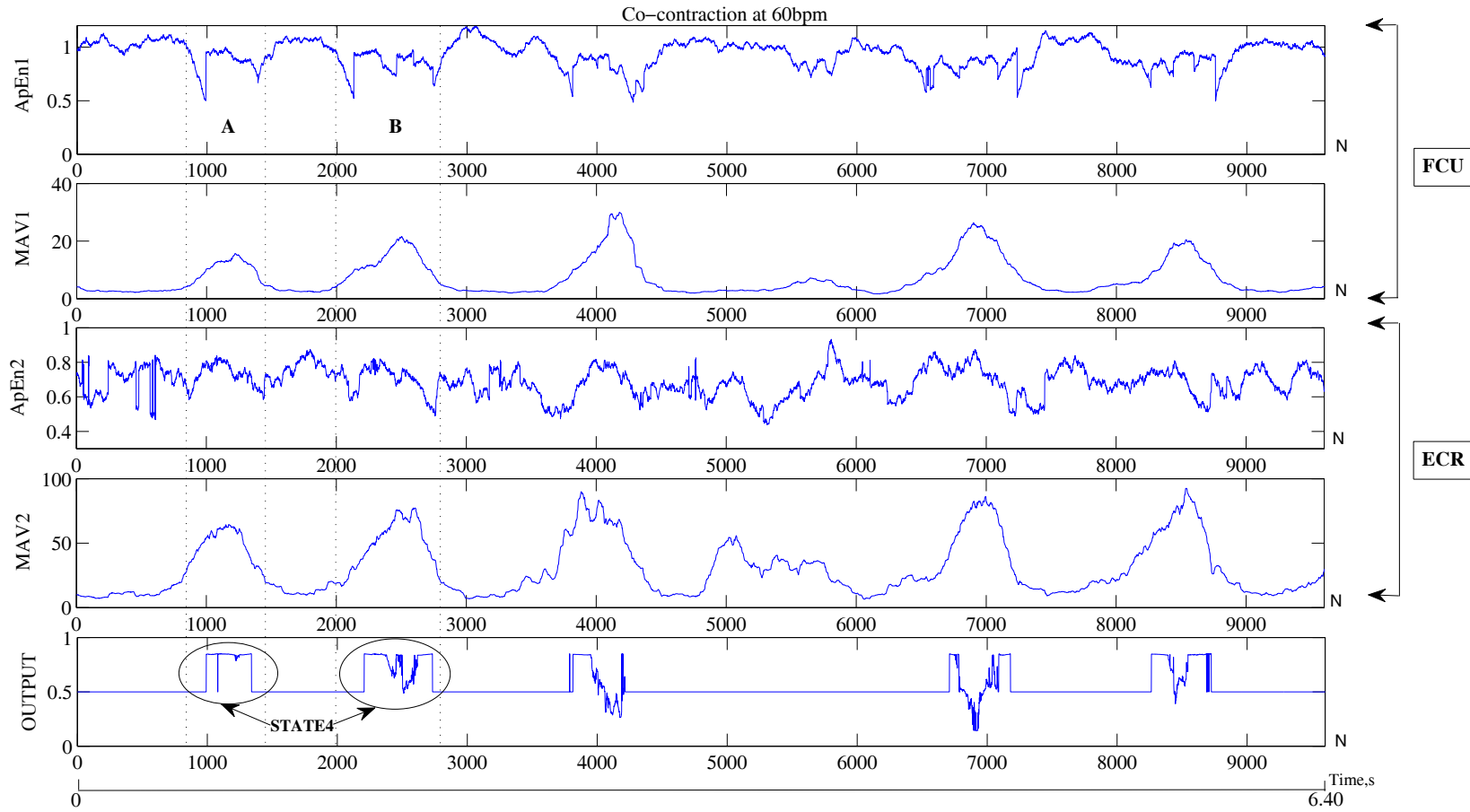
FIGURE E.3: The result of the revised four states classification system during co-contraction at 60bpm. Label STATE4 (0.75 - 1.00) is the classification result during co-contraction (region A and B).

Appendix F

The classification results - three states ECS system
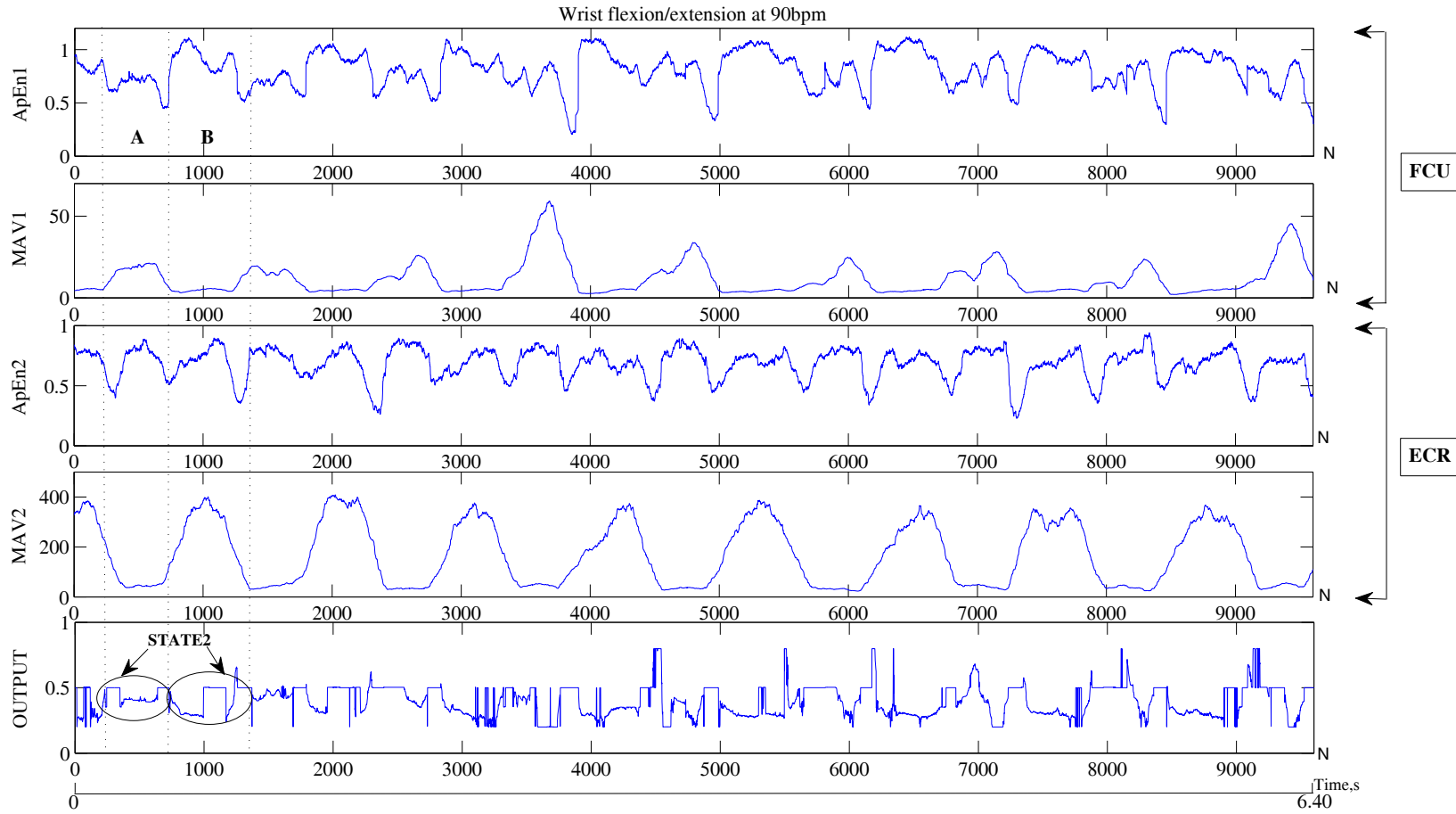
FIGURE F.1: The result of the three states classification system during wrist flexion/extension at 90bpm. Label STATE2 (0.30 - 0.70) is the classification result during wrist flexion (region A) and wrist extension (region B).
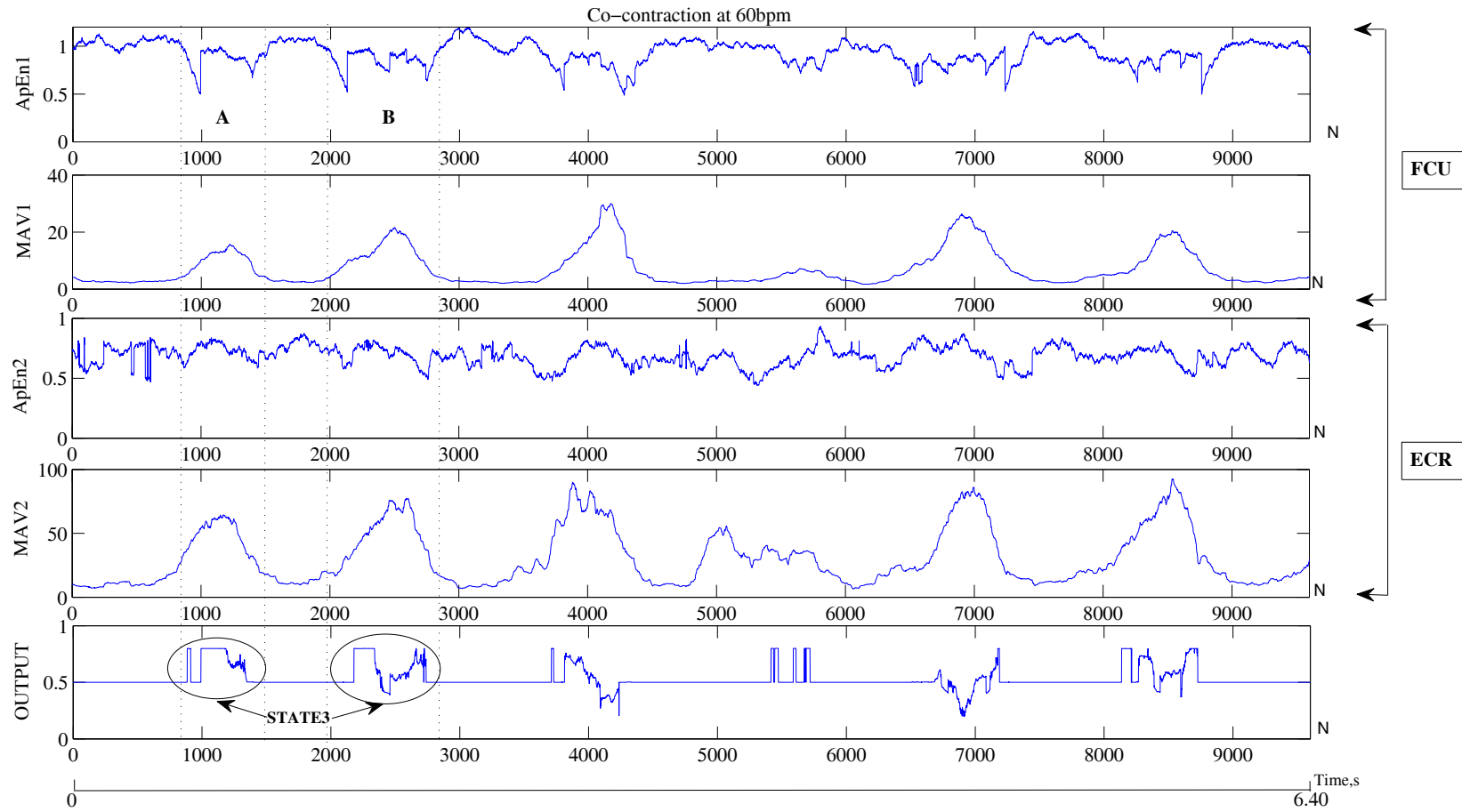
FIGURE F.2: The result of the three states classification system during co-contraction at 60bpm. Label STATE3 (0.60 - 1.00) is the classification result during co-contraction (region A and B).

Appendix G

The classification results - five states ECS system
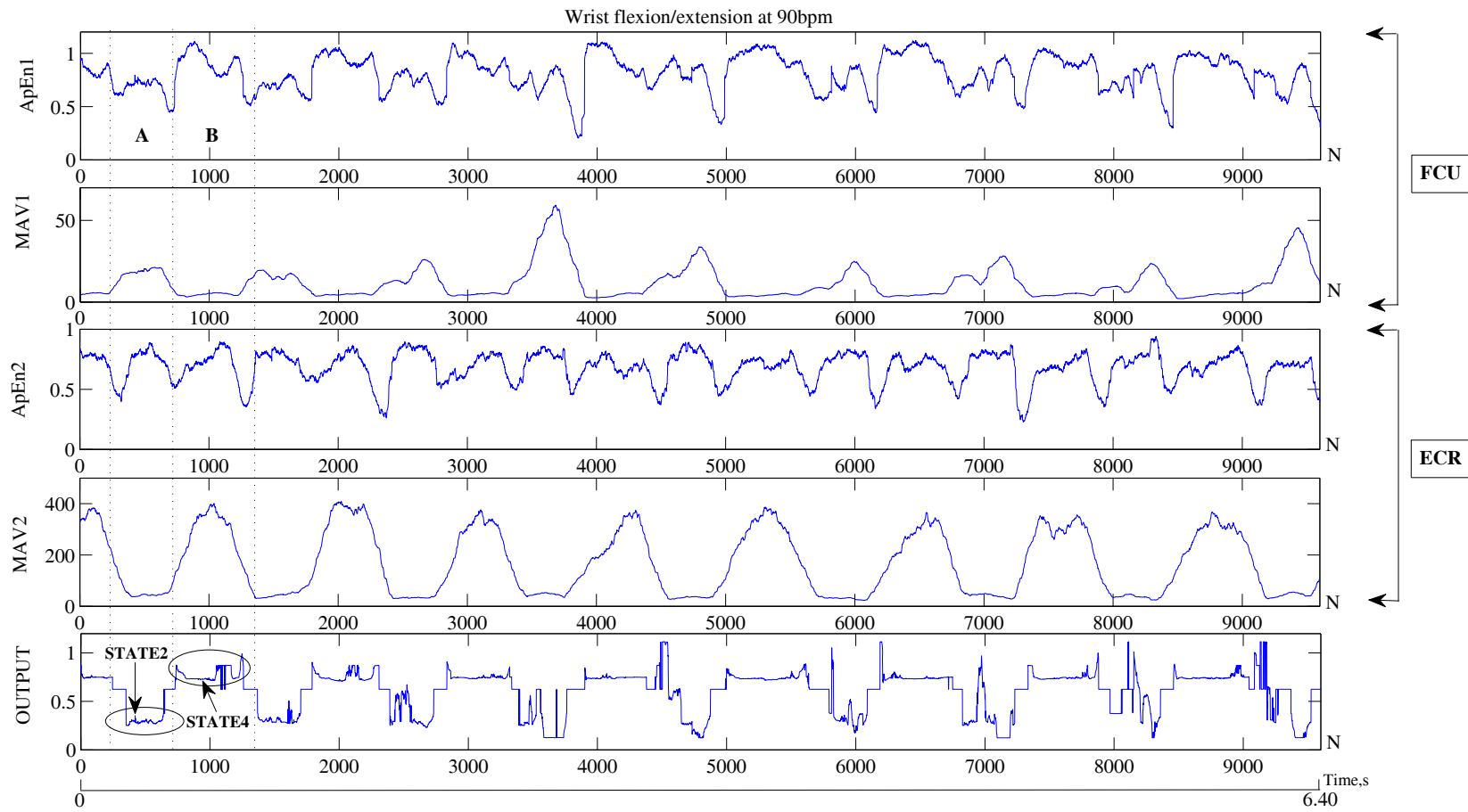
FIGURE G.1: The result of the five states classification system during wrist flexion/extension at 90bpm. Label STATE2 (0.25 - 0.51) is the classification result during wrist flexion (region A) and label STATE4 (0.77 - 1.00) is the classification result during wrist extension (region B)
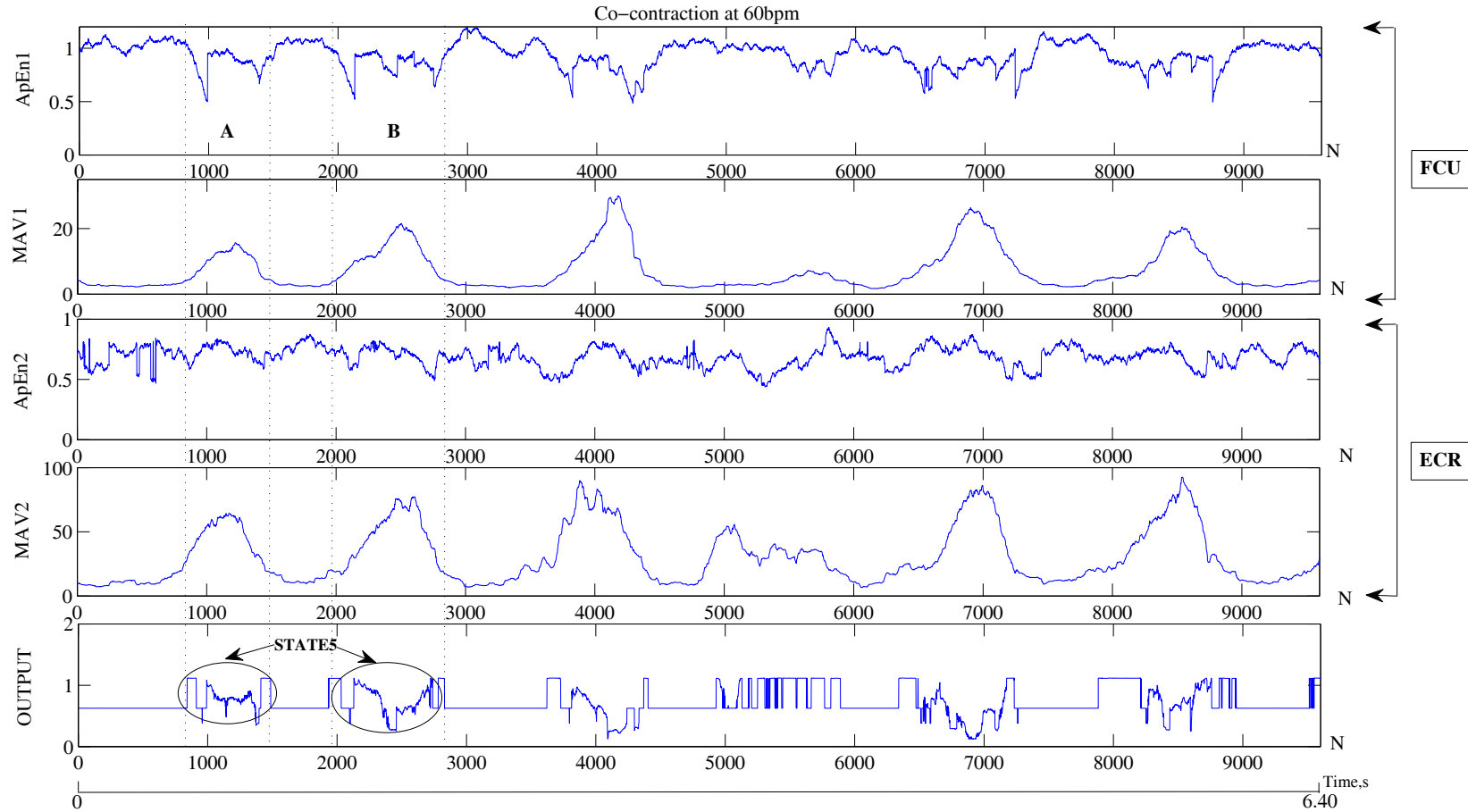
FIGURE G.2: The result of the five states classification system during co-contraction at 90bpm. Label STATE5 (1.00 - 1.25) is the classification result during co-contraction (region A and B).

Appendix H

The classification result - state based ECS system
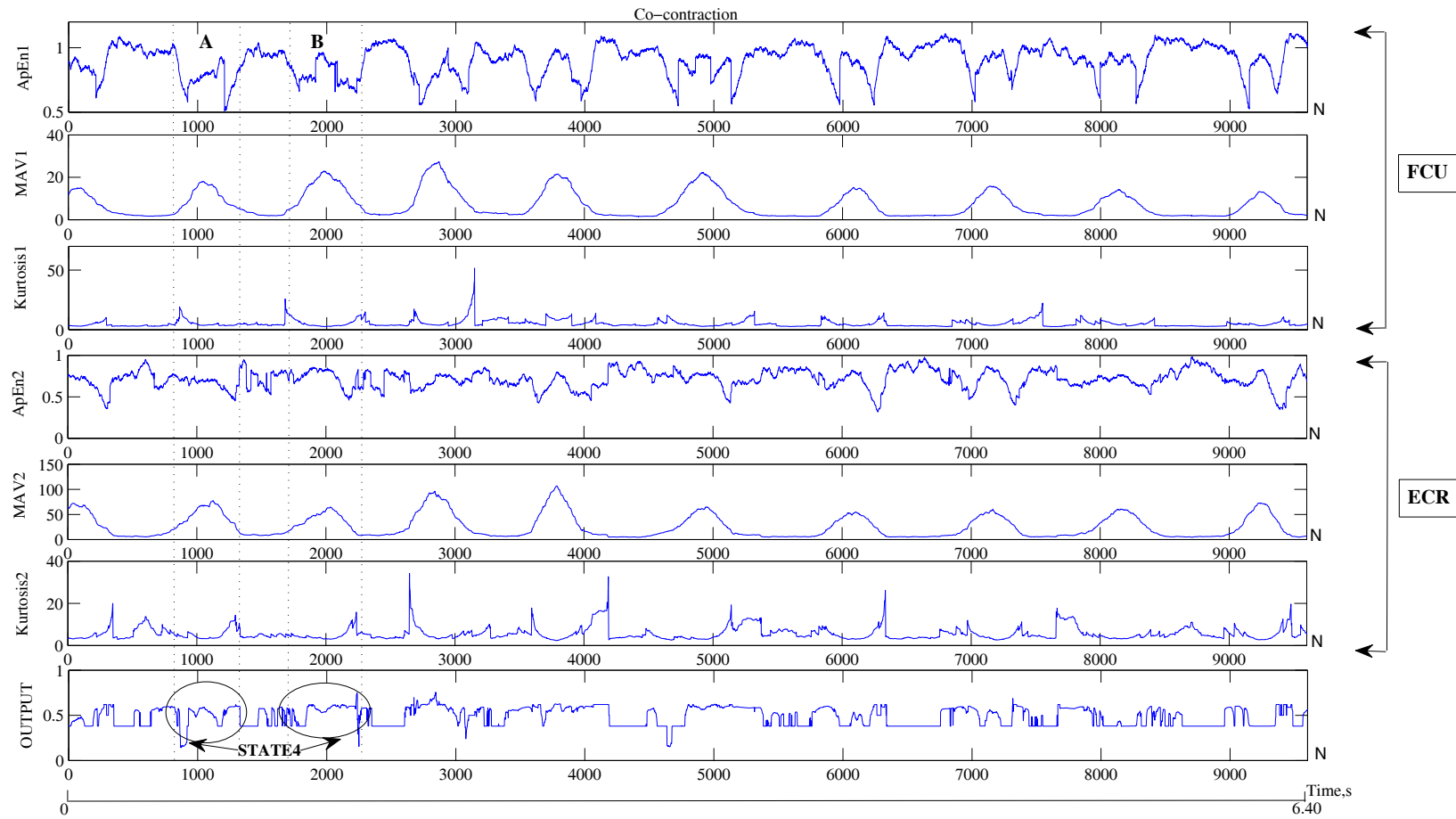
FIGURE H.1: The result of the contraction's state based classification system during co-contraction. Label STATE4 (0.71 - 1.00) is the classification result during co-contraction (region A and B).

Appendix I

Investigation of an Artificial Prehension System

This appendix describes an investigation of the fundamental operation of an artificial hand. The hand is modeled as a simple prehension system with three sensing elements; force, acceleration and slip. An overview of the operation and the experimental setup are described and the results from the sensors's analysis are included. A proposed automatic closed loop feedback algorithm is also described.

I.1   Artificial prehension system

The Oxford English dictionary defines prehension as the action of physically grasping or holding something and is done uncognitively [Oxford, 2009]. It also involves manipulation of the hand and the movement of object within the hand. The most important function of a human hand is prehension. An example is picking up a ball using a spherical grip posture. Several designs and developments of artificial hand have been reported, but none of them have included the study of prehension [Light et al., 2002b; Carrozza et al., 2002b; Dechev et al., 2001]. There is growing interest in studying methods to avoid the object from slipping when being held. A robust control solution is needed to overcome this matter where robust sensors are essential for the measurement of variables in a control loop.

The objective of this work is to investigate the artificial hand's operation and is represented by an experimental prehension system. The long term objective is to

develop an automatic closed loop feedback control system that will work together with the ECS developed in this research.

The prehension system has three sensors integrated in it which are force sensor, slip sensor and accelerometer. Experimental tests are developed to mimic the behavior of an artificial hand and is focused on an understanding of a hand's operation associated with object's gripping and slippage. The idea of the system is shown in Figure I.1 where it performs a single-degree of freedom operation. The object is gripped securely when force, F is applied where the gravitation force, *mg* equals the friction force, 2μF
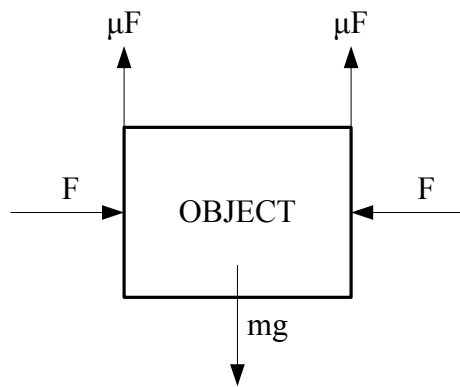
FIGURE I.1: A diagram of the object gripping of the prehension system

The control system is similar in form to Hooke's Law as follows:

$$F = k\hat{x} \tag{I.1}$$

where F is the force, k is the constant and $\hat{x}$ is the distance that the object has slipped. The distance, $\hat{x}$ will determine the amount of force required to tighten the object after it slips.

The block diagram of the prehension system is shown in Figure I.2. The operation of the system is described as follows: after receiving information from the HOLD switch which is either ON ('1') or OFF ('0'), the microcontroller will determine when to start the DC motor to hold the object. The object will be held if the 'ON' instruction is received. Upon gripping the object securely, the amount of the applied force can be measured. When the object starts to slip, a signal from the slip signal will be sent to the microcontroller. An audio cartridge is used to sense vibration when the object starts to slip. The system will then try to re-grip the object by estimating the distance of the object has dropped by double integrating
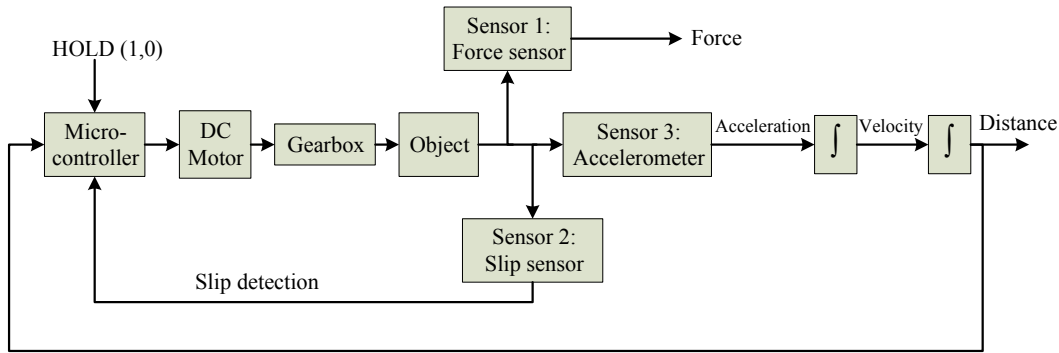
FIGURE I.2: The artificial prehension system general block diagram

the acceleration signal and apply a sufficient amount of force required to re-grip the object.

I.2   Experimental setup

The experimental setup for the system is shown in Figure I.3. The apparatus arrangement allows for linear and horizontal movement to refelct the pinching action between a finger and thumb. The mechanical components of the system are actuator, gripper, object and a stylus of an audio cartridge. The electronics components are the motor controller circuit, force sensor and its amplification circuit, an accelerometer and the cartridge's circuit.

The rack and pinion system is used to provide a linear motion in the system and is attached to the DC motor with gearbox. The spur gear is driven by a DC motor along the rack. The rack is attached to the ball slide 2 to ease its movement. The gripper, is a simple parallel jaw formed with two discs. One of the discs is attached to the rack and the other one is attached to ball slide 3. With this arrangement, the object is constrained to move either vertically or horizontal and is not allowed to rotate about the x-y axis. The DC motor/gearbox generates a force to move the rack until the gripper holds the object and pushes slide 3 until it touches the force sensor. An aluminium bar with a 'U' cross section is used as an object to test the operation of the system, is attached to 2 ball slides that moves vertically and horizontally. This arrangement ensures that the object can be held easily by the gripper.

The following section describes the electronics design for the prehension system.

A – 2 ball slides in parallel (Ball slide 1)	F – Additional circuit for G and D
B – DC motor	G – Force sensor
C – Rack and pinion system, and ball slide 2	H – Ball slide 3
D – Audio cartridge	I – Gripper
E – Accelerometer and its circuit	
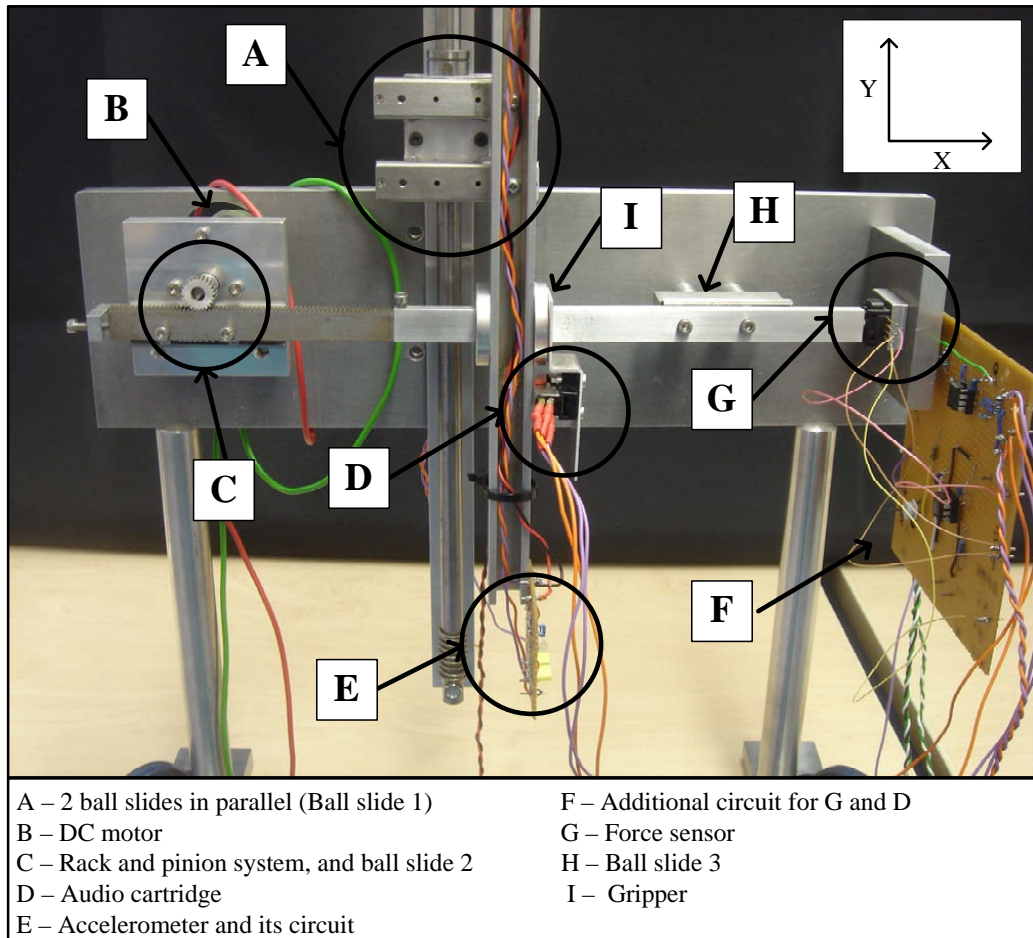
FIGURE I.3: The artificial prehension system

I.2.1 DC motor controller circuit

A motor controller circuit was designed to control the voltage applied to the DC motor. The IG33 20:1 gear DC motor with maximum torque of 100mNm is used to generate the gripper force. The circuit design is shown in Figure I.4 where it represents a 2 stage amplifier. The first amplifier is using ICL7621, acts as a unity gain buffer. The input of the ICL7621 is connected to 50kΩ potentiometer. The potentiometer controls the direction of the motor by turning the pin to one side or another. When the pin is in the middle, the motor stops moving. The power op-amp, L165 is used in the second stage of the amplifier as the inverting amplifier and IC is suitable for the actuator speed control application. A heat sink is attached to the L165 to protect the circuit as it can easily heat up.

The initial testing on the system is to carry out a frequency response analysis between the input of the motor controller circuit and output (see Figure I.5). This is to ensure the stability in the prehension process. In the analysis, the
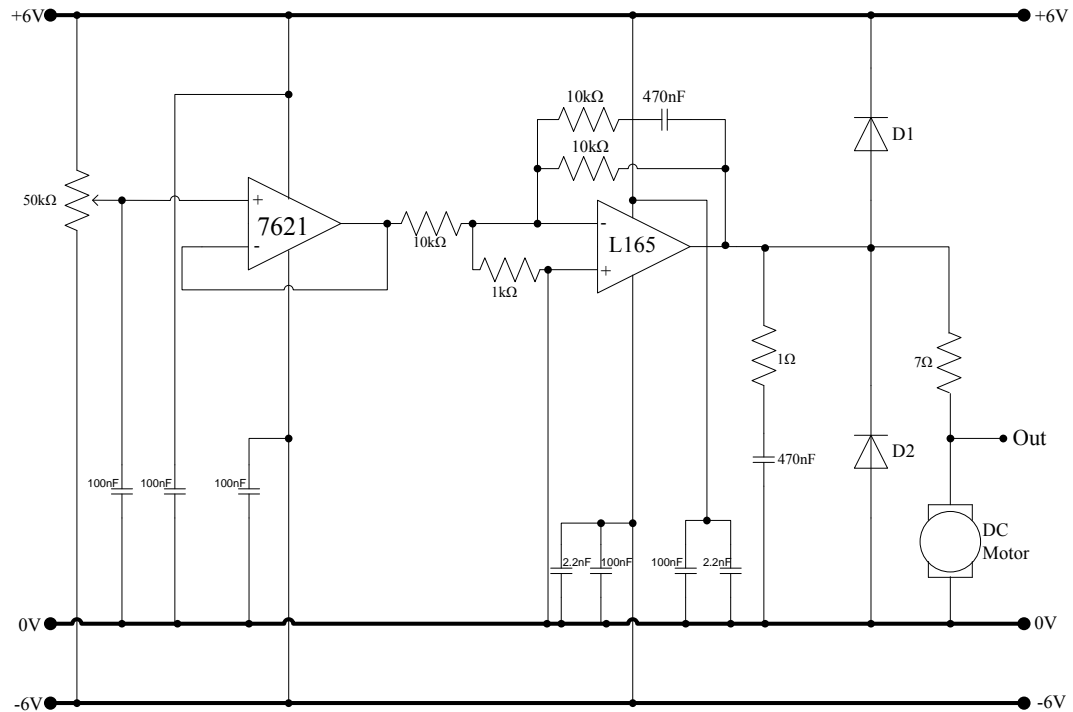
FIGURE I.4: The DC motor controller circuit
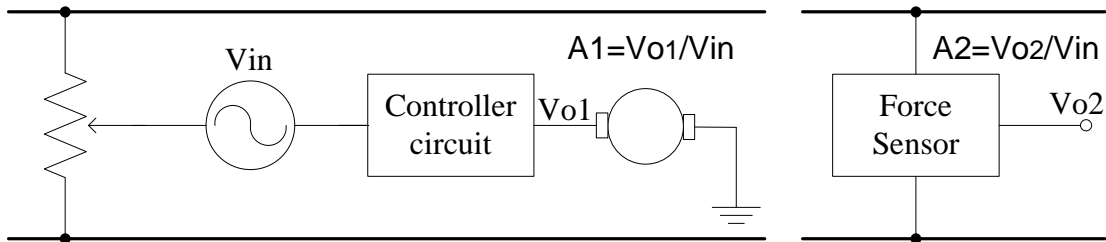
FIGURE I.5: The block diagram of the frequency response analysis.

potentiometer is set for the DC motor to grip the object. Then alternate current (AC) signal is applied to the V_{in} and the AC output is observed at the V_{o1}. The gain, $A1$ was then calculated. Similar procedures were done in determining the gain, A_2.

Figure I.6 shows the frequency response of the system and it shows that it is a third order system. The analysis shows that the amplifier circuit has a first order system and the gearbox behaves as a second order system.
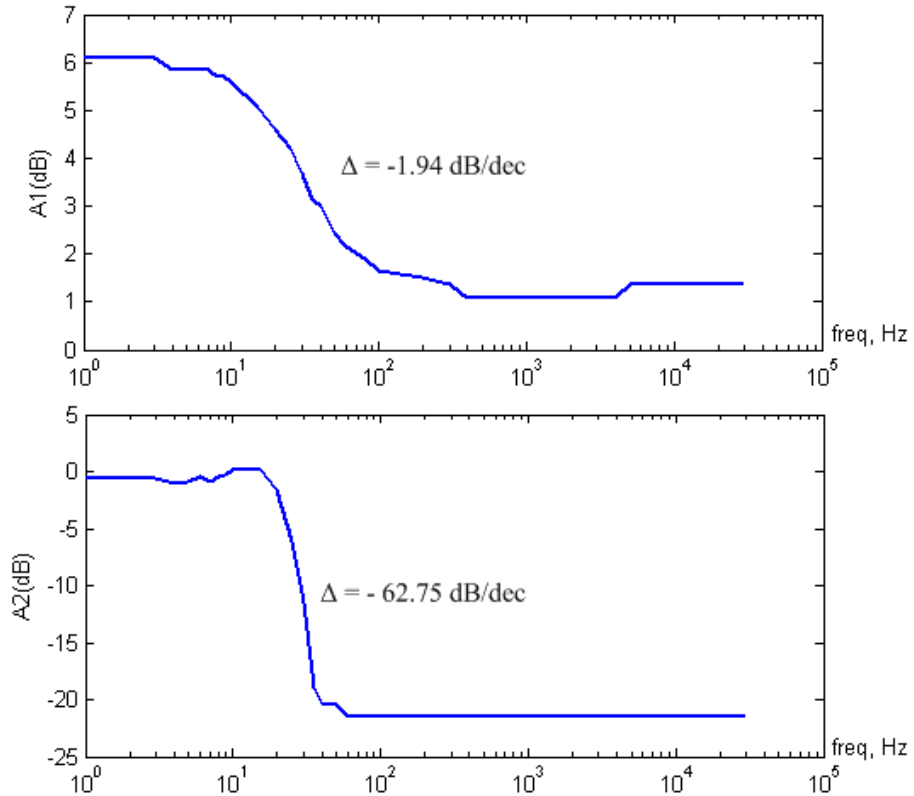
FIGURE I.6: The frequency response in the amplifier (top) and in the system (bottom)

I.2.2 Force sensor

A force sensor, Honeywell FSG15N1A is used to measure the gripper force. The sensor operates on the principle that the resistance of silicon implanted piezoresistors will increase when the resistors strain under an applied force. It can measure force up to 15N and sensitivity 24mV/N.

The force sensor and its amplification circuit is shown in Figure I.7. An instrumentation amplifier, INA118P is used to amplify the signal where the input signal from the force sensor are applied to the two differential inputs. The gain is set up by an external resistor R_G and the following equation is used to achieve the gain of 20, where $R_G = 2.63k\Omega$.

$$G = 1 + \frac{50k\Omega}{R_G} \tag{I.2}$$

The reference voltage, V_{ref} of the instrumentation amplifier is adjusted to $30mV$, which is the same with the null offset of the force sensor. The output of the circuit is in volts and the force in Newton can be determined by the following equation:

$$F = \frac{V_{out}}{G} \frac{1}{24 \times 10^{-3}}(N) = 2.083V_{out}(N) \tag{I.3}$$
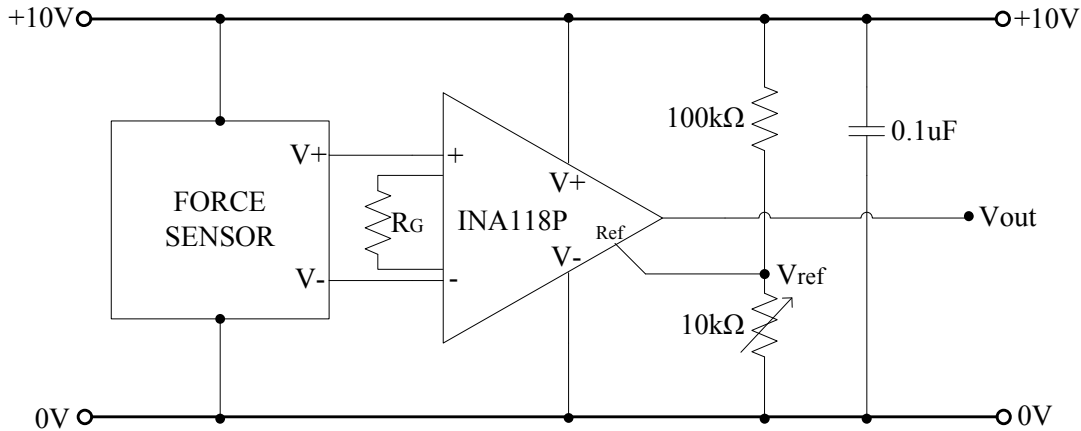
FIGURE I.7: The force sensor and its amplification circuit

I.2.3   Accelerometer

To measure the acceleration of the object when it drops, an accelerometer ADXL320 is used. The ADXL320 is a dual-axis (X-axis and Y-axis) accelerometer that can measure acceleration with a full-scale range of ± 5g. It has the sensitivity of 174mV/g. The functional block diagram of ADXL320 is shown in Figure I.8.
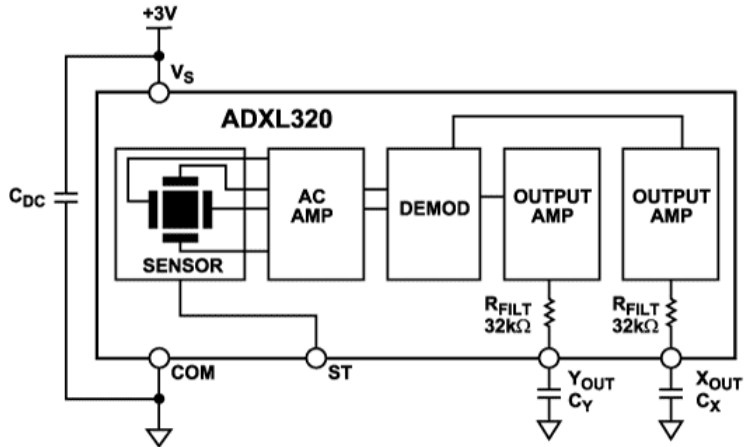
FIGURE I.8: The functional block diagram of ADXL320

C_x and C_y are added at the output pins to implement low-pass filtering for antialiasing and noise reduction. Both capacitors values are $0.01\mu F$ for 500Hz bandwidth and are obtained by using the following equation:

$$F_{-3dB} = \frac{5\mu F}{C_{(x,y)}}$$

(I.4)

From the acceleration signal, the velocity and the distance can be determined. This is done by double integrating the acceleration signal by using Simpson's rule method. Simpson's rule [PlanetMath, 2007] is a method of approximating the integral of function f using quadratic polynomials. In particular, let the function f be tabulated at points x_0, x_1 and x_2 equally spaced by distance h, and denote $f_n = f(x_n)$. The Simpson's rule is given by the following equation:

$$\int_{x_0}^{x_2} f(x)dx = \frac{h}{3}(f(x_0) + 4f(x_1) + f(x_2)) \tag{I.5}$$

For a series of number $X_0, X_1, X_2, \ldots, X_n$, the equation is as below:

$$X_0 = \frac{h}{3}(X_0 + 4X_1 + X_2) \tag{I.6}$$

$$X_1 = \frac{h}{3}(X_2 + 4X_3 + X_4) + X_0 \tag{I.7}$$

$$X_k = \frac{h}{3}(X_{n-2} + 4X_{n-1} + X_n) + X_{k-1} \tag{I.8}$$

I.2.4 Slip sensor

Another sensing element in the system is the slip sensor. A stereo magnetic phono cartridge is used for this purposes. The cartridge is a device that can convert vibration detect by the stylus on the cartridge into an electrical signal. The arrangement for the cartridge in the system is shown in Figure I.9.
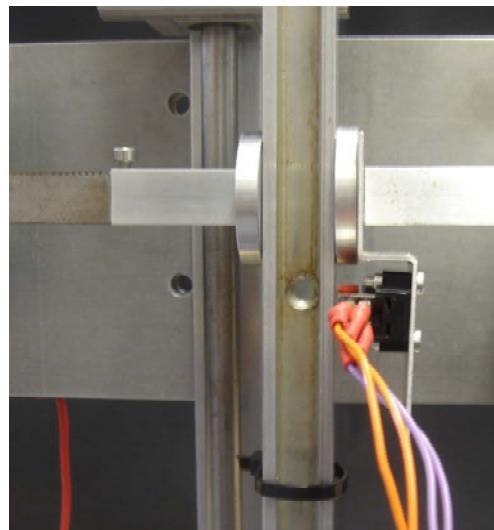
FIGURE I.9: The position of the stereo cartridge
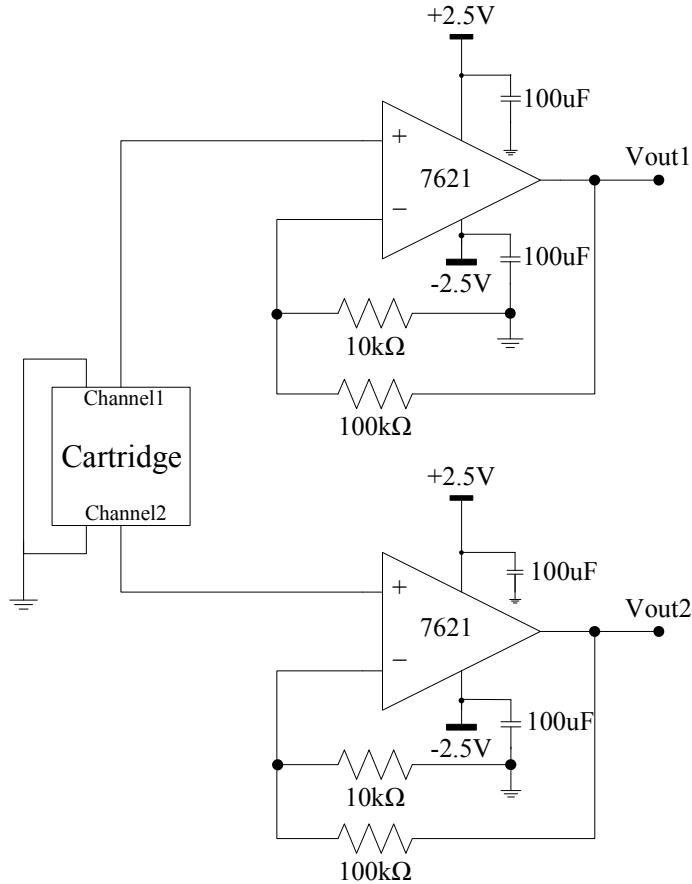
FIGURE I.10: The audio circuit and its amplification circuit

The stylus of the cartridge touches the object when it is held. A vibration will be detected when the object starts to slip. The slip signal from the cartridge is fed to an amplifier to amplify the signal with a gain of 10. The circuit design is shown in Figure I.10. The cartridge has two output channels. However, in this work only one output (Channel 1) is used in the analysis as it has been observed that both channels gave similar signal responses.

By applying an approximate integrator to the slip signal, the distance of the object slips could be estimated. Cotton et al. [2007] used the same method to get the distance from the slip signal obtained from the thick-film piezoelectric slip sensor attached on a fingertip. The flow chart of the approximate integrator is shown in Figure I.11. The V_T is chosen for the integration and this can be done by observing the absolute value of the slip signal. By moving the threshold up or down, it will effect the number of count of 1 where high V_T will give less count and oppositely, low V_T gives more count because of the noise. The V_T that give the most reasonable number of counts and good result is chosen. The distance obtained from the integration will be used as a control signal to provide automatic
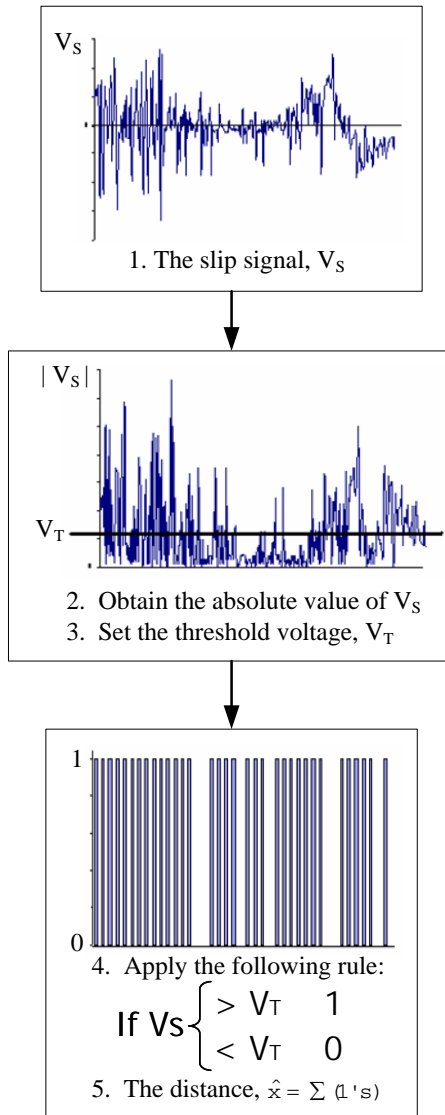
FIGURE I.11: The approximate integrator

closed loop feedback control to the prehension system as described in Equation I.1.

The slip signal is being investigated further using the ApEn algorithm, to see how it can be used to detect and avoid the object from slipping. Using the same parameters as in the SEMG investigation, where the data length, $N = 200$, vector, $m = 2$ and the tolerance range, $r = 0.25SD$, the ApEn algorithm is then applied to the slip signal. Figure I.12 shows the ApEn analysis when applied to the slip signal. It can be seen that the ApEn drops to a value about 0.4 when the object slips. When there is attempt to re-grip the object, there is an increase in the ApEn before it drops again. The ApEn is then increases again to about 1.0 when the

object is held again (the slip signal is 0V). The analysis shows that ApEn can be used to detect the object's slip.
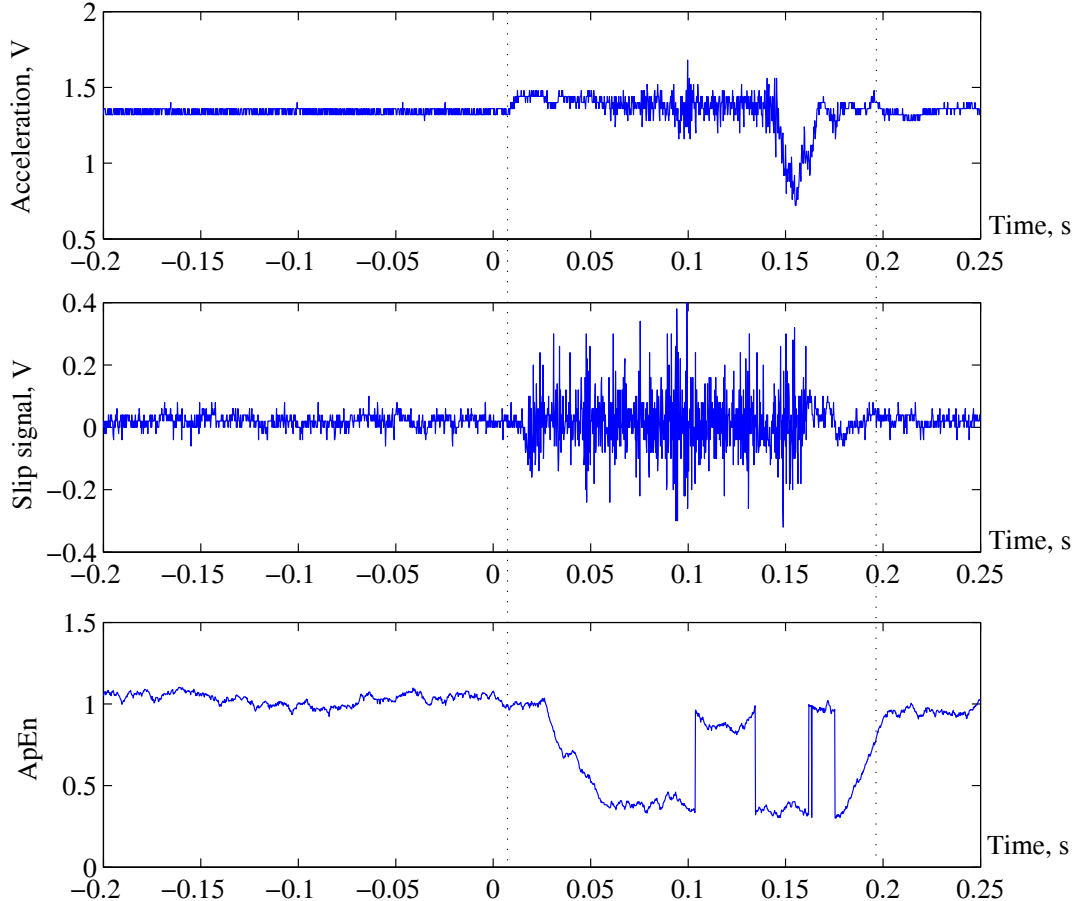
FIGURE I.12: Top: the acceleration signal, middle: the slip signal and bottom: the ApEn signal on the slip signal.

I.3   Results and discussion

The experiment on the prehension system was carried out by running an object gripping test. Initially, the force was applied to grip the object. After the object was held, the force was reduced and the object started to slip. The force was applied again to re-grip the object and prevent the object from slipping. The signals from the three sensors during the gripping and re-gripping processes were recorded and are shown in Figure I.13.

The study focuses on three phases of the object condition which are when it is held, it starts to slip and it is re-gripped. From the top plot, it shows that the
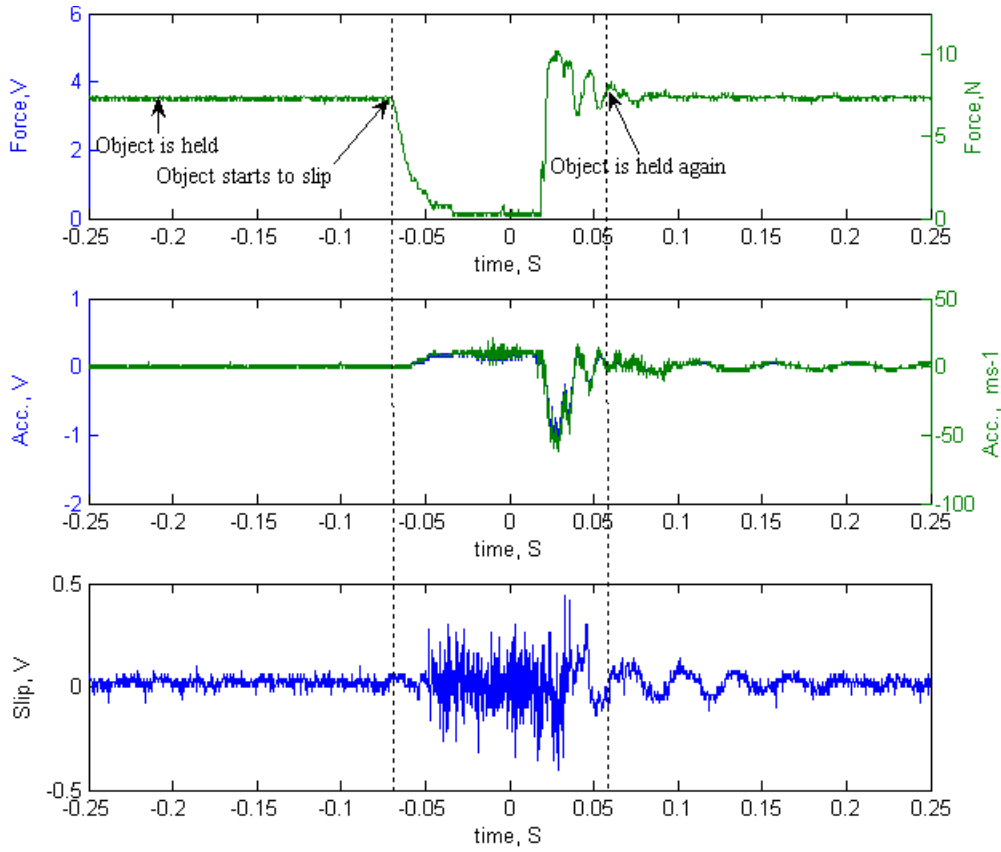
FIGURE I.13: The signals from the three sensors: force (top), acceleration (middle) and slip (bottom) measured from the experiment

average force required to grip the object is about 3.5V which is equivalent to $7N$. This value is typical of the finger force required to hold an object. When the object starts to slip, the force dropped at almost $0N$ and signal responses can be seen from the accelerometer and the slip sensor.

From the acceleration signal (middle plot in Figure I.13), it can be seen that the object accelerates when the force is reduced and it starts to decelerate when there's an attempt to re-grip the object. When an object experienced a free fall, it has the acceleration of 1g ($= 9.81 \text{m} s^{-1}$). From the acceleration plot, it shows that the object dropped under free fall condition. Simpson's rule was used to estimate the velocity and the distance from the acceleration signal and this is shown in the middle and bottom plot of Figure I.14 respectively. From the plots, it can be observed that the velocity and the distance of the object starts to increase when the object begins to slip. The velocity starts to decrease when attempt to re-grip the object is done. The velocity returns to zero eventually and the distance becomes a constant when the object is held again.
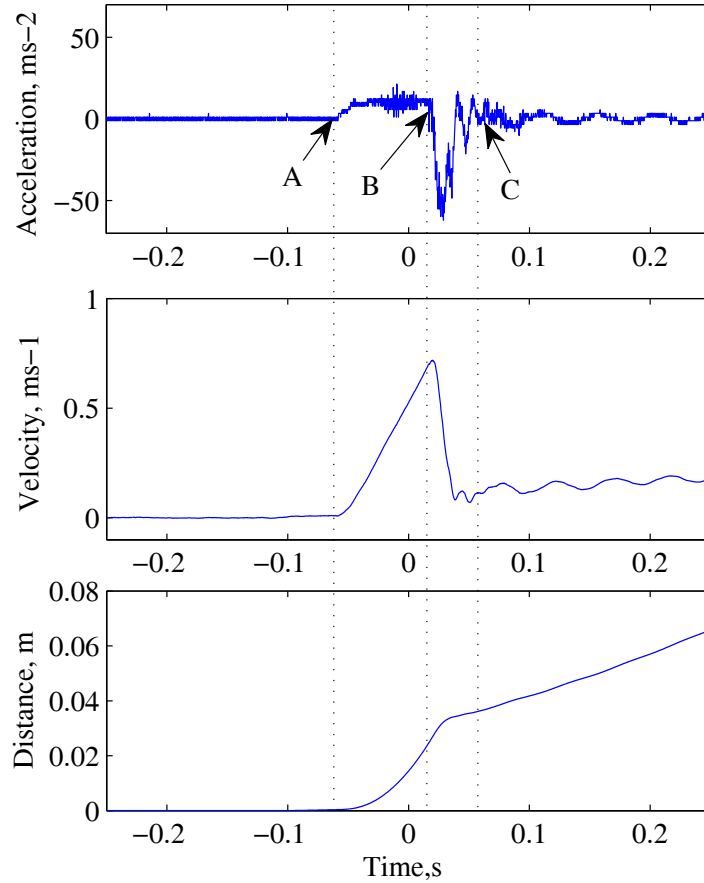
FIGURE I.14: By applying double integration the acceleration (top) signal, velocity (middle) and distance (bottom) are obtained. A: when the object starts to slip, B: attempt to re-grip the object and C: object is held again.

The slip signal (bottom plot in Figure I.13) is to detect when the object starts to slip. By applying approximate integrator to the signal, the distance of the object has slipped is computed. In approximate integration, the first step is to rectify slip signal (see Figure I.11 middle plot). A suitable V_t must be selected to get the safe range of vibration for the object. A right V_t will detect the vibration at the right velocity. Three different V_t were selected in investigating the signal which are 0.04V, 0.06V and 0.08V; and they are shown in Figure I.15.

The conditioning rule (see rule 4, Figure I.11) was applied to the rectified slip signal. Figure I.16 shows the results for three different V_ts after applying rule 4 and the bottom plot is the expanded view of the operation between the period of $5ms$ and $55ms$ in Figure I.16a ('X' label). It has been observed that at higher threshold levels, threshold crossing events are not recorded until later on in the experiment (i.e. at higher velocities)and oppositely, at lower velocities, threshold crossing events are observed much earlier in the experiment. Thus there is a
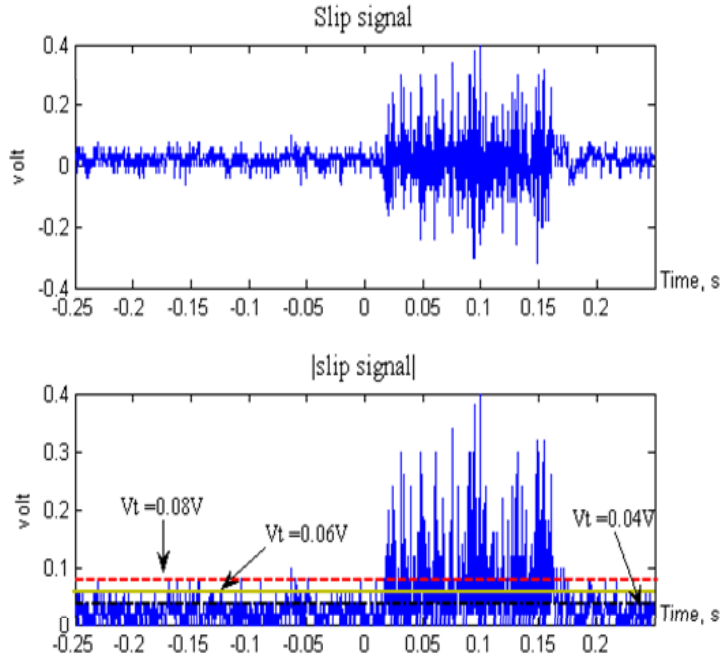
FIGURE I.15: Top: the slip signal. Bottom: The rectified slip signal with three superimposed threshold voltages, V_t

limiting velocity before which slip cannot be detected, and the value of this velocity is proportional to the magnitude of the threshold used when counting threshold crossing events. Ideally slip should be detected at the lowest velocity possible but this is where a trade off exists: setting a threshold level too low means that extraneous noise could register as a threshold crossing event giving the impression that slip had occurred when it hadn't [Cotton et al., 2007].

The sum of the count of 1s shown in Figure I.16 is proportional to the distance of object has slipped. Figure I.17 shows the distance on the object slipped from 3 different V_ts. It shows that V_t=0.08V gave the most reliable result compared to the other V_ts where it detects when the object starts to slip almost accurately. While at V_t=0.04V, it detects the event much earlier before it actually occurred.

Both information obtained from the accelerometer and the slip sensor could be used to estimate the distance that the object has slipped. The distance is used to determine the amount of force required to re-grip the object, as described earlier in Equation I.1. However, for the proposed algorithm of the automatic control feedback, the slip signal is used to detect the object's slip which will be then used to trigger the processing of the acceleration where the distance will be calculated. Figure I.18 shows the block diagram of the proposed control algorithm for the prehension system explaining the operation of the proposed system. The A, B
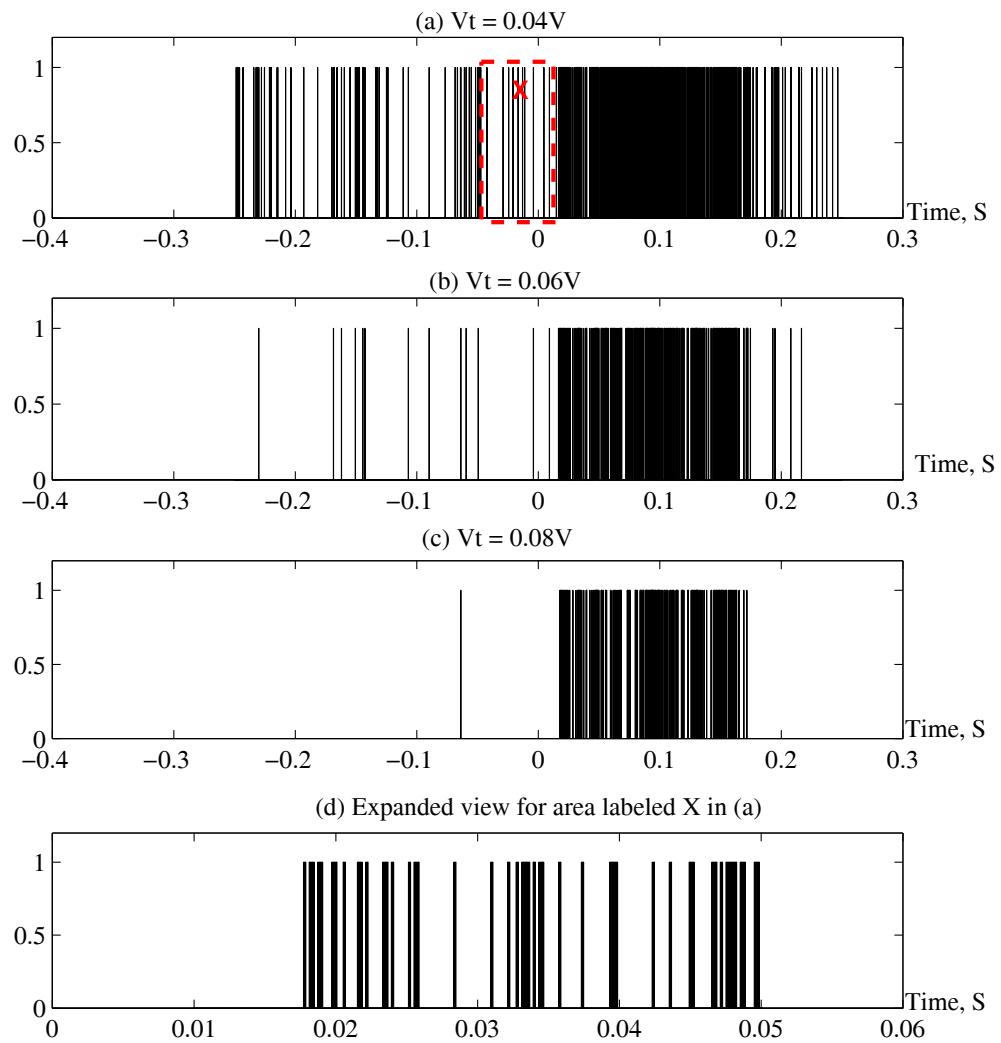
FIGURE I.16: The slip signal is 0 and 1 for three V_ts; (a) 0.04V, (b) 0.06V and (c) 0.08V. (d) is the expanded view for area X shown in (a)
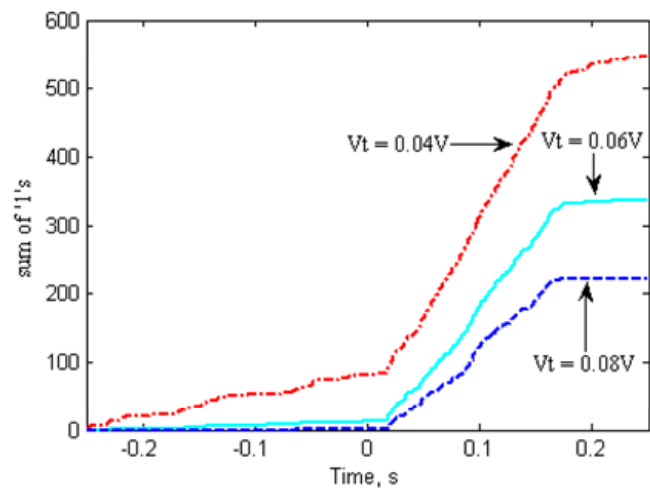
FIGURE I.17: The approximate distance based on sum of '1's of the slip signal at three different V_ts
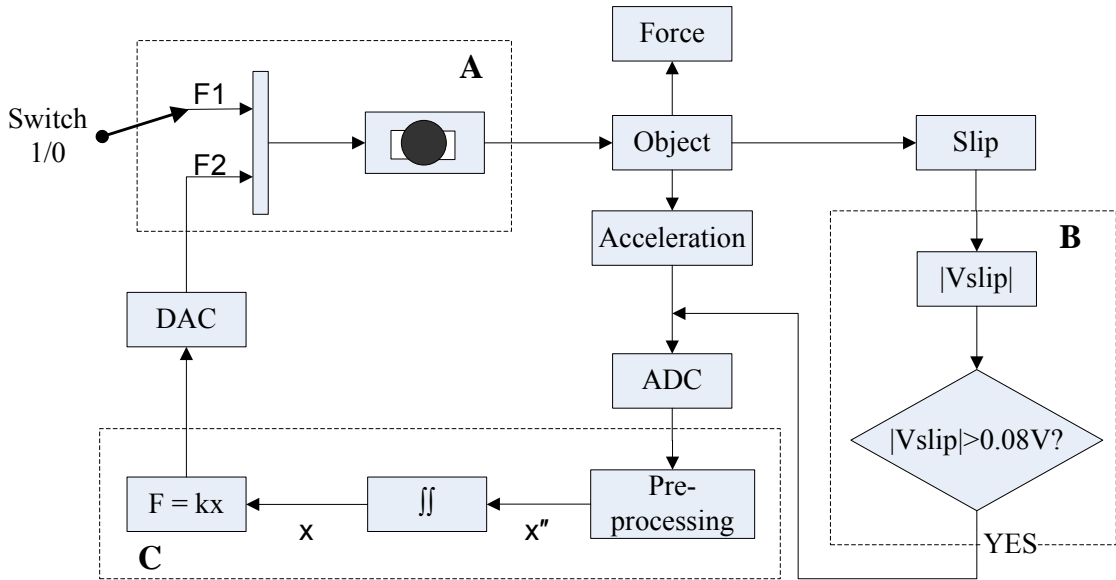
FIGURE I.18: The flowchart of the automatic control feedback algorithm for the artificial prehension system

and C label shown in the diagram are the signal processing stages which can be implemented in a microcontroller.

Prior to the implementation of the algorithm, the scalar 'k' in Equation I.1 will be determined. Fig. I.19 shows the relationship between the force and the distance obtained from the acceleration and the slip signals. From the right-axis of the bottom plot, it can be observed that when the object slipped, it has dropped about $30mm$ before it was re-gripped again. A force of $7N$ is required to grip the object securely. The result for three different V_ts of the approximate integration of the slip signal is shown in the bottom plot, left-axis. It can be observed that at higher threshold levels, threshold crossing events are not recorded until later on in the experiment and oppositely, at lower velocities, threshold crossing events are observed much earlier in the experiment. Also, it can be seen that the distance obtained from the acceleration is proportional to the sum of 1's obtained from the approximate integration of the slip signal.

Further analysis be-tween the distance obtained from the acceleration signal and the force during the re-gripping process was carried out. The experiment was repeated twenty times in determining the most appropriate value for 'k'. In the analysis, the average force when the system tried to re-grip the object until it's being gripped is calculated and the distance of the object has slipped during this period is measured. Fig. I.19 shows the range of values the average force (top plot) and the distance (middle plot). Using Equation I.1, the scalar 'k' is determined.
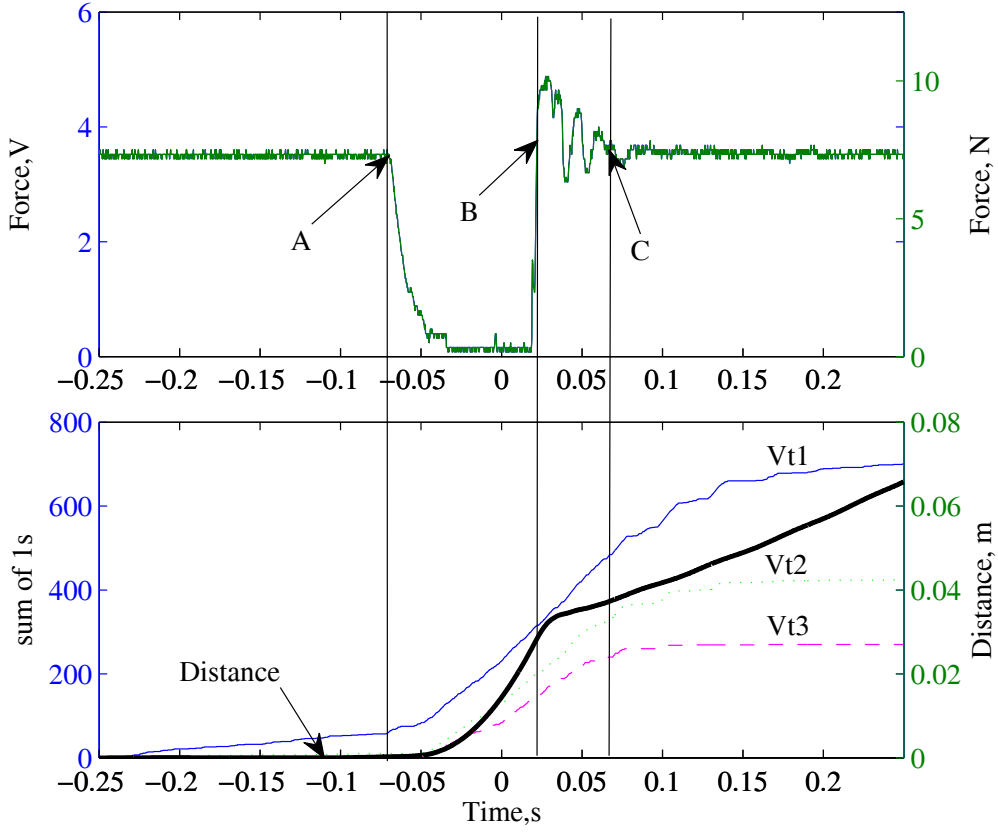
FIGURE I.19: The relationship between the force and the distance of the object has slipped during the re-gripping process. A: when the object starts to slip, B: attempt to re-grip the object and C: object is held again.

TABLE I.1: Summary of the force, distance and 'k' values from Figure I.20

	Force, N	Distance, mm	k
Minimum	2.08	30.8	29.69
Maximum	4.37	75.3	106.12
Mean	3.47	54.28	67.1
SD	0.68	12.27	19.28

The range of the 'k' values is between 30 and 107 (bottom plot in Fig. I.20). Table I.1 shows the statistics of the parameters shown in Fig. I.20. The average of the 'k' value is 67.10 with a SD of 19.28.
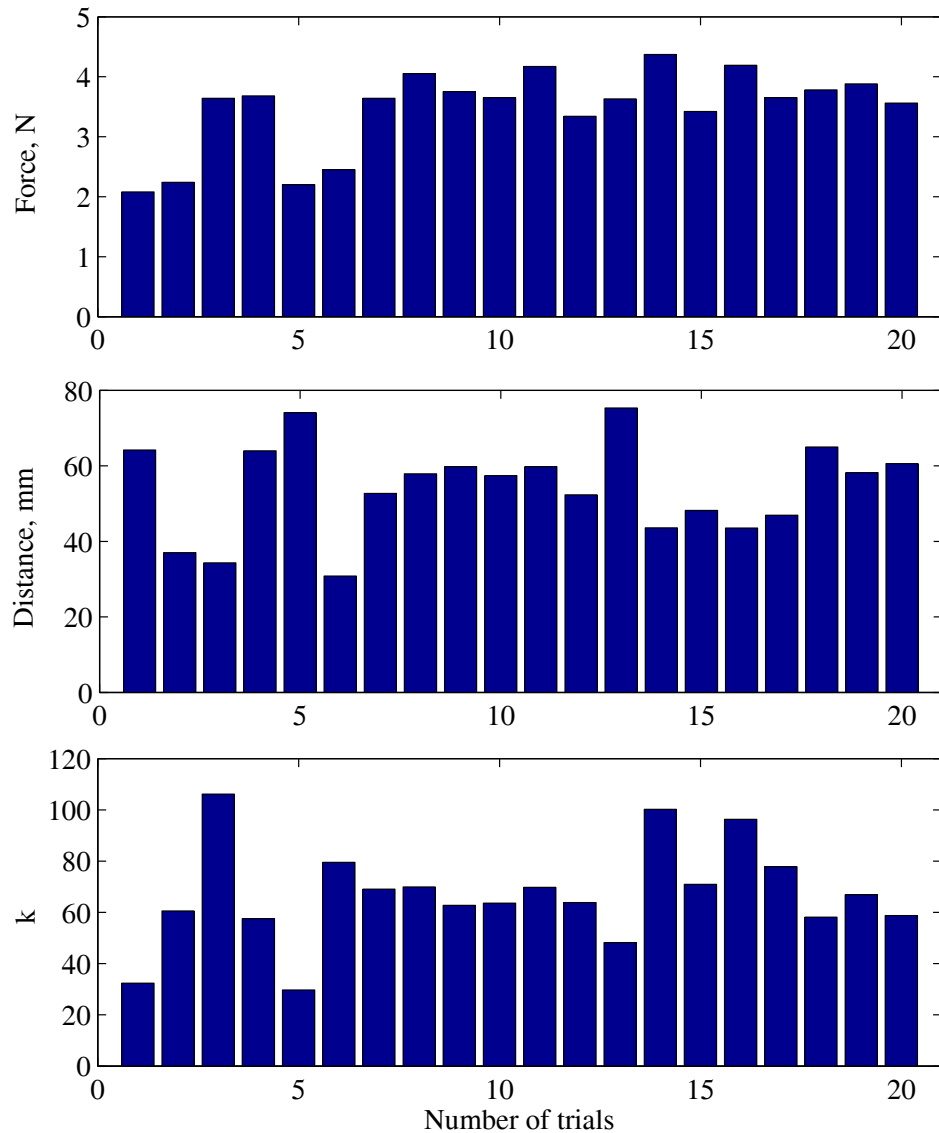
FIGURE I.20: Distribution of the force, distance and 'k' values over twenty trials

I.4   Conclusions

Tests and results from the apparatus used to investigate the artificial hand operation has been demonstrated that it is suitable to simulate the following: acceleration, object slippage and gripper force. It has also been observed that a large de-acceleration is required to obtain a small and acceptable slip distance. Also, an analysis of the slip signal using ApEn has shown when an object begins to slip. During re-gripping, there is a wide variation in the ratio of the applied average force to the object slip-distance.

An automatic control feedback system algorithm is proposed to be implemented into the prehension system. Also, in the future the information gained from the apparatus would be useful in improving the design of an artificial hand particularly the Southampton Hand and could be used with the ECS developed in this research.

References

Ajiboye, A., & Weir, R. (2005). A heuristic fuzzy logic approach to emg pattern recognition for multifunction prosthesis control. *IEEE Trans. on Biomedical Eng*, *52*(11), 280–291.

ARTSLab (2008). The cyberhand. [Accessed on: 24/12/2008].
URL http://www.cyberhand.org

Asghari Oskoei, M., & Hu, H. (2006). Ga-based feature subset selection for myoelectric classification. In *IEEE Int. Conf. on Robotics and Biomimetics*, (pp. 1465–1470).

Asghari Oskoei, M., & Hu, H. (2007). Myoelectric control systems - a survey. *Biomedical Signal Processing and Control*, *4*(4), 275–294.

Belaire-Franch, J., D. Contreras, D., & Tordera-Lled, L. (2002). Assessing nonlinear structures in real exchange rates using recurrence plot strategies. *Physica D*, *171*(4), 249–264.

Bezdek, J. C., & Pal, S. (1992). *Fuzzy models for pattern recognition : methods that search for structures in data*. IEEE Press, New York.

Bilodeau, M., Schindler-Ivens, S., Williams, D., Chandran, R., & Sharma, S. (2003). Emg frequency content changes with increasing force and during fatigue in the quadriceps femoris muscle of men and women. *J. Electromyogr Kinesiol*, *13*(1), 83–92.

Bonato, P., Boissy, P., Della Croce, U., & Roy, S. (2001). Changes in the surface emg signal and the biomechanics of motion during a repetitive lifting task. In *IEEE Trans. on Rehab Eng*, vol. 10, (pp. 38–47).

Carozza, M., Cappiello, G., Stellin, G., Zaccone, F., Vecchi, F., Micera, S., & Dario, P. (2005). On the development of a novel adaptive prosthetic hand with compliant joints: Experimental platform and emg control. In *IEEE/RSJ Int. Conf. on Intelligent Robots and Systems*, (pp. 1271–1276).

Carrozza, M., Cappiello, G., Beccai, L., Zaccone, F., Micera, S., & Dario, P. (2004). Design methods for innovative hand prostheses. In *IEEE Intl Conf on Eng. in Med. and Biol. Soc.*, vol. 2, (pp. 4345–4348).

Carrozza, M., Cappiello, G., Micera, S., Edin, B., Beccai, L., & Cipriani, C. (2006). Design of a cybernetic hand for perception and action. *Biological Cybernetics*, *95*(6), 629–644.

Carrozza, M., Dario, P., Vecchi, F., Roccella, S., Zecca, M., & Sebastiani, F. (2003). The cyberhand: on the design of a cybernetic prosthetic hand intended to be interfaced to the peripheral nervous system. In *IEEE Proc. on Intelligent Robots and Systems*, vol. 3, (pp. 2642–2647).

Carrozza, M., Dario, P., Zecca, M., & Micera, S. (2002a). Control of multifunctional prosthetic hands by processing the electromyographic signal. *Crit. Rev Biomed Engineering*, *30*, 459–485.

Carrozza, M., Massa, B., Micera, S., Lazzarini, R., Zecca, M., & Dario, P. (2002b). The development of a novel prosthetic hand - ongoing research and preliminary results. *IEEE/ASME Transactions on Mechatronics*, *7*(2), 108–114.

Carrozza, M., Micera, S., Massa, B., Zecca, M., Lazzarini, R., Canelli, N., & Dario, P. (2001). The development of a novel biomechatronic hand-ongoing research and preliminary results. In *Proc. of the IEEE/ASME International Conference on Advanced Intelligent Mechatronics*, vol. 1, (pp. 249–254).

Chai, L., Wang, Z., & Zhang, H. (1999). An emg classification method based on wavelet transform. In *Proc. of the First Joint BMES/EMBS Conf.*, (p. 565).

Chan, A., & Englehart, K. (2005). Continuous myoelectric control for powered prostheses using hidden markov models. *IEEE Transactions on Biomedical Engineering*, *52*(1), 121–124.

Chan, F., Yong-Sheng, Y., Lam, F., Yuan-Ting, Z., & Parker, P. (Sept. 2000). Fuzzy emg classification for prosthesis control. *IEEE Trans. On Rehabilitation Engineering, Vol. 8(3)*.

Chen, W. T., Wang, Z., & Ren, X. (2006). Characterization of surface emg signals using improved approximate entropy. *Zhejiang University Science B*, *7(10)*, 844–848.

Chen, X., Solomon, I., & Chon, K. (2005). Comparison of the use of approximate entropy and sample entropy: Applications to neural respiratory signal. In *Proc. of the 27th Ann. Intl Conf. of the IEEE-EMBS*, (pp. 4212–4215).

Christodoulou, C., & Pattichis, C. S. (1995). A new technique for the classification and decomposition of emg signals. In *Proc. of IEEE Int. Conf. on Neural Networks*, vol. 5, (pp. 2303–2308).

Chu, J., Moon, I., & Mun, M. (2006). A real-time emg pattern recognition system based on linear-nonlinear feature projection for a multifunction myoelectric hand. *IEEE Trans. on Biomedical Eng*, *53*, 2232–2238.

Cipriani, C., Zaccone, F., Stellin, G., Beccai, L., Cappiello, G., Carrozza, M., & Dario, P. (2006). Closed loop controller for a bio-inspired multi-fingered underactuated prosthesis. In *IEEE Intl. Conf. on Robotics and Automation*, (pp. 2111–2116).

Codd, R. (1976). *Development and Evaluation of Adaptive Control for a Hand Prosthesis*. Ph.D. thesis, University of Southampton.

Cotton, D. P. J., Cranny, A., White, N. M., Chappell, P. H., & Beeby, S. P. (2007). A novel thick-film piezoelectric slip sensor for a prosthetic hand. *IEEE Sensors Journal: special edition on intelligent sensors*, *7*(5), 752–761.

Cranny, A., Cotton, D. P. J., Chappell, P. H., Beeby, S. P., & White, N. M. (2005a). Thick-film force and slip sensors for a prosthetic hand. *Sensors and Actuators A: Physical*, *123-124*, 162–171.

Cranny, A., Cotton, D. P. J., Chappell, P. H., Beeby, S. P., & White, N. M. (2005b). Thick-film force, slip and temperature sensors for a prosthetic hand. *Measurement Science and Technology*, *16*, 931–941.

de Andrade, M. M., do Carmo, J. C., Nascimento, F. A. O., Camapum, J. F., dos Santos, I., Mochizuki, L., & da Rocha, A. F. (2006). Evaluation of techniques for the study of electromyographic signals. In *28th Annual International Conference of the IEEE Engineering in Medicine and Biology Society*, 1335-1338.

Dechev, N., Cleghorn, W., & Naumann, S. (2001). Multiple finger, passive adaptive grasp prosthetic hand. *Mechanism and Machine Theory*, *36*, 1157–1173.

Del Boca, A., & Park, D. (1994). Myoelectric signal recognition using fuzzy clustering and artificial neural networks in real time. In *IEEE Intl Conf. on Neural Networks*, vol. 5, (pp. 3098–3103).

Delsys (2009). Electromyography. [Accessed on:26/05/2009].
  URL `http://www.delsys.com`

Disaboom (2008). Disability lifestyle info. [Accessed on: 24/12/2008].
  URL `http://www.disaboom.com`

Eckmann, J., Kamphorst, S. O., & Ruelle, D. (1987). Recurrence plots of dynamical systems. In *Europhysics Letters*, vol. 5, (pp. 973–977).

Englehart, K., Hudgin, B., & Parker, P. (2001). A wavelet-based continuous classification scheme for multifunction myoelectric control. *IEEE Trans. on Biomedical Engineering*, *48*(3), 302–311.

Englehart, K., & Hudgins, B. (2003). A robust, real-time control scheme for multifunction myoelectric control. *IEEE Transactions on Biomedical Engineering*, *Vol. 50*(7), 848–854.

Englehart, K., Hudgins, B., M, S., & P.A., P. (1995a). Classification of transient myoelectric signals using a dynamic feedforward neural network. In *World Congress Neural Net*.

Englehart, K., Hudgins, B., & Parker, P. (2000). Time-frequency based classification of the myoelectric signal: static vs. dynamic contractions. In *Proc. of IEEE Intl. Conf on Eng. in Med. & Biol. Soc.*, vol. 1, (pp. 317–320).

Englehart, K., Hudgins, B., Parker, P., & Stevenson, M. (1998). Time-frequency representation for classification of the transient myoelectric signal. In *Proceedings of the 20th Annual International Conference of the IEEE/EMBS*, vol. 5, (pp. 2627–2630).

Englehart, K., Hudgins, B., Parker, P., & Stevenson, M. (1999a). Classification of the myoelectric signal using time-frequency based representations. *Medical Engineering and Physics*, *21*, 431–438.

Englehart, K., Hudgins, B., Parker, P., & Stevenson, M. (1999b). Improving myoelectric signal classification using wavelet packets and principal components analysis. In *Proceedings of the First Joint BMES/EMBS Conference*, vol. 1, (p. 569).

Englehart, K., Hudgins, B., Stevenson, M., & Parker, P. (1995b). Classification of myoelectric signal burst patterns using a dynamic neural network. In *Proc. of the IEEE Intl. conf. on Bioengineering*, (pp. 63–64).

Englehart, K., Hudgins, B., Stevenson, M., & Parker, P. (1995c). A dynamic feed-forward neural network for subset classification of myoelectric signal patterns. In *IEEE 17th Annual Conference of the Engineering in Medicine and Biology Society*, vol. 1, (pp. 819–820).

Eom, G., Watanabe, T., Futami, R., Hoshimiya, N., & Handa, Y. (2000). Artifact-free sensory nerve signals obtained from cuff electrodesduring functional electrical stimulation of nearby muscles. *Frontiers of Med. & Biol. Eng.*, *10*(3), 213–231.

Evans-Pughe, C. (2006). Smarter prosthetics. Tech. rep., IET - Engineering and Technology.

Farina, D., & Merletti, R. (2000). Comparison of algorithms for estimation of emg variables during voluntary isometric contractions. *Jnl. of Electromyography and Kinesiology*, *10*, 337–349.

Farrell, W. R., T.R. (2005). Pilot comparison of surface vs. implanted emg for multifunctional prosthesis control. In *International Conference on Rehabilitation Robotics*, (pp. 277–280).

Ferenets, R., Lipping, T., Anier, A., Jantti, V., Melto, S., & Hovilehto, S. (2006). Comparison of entropy and complexity measures for the assesment of depth sedation. *IEEE Trans. of Biomed Eng*, *53*(6), 1067 – 1077.

Gautama, T., Mandic, D., & Van Hulle, M. (2003). A differential entropy based method for determining the optimal embedding parameters of a signal. In *Proceedings of the IEEE International Conference on Acoustics, Speech, and Signal Processing (ICASSP '03)*.

Graupe, D., Salahi, J., & Kohn, K. (1982). Multifunction prosthesis and orthosis control via microcomputer identification of temporal pattern differences in single-site myoelectric signals. *Jnl of Biomedical Engineering*, *4*, 17–22.

Hargrove, L., Englehart, K., & Hudgins, B. (2006). The effect of electrode displacements on pattern recognition based myoelectric control. In *IEEE Ann. Intl. Conf. on Engineering in Medicine and Biology Society*, (pp. 2203–2206).

Hargrove, L., Englehart, K., & Hudgins, B. (2007). A comparison of surface and intramuscular myoelectric signal classification. *IEEE Transactions on Biomedical Engineering*, *54*(5), 847–853.

Hermans, H., Freriks, B., Merletti, R., Stegeman, D., Blok, J., Rau, G., Disselhorst-Klug, C., & Hagg, G. (1999). *SENIAM 8, European Recommendations for surface Electromyography, results of the SENIAM project*. Rossingh Research and Development.

Hudgins, B., Parker, P., & Scott, R. (1994). Control of artificial limbs using myoelectric pattern recognition. *Med. Life Sci. Eng.*, *13*, 21–38.

Hudgins, B., Parker, P., & Scott, R. N. (1993). A new strategy for multifunction myoelectric control. *IEEE Trans. on Biomedical Eng*, *40(1)*(1), 82–94.

Jansen, R., Ament, W., Verkerke, G., & Hof, A. (1997). Median power frequency of the surface electromyogram and blood lactate concentration in incremental cycle ergometry. *European Journal of Applied Physiology*, *75*(2), 102–108.

Jingdong, Z., Zongwu, X., Li, J., Hegao, C., Hong, L., & Hirzinger, G. (2006). A five-fingered underactuated prosthetic hand control scheme. In *IEEE/RAS-EMBS Intl Conf on Biomedical Robotics and Biomechatronics*, (pp. 995–1000).

Kalon, K. L., Moody, G., Chung-Kang, P., Mietus, J., Larson, M., Levy, D., & Goldberger, A. (1997). Predicting survival in heart failure case and control subjects by use of fully automated methods for deriving nonlinear and conventional indices of heart rate dynamics. *Circulation*, *96*, 842–848.

Karlik, B., M.O., T., & M., A. (2003). A fuzzy clustering neural network architecture for multifunction upper- limb prosthesis. *IEEE Trans. on Biomedical Engineering*, *50*, 1255–1261.

Kyberd, P. (1990). *Algorithmic Control of a Multifunction Hand Prosthesis*. Ph.D. thesis, University of Southampton.

Kyberd, P., Holland, O., Chappell, P., Smith, S., Tregidgo, R., Bagwell, P., & Snaith, M. (1995). Marcus: a two degree of freedom hand prosthesis with hierarchical grip control. *IEEE Transactions on Rehabilitation Engineering*, *3*(1), 70–76.

Kyberd, P. J., & Chappell, P. H. (1994). The southampton hand: An intelligent myoelectric prosthesis. *J Rehabil Res Dev*, *31*(4), 326–334.

Lake, D., Richman, J., Griffin, M. P., & Moorman, J. R. (2002). Sample entropy analysis of neonatal heart rate variability. *Am J Physiol Regul Integr Comp Physiol*, *283*(3), 789–797.

Li, X., & Aruin, A. (2005). Muscle activity onset time detection using teager-kaiser energy operator. In *Proc. of the 2005 IEEE/EMBS 27th Annual Conference*, (pp. 7549–7552).

Li, X., Zhou, P., & Aruin, A. (2007). Teager-kaiser energy operation of surface emg improves muscle activity onset detection. *Annals of Biomedical Engineering*, *35*, 1532–1538.

Light, C., Chappell, P., & Kyberd, P. (2002a). Establishing a standardized clinical assessment tool of pathologic and prosthetic hand function: normative data, reliability, and validity. *Arch Phys Med Rehabil*, *83*(6), 776–783.

Light, C. M. (2000). *An intelligent hand Prosthesis and Evaluation of Pathological and Prosthetic Hand Function*. Ph.D. thesis, University of Southampton.

Light, C. M., & Chappell, P. H. (2000). Development of a lightweight and adaptable multiple-axis hand prosthesis. *Med Eng Phys*, *22*(10), 679–684.

Light, C. M., Chappell, P. H., Hudgins, B., & Engelhart, K. (2002b). Intelligent multifunction myoelectric control of hand prostheses. *J Med Eng Technol*, *26*(4), 139–146.

Mamdani, B., & Assilian, S. (1999). An experiment in linguistic synthesis with a fuzzy logic controller. *Int. J. Hum.-Comput. Stud.*, *51*, 135–147.

Manette, O., & Maier, M. (2004). Temporal processing in primate motor control: relation between cortical and emg activity. *IEEE Trans. on Neural Networks*, *15*(5), 1260–1267.

Martinez, A., & Kak, A. (2001). Pca versus lda. *IEEE Trans. on Pattern Analysis and Machine Intelligence*, *23*(2), 228–233.

Marwan, N. (2003). *Encounters With Neighbours - Current Developments Of Concepts Based On Recurrence Plots And Their Applications*. Ph.D. thesis, University of Potsdam, ISBN 3-00-012347-4.

Meng, Y., Liu, Y., & Liu, B. (2001). A comprehensive nonlinear analysis of electromyogram. In *Proc. of the 23rd Annual International Conference of the IEEE-EMBS*, vol. 2, (pp. 1078–1081).

Meng, Y., Liu, Y., & Liu, B. (2005). Test nonlinear determinacy of electromyogram. In *Proc. of the 27th Annual International Conference of the IEEE-EMBS*, (pp. 4592–4595).

Mitchell, W. R., M. (2008). Development of a clinically viable multifunctional hand prosthesis. In *MyoElectric Controls/Powered Prosthetics Sympossium*.

Moore, D. (1980). *Development of a Multifunctional Adaptive Hand Prosthesis*. Ph.D. thesis, Univeristy of Southampton.

Morrison, S., Hong, S., & Newell, K. (2007). Inverse relations in the patterns of muscle and center of pressure dynamics during standing still and movement postures. *Experimental Brain Research*, *181*(2), 347–358.

MotionControl (2007). The prohand. [Accessed on: 19/09/2007].
URL `http://www.utaharm.com/tds.htm`

New Brunswick University, C. (2009). Institute of biomedical engineering. [Accessed on: 20/01/09].
URL `http://www.unb.ca/biomed/`

OttoBock (2007). The sensorhand and the systemhand. [Accessed on: 18/09/2007].
URL `http://www.ottobock.com`

Oxford, U. (2009). Oxford online dictionary. [Accessed on: 01/11/2007].
URL `http://dictionary.oed.com/`

Parker, P., Englehart, K., & Hudgins, B. (2006). Myoelectric signal processing for control of powered limb prostheses. *Jnl. of Electromyography and Kinesiology*, *16*, 541–548.

Perry, S., Housh, T., Weir, J., Johnson, G., Bull, A., & Ebersole, K. (2001). Mean power frequency and amplitude of the mechanomyographic and electromyographic signals during incremental cycle ergometry. *Journal of Electromyography and Kinesiology*, *11*(11), 299–305.

Pincus, S., & Singer, B. H. (1996). Randomness and degrees of irregularity. *Proc Natl Acad Sci U S A*, *93*(5), 2083–2088.

Pincus, S. M. (1991). Approximate entropy as a measure of system complexity. *Proc Natl Acad Sci U S A*, *88*(6), 2297–2301.

Pincus, S. M., Cummins, T. R., & Haddad, G. G. (1993). Heart rate control in normal and aborted-sids infants. *Am J Physiol*, *264*(3 Pt 2), 638–646.

Pincus, S. M., Gevers, E. F., Robinson, I. C., van den Berg, G., Roelfsema, F., Hartman, M. L., & Veldhuis, J. D. (1996a). Females secrete growth hormone with more process irregularity than males in both humans and rats. *Am J Physiol*, *270*(1 Pt 1), E107–E115.

Pincus, S. M., Gladstone, I. M., & Ehrenkranz, R. A. (1991). A regular statistic for medical data analysis. *Clinical Monitoring*, *7*(4), 335–345.

Pincus, S. M., & Goldberger, A. L. (1994). Physiological time-series analysis: what does regularity quantify? *Am J Physiol*, *266*(4 Pt 2), H1643–H1656.

Pincus, S. M., Mulligan, T., Iranmanesh, A., Gheorghiu, S., Godschalk, M., & Veldhuis, J. D. (1996b). Older males secrete luteinizing hormone and testosterone more irregularly, and jointly more asynchronously, than younger males. *Proc Natl Acad Sci U S A*, *93*(24), 14100–14105.

Pincus, S. M., & Viscarello, R. R. (1992). Approximate entropy: a regularity measure for fetal heart rate analysis. *Obstet Gynecol*, *79*(2), 249–255.

PlanetMath (2007). Simpson's rule. [Accessed on: 4/12/2007].
URL http://planetmath.org/encyclopedia/SimpsonsRule.html

Plettenburg, D. H. (2006). *Upper Extremity Prosthetics, Current Status & Evaluation*. VSSD.

Polikar, R. (2007). The wavelet tutorial. [Accessed on: 18/10/2007].
URL http://users.rowan.edu/~polikar/WAVELETS/Wtutorial.html

Richman, J. S., & Moorman, J. R. (2000). Physiological time-series analysis using approximate entropy and sample entropy. *Am J Physiol Heart Circ Physiol*, *278*(6), H2039–H2049.

Roberto Merletti, P. P. (Ed.) (2004). *Electromyography Physiology, Engineering and Noninvasive Applications*. IEEE Press, John Wiley & Sons Inc.

Romaiguere, P., Vedel, J., & Pagni, S. (1993). Comparison of fluctuations of motor unit recruitment and de-recruitment thresholds in man. *Exp Brain Res*, *95*(3), 517–522.

Samanta, A., Musharaf Ali, S., & Ghosh, S. (2004). New universal scaling laws of diffusion and kolmogorov-sinai entropy in simple liquids. *Phys. Rev. Lett.*, *92*, 145901.

Schug, J., Schuller, W.-P., Kappen, C., Salbaum, J., Bucan, M., & Stoecker, C. (2005). Promoter features related to tissue specificity as measured by shannon entropy. *Genome Biology*, *6*(4).

Scott, R. (1984). *An introduction to myoelectric prostheses in UNB Monographs on Myoelectric Prostheses Series*. Institute of Biomedical Engineering, UNB Canada.

Scott, R., & Parker, P. (1988). Myoelectric prostheses: state of the art. *Medical Eng. tech.*, *12*, 143–151.

Shannon, C. (1948). A mathematical theory of communication. *Bell System Technical Journal*, *27*, 379–243.

Silva, J., Chau, T., Naumann, S., & Heim, W. (2003a). Systematic characterisation of silicon-embedded accelerometers for mechanomyography. *Medical and Biological Engineering and Computing*, *41*(3), 290–295.

Silva, J., Chau, T., Naumann, S., Helm, W., & Goldenberg, A. (2003b). Optimization of the signal-to-noise ratio of silicon-embedded microphones for mechanomyography. In *IEEE Conf. on Elec. and Comp. Eng.*, vol. 3, (pp. 1493–1496).

Silva, J., Heim, W., & Chau, T. (2004). Mmg-based classification of mucle activity for prosthesis control. In *IEEE Proc. on Eng. in Med. and Biol. Soc.*, vol. 2, (pp. 968–971).

Simpson, D. (1994). *Maximum Entropy Image Processing in Two and Three Dimensional Single Photon Nuclear Medicine Imaging*. Ph.D. thesis, University of Southampton.

Storey, N. (1978). *Control of an Arm Prosthesis*. Ph.D. thesis, Univesity of Southampton.

Stots, P., & Bawa, P. (2001). Motor unit recruitment during lengtening contraction of human wrist flexors. *Muscle Nerve*, *24*, 1535–1541.

Swain, I. (1982). *Adaptive Control of an Arm Prostheses*. Ph.D. thesis, University of Southampton.

Thiel, M., Romano, M., & Kurths, J. (2004). How much information is contained in a recurrence plot? In *Physics Letters*, vol. A330, (pp. 343–349).

Todd, R. W. (1970). *Adaptive Control of a Hand Prosthesis*. Ph.D. thesis, University of Southampton.

TouchBionics (2007). The i-limb hand. [Accessed on: 19/09/2007].
  URL `http://www.touchbionics.com`

Van Cutsem, M., Duchateau, J., & Hainaut, K. (1998). Changes in sinle motor unit behaviour contribute to the increase in contraction speed after dynamic training in humans. *Jnl of Physiology*, *513*(1), 295–305.

van Drongelen, W., Nayak, S., Frim, D., Kohrman, M., Towle, V., Lee, H., McGee, A., Chico, M., & Hecox, K. (2003). Seizure anticipation in pediatric epilepsy: Use of kolmogorov entropy. *Pediatric Neurology*, *29*(3), 207–213.

von Berlichingen, G. (2007). [Accessed on:17/09/2007].
  URL `http://www.wikipedia.org`

Wang, G., Yan, Z., Hu, X., Xie, H., & Wang, Z. (2006). Classification of surface emg signals using harmonic wavelet packet transform. *Physiological Measurement*, *27*, 1255–1267.

Webber, C., & Zbilut, J. (1994). Dynamical assessment of physiological systems and states using recurrence plot strategies. *Jnl of Applied Physiology*, *76*(2), 965–973.

Weir, R., & Ajiboye, A. (2003). A multifunction prosthesis controller based on fuzzy-logic techniques. In *Proceedings of the 25th Annual International Conference of the IEEE/EMBS*, vol. 2, (pp. 1678–1681Vol.2).

Y. Al-Assaf, H. A.-N. (2005). Surface myoelectric classification for prostheses control. *Jnl. of Med. Eng & Tech*, *29*(5), 203–207.

Yonghong, H., Englehart, K., Hudgins, B., & Chan, A. (2005). A gaussian mixture model based classification scheme for myoelectric control of powered upper limb prostheses. *IEEE Tran. on Biomedical Engineering*, *52*(11), 1801–1811.

Zadeh, L. (1965). Fuzzy sets. *Information Control*, *8*, 338–353.

Zardoshti-Kermani, M., Wheeler, B., Badie, K., & Hashemi, R. (1995). Emg feature evaluation for movement control of upper extremityprostheses. *IEEE Trans. on Neural Systems and Rehabilitation*, *3*(4), 324–333.

Zhao, J., Jiang, L., Shi, S., Cai, H., Liu, H., & Hirzinger, G. (2006a). A five-fingered underactuated prosthetic hand system. In *Proc. of the IEEE Intl Conf. on Mechatronics and Automation*, (pp. 1453–1458).

Zhao, J., Xie, Z., Jiang, L., Cai, H., Liu, H., & Hirzinger, G. (2006b). Emg control for a five-fingered underactuated prosthetic hand based on wavelet transform and sample entropy. In *IEEE/RSJ International Conference on Intelligent Robots and Systems*, (pp. 3215–3220).